The quantitative effect of gas-to-particle conversion on ammonia fluxes

UMIST Transfer Report

- Eiko Nemitz -

Supervisors: Prof. T.W. Choularton (UMIST) and Dr. M.A. Sutton (ITE)
University of Manchester Institute of Science and Technology, UMIST
Department of Physics
Sackville Street
Manchester
M60 1QD

Institute of Terrestrial Ecology, ITE
Bush Estate
Penicuik
Midlothian
EH26 OQB

November 1995

1. INTRODUCTION

1.1 AMMONIA AS A POLLUTANT

During the last ten years there has been a growing interest in the atmospheric emission and transport of nitrogen species. As oxides of nitrogen (NO_2, NO and HNO_3) are mainly produced by anthropogenic sources, their increasing concentrations are expected to have an effect on the global nitrogen cycle and budget. However, it has also been shown that the increase of the emission of reduced nitrogen in the form of ammonia (mainly due to rising live stock numbers, over the last 200 years) has effects. Ammonia is the only major gaseous base in the atmosphere. It plays an important role for the neutralisation of atmospheric acids such as nitric acid (HNO_3), sulphuric acid (H_2SO_4) and hydrochloric acid (HCl) as well as in the global nitrogen cycle (see Figure 1).

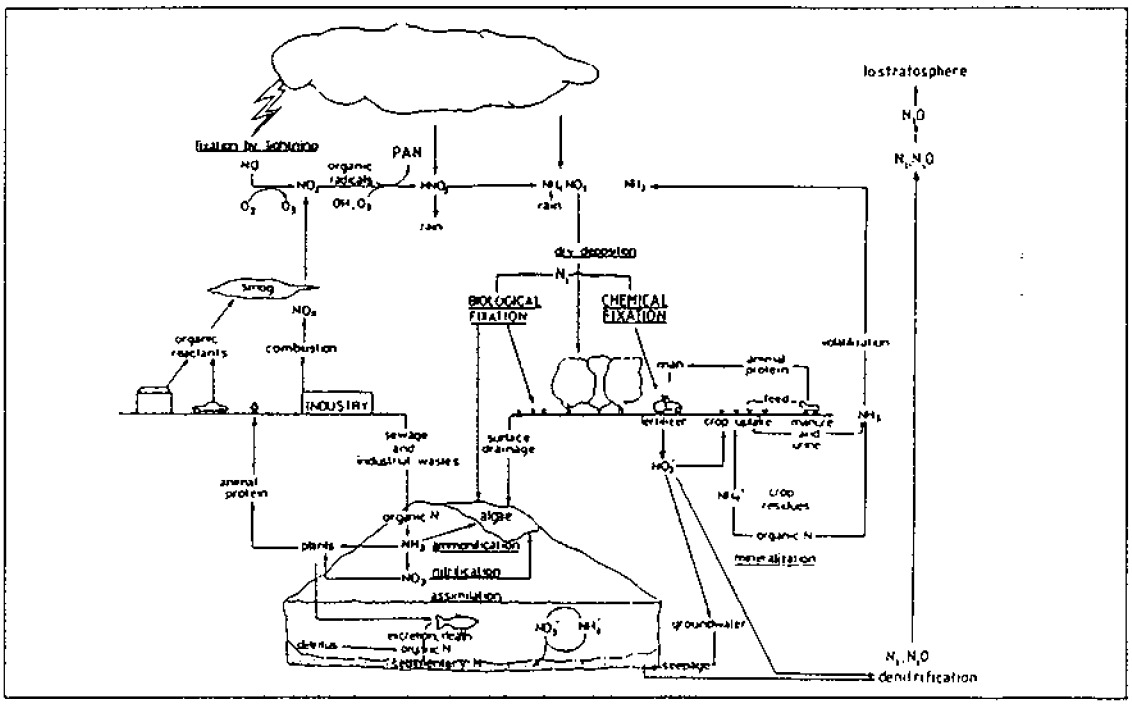

Figure 1: The schematic nitrogen cycle taken from The Royal Society (1983)

The atmospheric deposition of NH_3 into ecosystems is known to have the following main environmental impacts:

1. Eutrophication:

   The deposition of nitrogen compounds is a potential source of nutrient import. Whereas this deposition had been considered to be a beneficial source of nitrogen for plants it is now suspected to disturb the balance of the nutrient economy. For example, eutrophication of lakes is known to increase the possibility of algal booms. Additional nitrogen supply favours the growth of plant communities needing high amounts of nutrients and might suppress species favouring oligotrophic conditions. This way heather is endangered to be gradually replaced by grass and short grassland species by taller, rougher grasses. Moreover additional nitrogen supply can induce imbalance of

other nutrients and hormones leading to a higher sensitivity to frost damage or fungal infection as well as fast growth and the production of high volume cells resulting in wind sensitivity as far as trees are concerned (e.g. Sutton *et al.*, 1993).

2. Acidification of ecosystems:

   Additional to the direct deposition of nitric acid, ammonia deposition can also lead to soil acidification. Transformation of NH_3 to NH_4^+ consumes one H^+, however, subsequent oxidation of the NH_4^+ to nitrate by soil bacteria releases two H^+, resulting in a net acidification. Other plant and soil uptake processes act in competition so that it is difficult to estimate the net contribution of NH_3 to acidification. Since additional nitrate ions might catch nutrient cations (eg. Ca^{2-}, K^-), they limit the availability of nutrients for the plant causing growth problems associated with nutrient shortages. This effect has become known as the 'ammonium hypothesis' for forest decline (Nihlgård, 1985).

3. Modification of atmospheric and surface chemistry:

   As the predominant atmospheric base the pH change due to ammonia and ammonium solved in aqueous aerosol, in cloud droplets or in leaf water films, is known to strongly influence the reaction rates of many aqueous phase reactions. It has been suggested that deposition of ammonia and deposition of sulphur dioxide enhance each other (known as NH_3-SO_2 co-deposition, e.g. Erisman and Wyers, 1993) as the oxidation of SO_2 increases with pH (Behra *et al.* 1989) acting as a sink for NH_3 in return lowering the pH and thus allowing a higher deposition flux of ammonia.

4. In high concentrations airborne ammonia itself may be **directly phytotoxic** as suggested by van der Eerden (1982).

These negative effects make it necessary to monitor ammonia concentrations and to estimate the inputs of ammonia into the biosphere. For this a better understanding of transfer mechanisms to canopy and surface is important along with new and more precise measuring techniques for ammonia concentrations and fluxes.

1.2 EMISSION AND DISTRIBUTION

The contribution of the different sources to the emission of ammonia has been controversially discussed throughout time and literature. Natural emission rises from soil, anthropogenic from animal manure, synthetic fertiliser and livestock waste (see Table 1). Asman (1992) estimates that the latter contributes about 81% to the estimated total emission of 6.4 Tg NH_3 per year in Europe. Dentener and Crutzen (1994) assume a worldwide NH_3 emission from anthropogenic sources of 30.4 Tg N yr^{-1}.

Sensitive to local sources ammonia emissions and concentrations show a high spatial and temporal variability. Allen *et al.* (1988) who carried out a study for Colchester, UK, found mean ammonia concentrations decreasing from 28 to 2 µg over a distance of less than 2 km. Moreover, ammonia can be either emitted or deposited depending on air concentration and the state and nature of the ecosystem. This leads to some complications for a uniform description of the micrometeorological theory as some common techniques cannot sensibly applied to bi-directional transfer (see next section). Sutton (1990)

made flux measurements over different ecosystems and measured mean deposition fluxes over natural ecosystems as: 31 ng $m^{-2} s^{-1}$ over neutral-calcareous grassland, 23 ng $m^{-2} s^{-1}$ over moor land, of 10 ng $m^{-2} s^{-1}$ over forest. Fluxes over agricultural surfaces differed with meteorological conditions and the time of year indicating an influence of the state of the crop, the intensity of grazing or temperature. A mean deposition flux of 12.2 ng $m^{-2} s^{-1}$ in winter and an emission flux of -4.8 ng $m^{-2} s^{-1}$ in summer for the same agricultural grassland show this seasonal dependency. Fluxes in summer differed from 10.6 ng $m^{-2} s^{-1}$ under wet to -15 ng $m^{-2} s^{-1}$ under dry conditions.

Table 1: Sources of ammonia divided into naturally and anthropogenically induced. Numbers are global emission according to Dentener and Crutzen (1994) in [Tg N yr^{-1}]

importance of source	natural sources	anthropogenic sources	global emission [Tg N yr^{-1}]
major:		- animal wastes	22.0
		of which	
		. cattle	14.2
		. pigs	2.8
		. horses/mules/asses	1.2
		. sheep/goats	2.5
		. poultry	1.3
		- fertilisers	6.4
		- industrial activities	N/A
minor:	- natural soils and vegetation (5.1)	- coal combustion	2.0
	- wild animals (2.5)	- human respiration	N/A
	- ocean (7.0)	- sewage sludge	N/A
		- cats and dogs	N/A

In contrast to NH_3 the concentration of NH_4^+ aerosol was found to show much less spacial and temporal variablity throughout the study of Allen *et al.* (1988). This can be explained by NH_4^+ undergoing mainly long-range transport mechanisms and being produced as a secondary pollutant.

1.3 Deposition paths of Ammonia

As for any trace gases, the mechanisms for removal of NH_3 from the atmosphere are:

1. Wet deposition

   NH_3 is dissolved in rain, snow and fog droplets and removed by precipitation.

2. Dry deposition

   Pollutant gases can be absorbed by canopy, soil and water surfaces and thus be depleted near the ground. As higher parts of the atmosphere can often be regarded as a infinite reservoir of the tracer, a concentration gradient forms leading to a flux. The rate of the flux is governed by the magnitude of the gradient, atmospheric turbulence, atmospheric stability and the (molecular or Brownian) diffusivity of the tracer. Whereas for some gases (HNO_3, HCl) any canopy is thought to act as a perfect sink (e.g. Huebert *et al.*, 1988) there can be a considerable concentration of NH_3 in the plant

stomata, limiting the NH_3 gradient or even leading to counter gradients, i.e. emission, if it exceeds the air concentration. Thus the surface atmosphere exchange of NH_3 is bi-directional.

3. Chemical conversion processes

Reaction with atmospheric acids can lead to formation of aerosol, which, depending on the relative humidity, can be found in either a solid or aqueous state, and contribute to the removal of gaseous ammonia. The mechanisms and thus the rate of dry deposition, described by the deposition velocity (V_d) for aerosols differ significantly from those of gases (see section 2.6.5). Hence gas-to-particle-conversion can alter the rate of atmosphere surface exchange as discussed in more detail in the following section.

1.4 THE INFLUENCE OF GAS-TO-PARTICLE CONVERSION ON THE NET EXCHANGE OF AMMONIA: MOTIVATION FOR THIS WORK

Direct measurements of pollutant fluxes at one height require high frequency detectors (see section 2.5.1), which are not yet available for NH_3. Instead, gradient methods are frequently used to derive the flux from the concentration gradient in the atmosphere. They are based on the assumption that a layer, in which the fluxes are independent of height (the constant flux layer, CFL), forms above a homogenous surface. This assumption requires homogeneity of the area and the absence of advection; but it is also essential that there are no sources or sinks within the atmosphere. The latter requirement is fulfilled for heat and non-reactive entities but is violated if chemical conversion processes occur.

Ammonia forms equilibria with HCl and HNO_3 forming ammonium salts and can also be depleted by the irreversible reaction with H_2SO_4. Ammonia, gaseous acids and ammonium aerosols obey different deposition mechanisms and are hence differently quickly removed from the atmosphere. The difference in the deposition velocity results in deviations from the chemical equilibrium given by the concentration product of NH_3 and HNO_3 (or HCl) and the concentration of NH_4NO_3 (or NH_4Cl). Dis-equilibrium then leads to non-conserved fluxes. The magnitude of the flux divergence depends on the reaction rates governed by the concentrations themselves as well as temperature and humidity. For NH_3 the true flux can, strictly speaking, not be evaluated by gradient methods without correcting for the influence of gas-to-particle conversion (GPC). However, so far the effect of GPC has largely been considered as negligible and consequently been ignored. Figure 2 illustrates an example of NH_3 emission with formation of NH_4NO_3 aerosol close to the ground. The high NH_3 emission leads to a concentration product of the gases, $[NH_3]x[HNO_3]$, which is bigger than the equilibrium product determined by the NH_4NO_3 concentration, temperature and relative humidity. As the NH_3 concentration and possibly the ralative humidity decrease with height the dis-equilibrium becomes smaller. In this example the application of gradient techniques would not derive the surface/atmosphere exchange but an average value for the height dependent flux over the height range of the measurements. Thus the true emission flux would be underestimated.

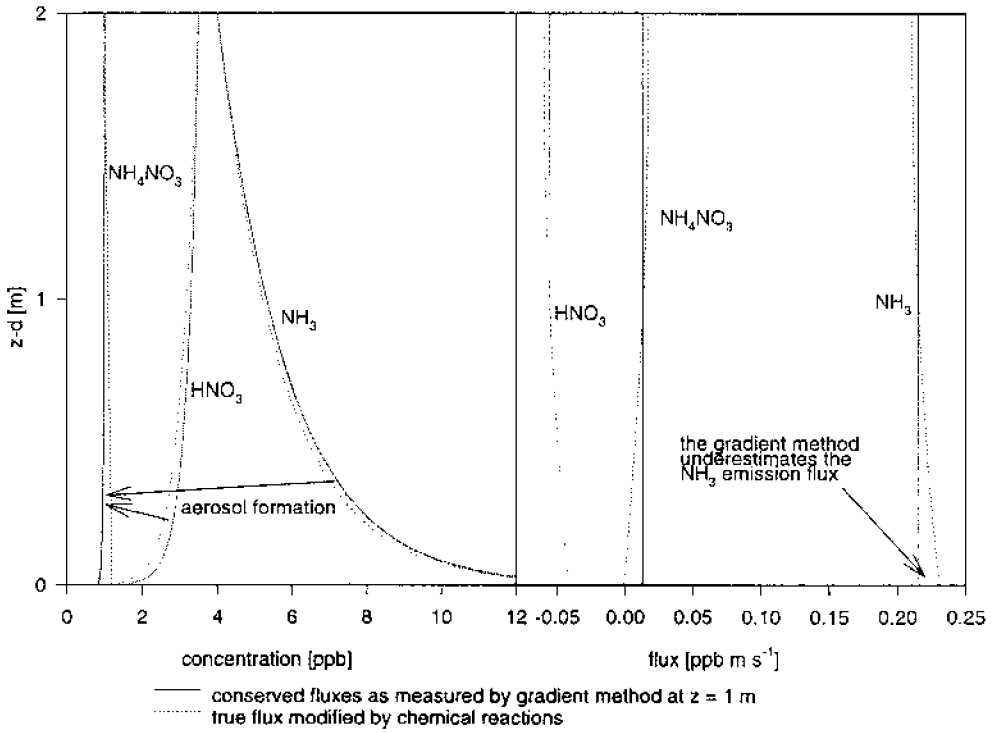

Figure 2. Schematic outline of the principle of gas-to-particle conversion. In this example emission of NH_3 in the presence of a considerable HNO_3 concentration leads to formation of NH_4^+ aerosol which is highest at the ground.

A variety of measurements carried out by different authors have shown features which cannot be explained by constant flux micrometeorology and indicate that the effect of gas-to-particle conversion can, under certain conditions, indeed be substantial. Zhang *et al.* (1995) found upward fluxes of HNO_3 of up to 0.4 μg m^{-2} s^{-1} whereas theory predicts deposition, and explain it with height dependent depletion through the high NH_3 concentration of about 10 μg m^{-3}. Sutton (unpublished data, see section 4.3) found emission of particulate NH_4^+ of up to 60 ng m^{-2} s^{-1} during a field campaign in Halvergate in September 1989. Huebert *et al.* (1988) also report apparent emission of HNO_3 and higher deposition rates of NH_4^+. Brost and Delany (1988) were able to qualitatively simulate these features in a numerical model taking chemical conversions into account.

Some models have been written for modelling the equilibrium reaction between HNO_3, NH_3 and NH_4NO_3, but neither has the reaction of NH_3 with HCl or humidity effects been included in the models, nor have the model predictions been thoroughly compared to experimental data. A variety of approaches to calculate the similar photochemical reaction cycle of NO_2, NO and O_3 exist showing that measured fluxes might have to be corrected by up to 20% (Coe, 1993). Because of the similarity to the nitrate triad these models can easily be adopted for the chemistry of NH_3. The accuracy of models dealing with the chemistry of NH_3 appeared to be limited by insufficient knowledge of the reaction kinetics but according to Kramm and Dlugi (1994) NH_3 fluxes could be overestimated by several 100% if the reaction rates are assumed to be very high, while they also found that sign changes of the true NH_3 flux can occur.

The reported measurements and first model results of other authors show that situations occur in which the effect of GPC on NH_3 flux measurements cannot be neglected. The effect on the flux measurements might lead to considerable error in the net exchange of NH_3 with ecosystems. Beside the effect on measurements, GPC is also likely to effect the physical exchange processes themselves. For example, evaporation of particulate NH_4^+ into fast depositing gaseous NH_3 would potentially enhance the total deposition of reduced nitrogen in highly polluted areas. This would obviously have important consequences for the exceedance of critical loads of nitrogen. If, on the other hand, NH_3 is emitted in the presence of a high background concentration of HNO_3, aerosol formation can deplete NH_3 near the surface resulting in bigger gradients and increased NH_3 emission.

1.5 AIM AND STRUCTURE OF THE REPORT

The aim of this work is to compare the predictions of different NH_3 chemistry models to measured data and to establish requirements for both further input data and necessary model changes. Field campaigns are to be set up focusing on obtaining suitable and representative data which can be fed into the modified models. Here a first emphasis has to be put on the examination of the reaction kinetics. After the models have been improved the net effect of GPC on ammonia exchange under different micrometeorological situations and the true surface fluxes are to be estimated so that instructions for the correction of flux measurements by gradient methods can be formulated. As a last step the results obtained shall be used for overlaying maps of NH_3 deposition data with concentration maps of the other relevant chemical species in order to estimate the effect of GPC on the NH_3 budget for the UK.

As the reaction kinetics are closely linked to the chemistry and physics of NH_4^+ aerosol, investigations in the transport, formation, coagulation and evaporation processes of aerosol have to be carried out.

This report presents the state of the work after eleven months time. It starts with an overview over the micrometeorological background of flux measurements (chapter 2), which is kept relatively comprehensive reflecting the variety of techniques used throughout the work. However, as it does not exceed common theory, it is meant as a reference for the following chapters and future work of the author himself rather than as a substantial part of the work itself. It can thus be skipped by the reader without effecting the understanding of subsequent chapters as necessary cross-references on micrometeorological equations will be given.

Chapter 3,

The chemistry of ammonia and ammonium aerosol" recapitulates work carried out by former authors on the reaction kinetics of NH_3.

The next chapter (chapter 4) gives a summary of existing models for the calculation concentration and flux profiles of the nitrate triad HNO_3, NH_3 and NH_4NO_3 and the NO_x triad, NO_2, NO and O_3,. These models have here been re-decoded and extended by methods to

a) simultaneously deal with the nitrate and chloride triad,

b) extrapolate profiles calculated between two input heights down to the surface, z_o,

c) calculate the height dependent equilibrium constants as functions of the temperature and relative humidtiy so that gradients in temperature and relative humidity can be accounted for.

The first findings of applying these models to measured data are given followed by a brief discussion on further data requirements.

Chapter 5 deals with common techniques to measure the concentration of NH_3 and other tracers and shows how experience was gained in these techniques. The preliminary findings of a field campaign (EXAMINE '95) are then reported (chapter 6) showing results of NH_3 gradients both above and within the canopy as well as particle fluxes.

The report finishes off (chapter 7) by outlining plans and perspectives for further modelling and measuring activities.

2. MICROMETEOROLOGICAL THEORY

2.1 THE STRUCTURE OF THE ATMOSPHERIC BOUNDARY LAYER

The boundary layer is defined as the region of the troposphere closest to the earth surface where atmospheric motion is influenced by friction effects. Up to a height of 50-100 m, depending on the surface properties and the stability conditions, air flows are mainly determined by friction and temperature gradients (surface layer). Here shear stress and heat fluxes are nearly constant with height. In the upper part of the boundary layer, the Ekman layer, the flow is increasingly influenced by the coriolis force. Transport processes between the surface layer and the surface itself take place through a very shallow (depth of less than 1 mm) laminar (or viscous) sub-layer which encloses all surface elements. Whereas here the transport mechanism is due to molecular or Brownian diffusion, mixing and advective effects of differently sized circular motions, eddies, play the major role within the boundary layer.

As the wind passes over a homogenious surface a layer forms above the ground in which the fluxes are expected to be in equilibrium with the surface and constant with height. The thickness of this constant flux layer depends largely on the fetch, i.e. the distance from the closest upwind inhomogeneity. Monteith and Unsworth (1990) state the rule that fluxes of heat and chemically inert entrained properties are sufficiently constant within the boundary layer up to a height of 0.5 % to 1 % of the fetch, e.g. for measurements up to 1 m an upwind fetch of 100 m, better 200 m, is required. It is within this constant flux layer that flux measurements can be carried out as the measured flux is expected to equal the surface flux.

From empirical results it is known that the increase in mean horizontal wind speed, u, with height is inversely proportional to the height, z, itself:

$$\frac{\partial \bar{u}}{\partial z} \propto \frac{1}{z} \qquad \text{eq 1}$$

Obviously, integration of this equation leads to a logarithmic wind profile. Under neutral conditions ($u'=w'$) the factor of proportionality is found to equal a characteristic velocity, the friction velocity u_*, divided by an empirical constant, known as the von Karman constant ($\kappa=0.41$).

Considering the roughness of a surface containing roughness elements of the mean height, h, the relationship in equation 1 breaks down near the surface. However, the wind profile can be extrapolated to the ground and a virtual height, z_o, can be found at which the wind speed is expected to equal zero. This height is called roughness length and is of the order $^1/_5$ to $^1/_{30}$ h. A further correction needs to be done as to account for the atmospheric stability. In stable condition (negative temperature gradient) vertical mixing and transport of momentum is diminished which leads to a flattened wind profile ($w'<u'$) whereas in unstable conditions (strongly positive temperature gradient) the eddies are vertically 'stretched' ($w'>u'$) and steepen the wind profile. The expression for the wind speed has to be multiplied by a dimensionless stability function, Φ_M, for the transfer of momentum, which is greater or less than

unity for stable or unstable conditions, respectively. However, even in neutral conditions the plot of wind speed against the logarithm of height would not lead to a straight line as far as measurements over plant canopies are concerned. A zero plane displacement level (d) of the flow above ground which is a major fraction of plant height (h) (often assumed to be 2/3 h or 3/4 h) must be introduced yielding the relationship:

$$\frac{\partial \bar{u}}{\partial z} = \frac{u_* \Phi_M}{\kappa (z-d)} = \frac{u_*}{l} \qquad \text{eq 2}$$

l can be identified with the mean eddy size or mixing length and is roughly proportional to the height above d, i.e. z-d. Equation 3 gives the solution for this differential equation considering the stability function as independent of height. As this is only an approximation the exact integration will be carried out in section 2.5.2.1.

$$\bar{u}(z) = \frac{u_*}{\kappa} \ln \frac{z-d}{z_0} \Phi_M \qquad , z-d > z_0 \qquad \text{eq 3}$$

2.2 ATMOSPHERIC STABILITY

Atmospheric stability describes the thermal stratification of the atmosphere. As an air parcel is displaced adiabatically up or downwards its density changes. Depending on whether it becomes lighter or heavier than the surrounding air it either experiences a restoring force or the perturbation is supported.

In order to quanitify the stability conditions it is necessary to parameterize the stability. One measure for the degree of stability or instability is the Richardson number, Ri. It describes the ratio of the gain in kinetic energy an air parcel experiences when it follows one cycle of the mean eddy motion of the length, l, KE_b, and its initial kinetic energy, KE_i. The detailed derivation can be found in Garrant (1992).

$$Ri(z) = \frac{KE_b}{KE_i} = \frac{g}{T} \frac{\partial T}{\partial z} \left(\frac{\partial \bar{u}}{\partial z} \right)^{-2} \qquad \text{eq 4}$$

where g is the acceleration due to gravity and T the absolute temperature in degrees Kelvin. Ri is positive in stable, equals zero in neutral and is negative in unstable conditions. It changes with height (as the eddy size) and is for any given situation roughly proportional to height.

Another parameter which is often used is the Monin-Obukhov stability length, L. L describes the height at which buoyancy contributes more to the gain in turbulent kinetic energy an air parcel experiences than the wind shear. Since the influence of the shear is more sensitive to height than buoyancy this threshold can always be found. If buoyancy counteracts an upward motion this length is negative (stable

condition), in unstable condition it is positive. L is infinite and changes sign in the case of atmospheric neutrality. Garrant (1992) derives L as:

$$L = -\frac{u_*^3}{\kappa(g/T)(H/\rho c_p)} \qquad \text{eq 5}$$

where H is the sensible heat flux (positive, if upwards), c_p the specific heat capacity of air at constant pressure and ρ the density of air. L has the dimension of length and in contrast to Ri it remains constant with height.

2.3 DEFINITION OF FLUXES ACCORDING TO THE VARIANCE THEORY

Eddies lead to disordered and random fluctuations of wind speed, temperature, concentrations and other quantities. These can be divided into an averaged and a fluctuating component as might be shown for the horizontal wind speed: $u = \bar{u} + u'$ (Reynolds decomposition).

Using this concept the following scaling parameter of an entity can be defined by the co-variance of the entity with the vertical wind speed component:

$$u_* = -\frac{\overline{u'w'}}{u_*} \qquad \text{eq 6}$$

$$\chi_* = -\frac{\overline{w'\chi'}}{u_*} \qquad \text{eq 7}$$

$$\theta_* = -\frac{\overline{w'\theta_v'}}{u_*} \qquad \text{eq 8}$$

Where w' and χ' are the fluctuation of vertical velocity and concentration of a pollutant, respectively. θ_v' is the fluctuating component of the virtual potential temperature, i.e. the temperature an air parcel would have if it was adiabatically transferred to a standard pressure of 1000 hPa and dried. u_* is called eddy velocity and is a measure for how fast horizontal momentum is transferred vertically onto the surface. The vertical fluxes of momentum (or shear stress per horizontal unit area), τ, sensible and latent heat (H and λE) and matter of concentration χ (F_χ) are defined as:

$$\tau = -\rho\overline{u'w'} \qquad \text{eq 9}$$

$$H = \rho c_p \overline{w'\theta'} \qquad \text{eq 10}$$

$$\lambda E = \lambda \overline{w'e'} \qquad \text{eq 11}$$

$$F_\chi = \overline{w'\chi'} \qquad \text{eq 12}$$

respectively. Here λ is the latent heat of evaporation of water, c_p is the specific heat capacity of air at constant pressure and θ' and e' are the variations of potential temperature and water vapour pressure, respectively. Time averaging of equation 9 and substituting in the definition of the eddy velocity (equation 6) leads to a further expression for the shear stress τ:

$$\tau = \rho u_* u_* \qquad \text{eq 13}$$

Equivalent expressions can be obtained for the other fluxes.

2.4 Definition of fluxes according to gradient methods - the constant flux assumption

As mentioned before a layer forms over a homogeneous surface in which the flux of heat and unreactive entrained entities is assumed to be constant with height. As the process of turbulent transport resembles that of Brownian diffusion (see Monteith and Unsworth, 1990) Fix's law can be applied replacing the Brownian diffusivity, D_χ, by an eddy diffusivity, K_χ, and the flux at a fixed height assumed to be proportional and opposite to the concentration gradient. Unlike D_χ K_χ itself is a function of height. The following equation are the analogues to the flux equations of the covariance method (equations 9 to 12).

$$\tau = -\rho K_M \frac{\partial \bar{u}}{\partial z} \qquad \text{eq 14}$$

$$H = -\rho c_p K_H \frac{\partial T}{\partial z} \qquad \text{eq 15}$$

$$\lambda E = -\lambda K_E \frac{\partial e}{\partial z} \qquad \text{eq 16}$$

$$F_\chi = -K_\chi \frac{\partial \chi}{\partial z} \qquad \text{eq 17}$$

Here the K_i represent the eddy diffusivities of momentum, latent and sensible heat and matter. Although scaling parameters like ρ in equation 14 have been taken out of the gradient the validity of their independence of height needs to be checked for the individual situation. Heavy, slow depositing particles may build up a density gradient at least. A more detailed analysis of the occurring forces for the deposition of matter would lead to:

$$F_\chi = -(K_\chi + D_\chi)\frac{\partial \chi}{\partial z} + v_{g_\chi}\chi \qquad \text{eq 18}$$

as Brownian diffusion and gravitational settling, with the settling velocity v_g, take place at the same time. Whereas the molecular diffusivity, D_χ, is always several orders of magnitude smaller than K_χ the drag force leading to a terminal settling velocity, v_g, cannot be neglected for heavy particles (see section 2.6.5).

Equation 3 can be transformed to yield a gradient expression for u_*:

$$u_* = \frac{\kappa(z-d)}{\Phi_M}\frac{\partial \bar{u}}{\partial z}, \qquad \text{eq 19}$$

this expression should be expected to be consistent with the definition of u_* as the root of the co-variance of vertical and horizontal wind component (equation 6). If an air parcel is lifted by an eddy by the height z' it experiences a change in wind speed given by the change in the overall background wind profile as:

$$u' = \frac{\partial \bar{u}}{\partial z} z' \qquad \text{eq 20}$$

If there are no other external forces the vertical fluctuation w' is proportional to the horizontal u' with a factor of proportionality depending on the stability class (w'=cu'). Thus w' can be substituted in equation 20 to yield

$$w' = c\left|\frac{\partial \bar{u}}{\partial z}\right| z' \qquad \text{eq 21}$$

Substitution of u' and w' into equation 6 leads to

$$u_* = \sqrt{\overline{u'w'}} = \sqrt{c\overline{z'^2}}\,\frac{\partial \bar{u}}{\partial z} \qquad \text{eq 22}$$

Here $c\overline{z'^2}$ is the variance of the vertical air parcel displacement and can thus be identified with l^2, the square of the mixing length, introduced in equation 1; the expressions of u_* are consistent. Combining the gradient and the co-variance expressions for τ (equations 13 and 14) an expression for the eddy diffusivity of momentum, K_M, can be obtained:

$$K_M = \frac{\kappa^2(z-d)^2}{\Phi_M^2}\frac{\partial \bar{u}}{\partial z} = \frac{\kappa(z-d)u_*}{\Phi_M} \qquad \text{eq 23}$$

2.5 FLUX MEASUREMENT TECHNIQUES

2.5.1 Eddy correlation method

The eddy correlation method makes direct use of the co-variance approach (equations 9 to 12) by measuring instantaneous concentrations, temperature and wind speed. This technique is simple, potentially accurate, as it lacks any empiricism, and measures the true flux at a single defined height. But in order to achieve reliable results even high frequency eddies need to be sampled so that a short sampling time becomes crucial; while the highest resolvable frequency equals half of the sampling frequency. A variety of instruments for measuring wind components and temperature, ultrasonic anemometers, with a sufficient sampling rate of more than the required 5-10 Hz are available. Furthermore, equipment has been developed to measure the instantaneous concentration of some pollutants (NO_x, O_3, CO_2 or CH_4) at a sufficiently high time resolution. Attempts have been made to measure NH_3 concentrations using tuneable diode lasers (TDLs) which can be operated at high sampling rates, but have shown that it is a) difficult to generate precise air standards and that b) the spectral absorption of NH_3 is weak resulting in a detection limit as high as 1 $\mu g\ m^3$. The detection time of more sensitive techniques is still too long so that this pollutant cannot yet be measured by the eddy correlation method. This leads to major restrictions of data acquisition for the assessment of GPC models. The flux measuring method, which is generally used instead, i.e. the aerodynamic gradient method, is, strictly speaking, not applicable if GPC takes place and derives the flux at only one height, whereas the numerical models calculate the flux as a function of height. Hence ammonia flux divergence is difficult to measure and model results are difficult to compare to field data.

During the work carried out so far the eddy correlation method was used to measure the size dependent deposition fluxes of aerosols with optical particle counters.

2.5.1.1 Relaxed eddy accumulation method

The eddy accumulation method is a relatively new technique which combines the advantage of the eddy correlation method, i.e. to measure the flux at a single height, with the advantages of gradient techniques, i.e. to allow for long detection times. A sonic anemometer is used to switch high speed valves so that air can be conditionally sampled into two different reservoirs depending on the sign of the fluctuation of the vertical wind component. The air collected in the reservoirs can subsequently be analysed by any method. Recent studies have shown the flux to be proportional to the product of the standard deviation of the vertical wind speed (σ_w) and the concentration difference in the two reservoirs:

$$F_\chi = \overline{w'\chi'} = b_\chi \sigma_w \left(\overline{\chi^+} - \overline{\chi^-}\right) \qquad \text{eq 24}$$

where χ^+ and χ^- are the concentrations measured during up and downdrafts, respectively. b_χ is an empirical constant which is currently assumed to be close to 0.6 (Businger and Oncley, 1990) but seems to decrease with height (Gao, 1995).

2.5.1.2 Other related methods

Other methods of flux measurements exist, which are based on the measurement of instantaneous values of the property under consideration. Here three of them shall be briefly described as they provide a means of checking the coherence of the results obtained by the eddy correlation method itself:

1. The **standard deviation method** makes use of the fact that for all entities undergoing the same vertical transport mechanism the correlation with wind speed should be the same. This is considered true for heat and entrained gases as discussed in chapter 2.5.2.1. If R_{wH} and $R_{w\chi}$ are the correlation coefficients of heat and matter with wind speed, respectively, it follows that one flux can be obtained from the other using the standard deviations by

$$\left|F_\chi\right| = \frac{\sigma_\chi}{\sigma_H}\left|F_H\right| \qquad \text{eq 25}$$

2. The **normalised standard deviation** method relates the flux of an entrained property to its standard deviation and the eddy velocity, i.e. the flux and standard deviation of the momentum, and requires the state of stability. The relationship is given by

$$\left|F_\chi\right| = \sigma_\chi u_* f\left(\frac{z-d}{L}\right) \qquad \text{eq 26}$$

where

$$\begin{aligned} f(\varsigma) &= 1.85 \qquad \text{for } \varsigma \geq -0.31 \\ f(\varsigma) &= -1.25\varsigma \quad \text{for } \varsigma < -0.31 \end{aligned} \qquad \text{eq 27}$$

Here the stability is expressed by the Monin-Obukhov-Length (L) and the stability parameter (ς = (z-d) L^{-1}) as defined in chapter 2.5.2.1.

3. The **correlation coefficient method** is also based on the hypothesis that in the surface layer the correlation coefficients are equal whatever the parameter considered. The correlation coefficient of an entrained property with the vertical wind component ($R_{w\chi}$) only depends on the stability class varying from 0.3 in stable conditions to 0.6 in the highly unstable atmosphere. It also can be deduced from L.

$$\left|F_\chi\right| = \left|R_{w\chi}\right|\sigma_w\sigma_\chi \qquad \text{eq 28}$$

2.5.1.3 Corrections required for the eddy correlation method

1. Misalignment of the sonic anemometer

Deviation of the sonic anemometer measuring the fluctuation of the vertical wind component from the vertical results in a non-zero mean vertical wind speed and a contribution of the fluctuation of the horizontal wind components to the measurement. Assuming the true vertical mean wind speed to be zero, an assumption which becomes incorrect when strong density gradients occur (see point 2), the misalignment can be corrected for applying a rotation of the co-ordinates, which is given by Neumann and den Hartog (1985) as

$$F_\chi = \left(\overline{w'\chi'} - \overline{w'}\,\overline{\chi'}\right)\cos\theta - \left(\overline{u'\chi'} - \overline{u'}\,\overline{\chi'}\right)\sin\theta\cos\nu - \left(\overline{v'\chi'} - \overline{v'}\,\overline{\chi'}\right)\sin\theta\sin\nu$$

$$\nu = \arctan\left(\frac{\overline{v}}{\overline{u}}\right); \qquad \theta = \arctan\left(\frac{\overline{w}}{\sqrt{u^2+v^2}}\right)$$

2. Density gradients:

However, $\overline{w}$ can be nonzero as a consequence of density gradients due to heat or water vapour fluxes. Webb *et al.* (1980) give the correction as

$$F = F_{raw} + \frac{\rho_\chi}{\rho_a}\left(\frac{\mu E}{1+\mu\sigma} + \frac{H}{c_p T}\right) \qquad \text{eq 29}$$

where ρ_χ, ρ_a are the densities of the tracer and dry air, respectively, μ identifies the ratio of the molecular weight of dry air to that of water vapour and σ the ratio of the densities of water vapour and air. This correction has to be applied if mass fluxes and not volume mixing ratio fluxes are calculated and becomes more significant the smaller the flux and the bigger the concentration of a tracer. This correction is not limited to eddy correlation. Whereas Sutton (1990) estimated the effect on NH_3 gradient measurements to be small, as NH_3 is a relatively light gas forming large gradients, it can become significant for fluxes of particles, which are heavy and deposit slowly.

3. Signal loss due to sensor response times

High sensor response times and low sampling frequencies might lead to fast eddies not being resolved. This effect becomes particularly important when fluxes are measured close to the canopy where the mean eddy size is small (see equation 1 and Figure 25) so that fast fluctuations significantly contribute to the total flux. In this case the flux can be underestimated if the measuring instrument acts as a low pass or an additional low pass is used. Otherwise, unresolved frequencies are folded back and detected as an apparent increased contribution of the highest still resolvable frequencies (aliasing). Whereas the first effect can be corrected for, the influence of the latter cannot be estimated afterwards. Fourier data series analysis is required as to compare power spectra and co-spectra of vertical wind component and tracer under consideration against spectra of fluxes assumed

to be sampled at a sufficiently high frequency, i.e. the heatflux, and to correct for sensor deficiencies.

4. **Contamination by low frequency noise:**

Aliasing can also occur at the low frequency end of the spectrum. Power spectra, of particle fluxes measurements in particular, show high contributions of low frequencies which do not refer to eddies contributing to vertical transport but horizontal transport mechanisms (e.g. gravity waves). Again these artefacts have to be estimated by time series analysis and high pass filtering might have to be applied. Lamaud *et al.* (1994) found frequencies of up to 0.01 Hz to be associated with horizontal particle fluxes and filtering corrected their flux measurements by about 50%.

2.5.2 Gradient methods

2.5.2.1 The aerodynamic gradient method

The aerodynamic gradient method makes use of the fluxe-gradient relationship given by equations 14 to 17. Once the stability correction has been found according to equation 23 the flux can be calculated from concentration gradient measurements. However, as concentration gradient and eddy diffusivity are non-linear functions of height many measuring points would be necessary to obtain a sufficiently accurate result. It is therefore desirable to reduce the problem to log-linear gradients:

Analogously to momentum a stability correction function, Φ_χ, for matter can be defined and a gradient expression for the other scaling parameter, e.g. χ_* (equation 7), can be obtained:

$$\chi_* = \frac{\kappa(z-d)}{\Phi_\chi}\frac{\partial\chi}{\partial z} \qquad \text{eq 30}$$

These expressions allow to formulate the flux in analogy to the eddy correlation method, but using eddy parameters which can be found from gradient measurements:

$$F_\chi = u_*\chi_* \qquad \text{eq 31}$$

The gradient expressions for the scaling parameters can be integrated and thus transformed into log-linear expressions. If we consider the stability function (Φ) to be height independent, for u_* equation 3 is re-obtained whereas $\chi(z)$ can be derived as:

$$\chi(z) = \frac{\chi_*}{\kappa}\ln\left(\frac{z-d}{z_\chi}\right)\Phi_H \qquad \text{eq 32}$$

Here z_χ is the notional height at which the concentration would be expected to be zero. Integration of equations 3 and 32 wrt. ln(z-d) rather than z results in:

$$\frac{\partial \bar{u}}{\partial \ln\{z-d\}} = \frac{u_*}{\kappa}\Phi_M$$
$$\frac{\partial \chi}{\partial \ln\{z-d\}} = \frac{\chi_*}{\kappa}\Phi_H \qquad \text{eq 33}$$

Substituting the eddy parameters into the flux equation 31 gives an expression for the flux containing gradients of log-linear plots:

$$F_\chi = \kappa^2 \frac{\partial \bar{u}}{\partial \ln\{z-d\}} \frac{\partial \chi}{\partial \ln\{z-d\}} (\Phi_M \Phi_H)^{-1} \qquad \text{eq. 34}$$

The term $f=(\Phi_M\Phi_H)^{-1}$ is called the stability factor (Thom, 1975).

Stability correction and integration

The stability function needs to be related either to the Richardson's number or the Monin-Obukhov-Length. Like the flux the Richardson's number can be expressed in terms of log-linear slopes rather than slopes of curves. To achieve this the gradients in equation 4 are to be replaced by the eddy parameters using the appropriate equations of the form of equation 23. The introduced eddy parameter can again be substituted by the log-linear expressions (equation 33).

$$Ri(z) = \frac{z-d}{g} \frac{\partial T}{\partial \ln(z-d)} \left(\frac{\partial \bar{u}}{\partial \ln(z-d)} \right)^{-2} \qquad \text{eq 35}$$

Here the effect of atmospheric stability has been neglected. Experiments have shown that in good approximation:

$$\Phi_M = \Phi_H = \Phi_\chi = \Phi_E \quad \textit{for stable}$$
$$\Phi_M \neq \Phi_H = \Phi_\chi = \Phi_E \quad \textit{for unstable} \qquad \text{eq 36}$$

conditions (Businger, 1966).

Consequently, the same equalities and inequalities apply to the eddy diffusivities. As the functions for all entrained entities and heat seem to be the same, only the index H is used throughout the rest of the text. Since the common transport mechanism is a fundamental presumption for the applicability of the atmospheric gradient method this technique is also called *similarity theory*.

Replacing the gradients in equation 4 by both the combination of equations 23 and 15 and equation 22 leads to an expression of Ri in terms of the stability functions:

$$Ri(z) = -\kappa \frac{g}{T} \frac{H}{\rho c_p} \frac{z-d}{u_*^3} \frac{\Phi_H}{\Phi_M^2} \qquad \text{eq 37}$$

so that by comparison with equation 5 a relationship between Ri and L can be obtained:

$$Ri(z) = \frac{z-d}{L}\frac{\Phi_H}{\Phi_M^2} = \varsigma\frac{\Phi_H}{\Phi_M^2} \qquad \text{eq 38}$$

where $\zeta=(z-d)/L$ is called the turbulent stability parameter. Although other semi-empirical expressions for the stability functions exist throughout the literature (e.g. Panofsky *et al.*, 1960) here the suggestion by Dyer and Hicks (1970), which was strongly supported by Paulson (1970) and has often been used since, is applied in unstable conditions. For stable conditions the method by Webb (1970) was chosen:

$$\begin{aligned} \Phi_M &= \Phi_H = (1+5.2\varsigma) \quad \textit{for stable,} \\ \Phi_M^2 &= \Phi_H = (1-16\varsigma)^{-1/2} \quad \textit{for unstable} \end{aligned} \qquad \text{eq 39}$$

conditions. These equations show that the stability correction is indeed a function of height and that therefore the treatment as a constant during the integration of the wind profile can only be regarded as a first approximation. The following expressions for the turbulent stability parameter and the relationship between Ri and L can obtained:

$$\begin{aligned} \varsigma &= \frac{z-d}{L} = \frac{Ri}{1-5.2Ri} \quad \textit{for stable} \\ \varsigma &= \frac{z-d}{L} \approx Ri \quad \textit{for unstable} \end{aligned} \qquad \text{eq 40}$$

conditions.

Although most authors seem to use the functions in relationship to the height dependent Richardson number the constant Monin-Obukhov stability length appears to be the more practical quantity (Sutton, 1990).

In the stable case the integration over the height independent stability function is straightforward:

$$\begin{aligned} d\bar{u} &= \frac{u_*}{\kappa(z-d)}\Phi_M dz = \frac{u_*}{\kappa(z-d)}(1+5.2\varsigma)dz \\ \overline{u(z)} &= \frac{u_*}{\kappa}\int_{z_0+d}^{z}\left(\frac{1}{z-d}+\frac{5.2}{L}\right)\partial z' = \frac{u_*}{\kappa}\left[\ln\left(\frac{z-d}{z_0}\right)+5.2\varsigma\right] \end{aligned} \qquad \text{eq 41}$$

This result might be re-arranged as to show that the correction results in re-scaling of the height axis (note that the last term is constant for a given micrometeorological situation):

$$\begin{aligned} u(z) &= \frac{u_*}{\kappa}\left[\ln(z-d)+5.2\varsigma\right]-\frac{u_*}{\kappa}\ln(z_0) \\ \chi(z) &= \frac{\chi_*}{\kappa}\left[\ln(z-d)+5.2\varsigma\right]-\frac{\chi_*}{\kappa}\ln(z_0') \end{aligned} \qquad \text{for stable conditions} \qquad \text{eq 42}$$

where z'_o indicates the notional height, at which the log-linear plot of the concentration meets the height axis, i.e. the mean height, at which the tracer χ is absorbed. Panofsky (1963) was the first to suggest the introduction of integrated stability functions, Ψ_M and Ψ_H, in the unstable situation because the integral cannot be solved analytically. These functions are defined by

$$\Psi_M(\varsigma) \equiv \int_0^{z/L} \frac{1-\Phi_M(\varsigma)}{\varsigma} \partial\varsigma \qquad \text{eq 43}$$

and thus the integration can partially be carried out to obtain

$$u(z) = \frac{u_*}{\kappa}\left[\ln\left(\frac{z-d}{z_0}\right) - \Psi_M(\varsigma)\right]$$

$$= \frac{u_*}{\kappa}\left[\ln(z-d) - \Psi_M(\varsigma)\right] - \frac{u_*}{\kappa}\ln(z_0) \qquad \text{for unstable conditions} \qquad \text{eq 44}$$

$$\chi(z) = \frac{\chi_*}{\kappa}\left[\ln(z-d) - \Psi_H(\varsigma)\right] - \frac{\chi_*}{\kappa}\ln(z'_0)$$

Dyer and Hicks (1970) calculated and tabulated distinct values of the integrated stability function based on measurement data and showed that this approach was valid up to an stability of Ri(1 m) = 1 which covers most of the environmental situations. In addition, Paulson (1970) provided analytical expressions of the form

$$\Psi_M(\varsigma) = 2\ln\left(\frac{1+x}{2}\right) + \ln\left(\frac{1+x^2}{2}\right) - 2\tan^{-1}(x) + \frac{\pi}{2}$$

$$\Psi_H(\varsigma) = 2\ln\left(\frac{1+x^2}{2}\right) \qquad \text{eq 45}$$

$$\text{with } x = (1-16\varsigma)^{1/4}$$

Practical considerations:

Equipped with the basic theoretical concept of the aerodynamic gradient method, it seems sensible to summarise a recipe how to proceed step by step:

1. The wind profile is to be measured under neutral conditions in order to obtain the zero plain displacement, d. This is done by plotting $\bar{u}$ versus ln(z-δ) where δ is to be varied until the plot approaches a straight line. (The curvature of the plot is positive if d is chosen too small, negative if the d used is too large.) This can be done either by best fit algorithms or by eyesight. The neutrality prevents that instability influences bend the plot at the same time. For simplicity reasons d must be assumed not to change with stability class although this is not completely correct.
2. z_o can be obtained as the distance of the intersection of the interpolated log-linear graph of the wind speed with the height axis from d.

3. A problem arises as Ri is to be calculated from the slopes of temperature and wind speed whereas the slopes need to be corrected according to the stability using Ri. This dilemma can be overcome using an iterative algorithm. However, neglecting stability effects for the calculation of Ri as a second order correction, the slopes of the graphs $\partial T/\partial \ln(z-d)$ and $\partial u/\partial \ln(z-d)$ are expected to give a value at a reference height, z_r (e.g. 1m), that is accurate enough if the linear regression uses an equal number of measuring points below and above z_r.
4. Now the approximate $Ri(z_r-d)$ can be calculated using equation 38 and thus the constant L according to equation 40.
5. For non-neutral conditions the values of the integrated stability functions are now obtainable and so are the values of the stability functions themselves.
6. The eddy parameter u_* and χ_* and thus the flux can now be calculated.

2.5.2.2 The energy balance method

The energy balance or bowen ratio method makes use of the conservation of the incoming heat flux. The energy balance at the ground surface is given by (Monteith and Unsworth, 1990):

$$R_n = H + \lambda E + D + G + J + \mu A \qquad \text{eq 46}$$

Here the vertical net radiation R_n is divided into the

H: vertical sensible heat flux,
λE: vertical latent heat flux,
D: net rate of energy which is removed horizontally by advection,
G: heat flux into the ground,
J: storage of energy in the ground and
μA: biochemical storage of energy.

All flux rates are regarded as positive if directed upwards and are of the dimension W m^{-2}.

In daytime conditions the vertical fluxes are the dominant terms in equation 47 so that the energy balance is given by:

$$R_n - G \approx H + \lambda E \qquad \text{eq 47}$$

In terms of a gradient method the sensible and latent heat flux are given by the equations 15 and 16, respectively. Combination leads to

$$R_n - G = -K_H\left(\rho c_p \frac{\partial T}{\partial z} + \lambda \frac{\partial e}{\partial z}\right) \qquad \text{eq 48}$$

Thus, measuring the gradients of temperature and water vapour contents, the eddy diffusivity can be found from the net radiation and the soil heat flux and then used in equation 17 to calculate the flux. The bowen ratio method is to be favoured over the aerodynamic gradient method if the wind speed is too small to allow reasonable measurements of the wind profile or if large stability corrections have to be applied. On the other hand it leads to poor results when the heat flux is small, e.g. during night time conditions. Therefore it does not allow diurnal measurements.

It is convenient to introduce the ratio of sensible to latent heat flux as the bowen ratio $\beta=H/\lambda E$. Given the equality of K_H and $K_{\lambda E}$ as discussed above it follows that:

$$\beta = \frac{\rho c_p}{\lambda}\frac{\partial T}{\partial e} \qquad \text{eq 49}$$

2.5.2.3 The mass balance method

Mass balance methods (Denmead, 1983, 1995) can be applied to measure plumes downwind of high emission areas of an extension of the order of 10 m. They derive the vertical emission flux from measurements of the horizontal flux across a vertical plane. From the law of mass conservation the flux into the atmosphere is given by

$$\begin{aligned} F_\chi &= \frac{1}{x}\int_0^z \overline{u(z)\left[\chi_g(z)-\chi_b(z)\right]}dz \\ &= \frac{1}{x}\int_0^z \left[\overline{u(z)}\;\overline{\chi_g(z)}-\overline{u(z)}\;\overline{\chi_b(z)}+u'(z)\chi_g'(z)\right]dz \end{aligned} \qquad \text{eq 50}$$

where x represents the width of the emission region along the horizontal mean wind direction and z denotes the upper boundary of the emission cloud. χ_g and χ_b are the concentration of the tracer downwind and the background concentration upwind of the emission area, respectively. Here the fluctuation of the background concentrations (χ_b') vanishes by definition. Whereas it is easy to measure the mean wind speed and mean concentration with height the last, co-variance, term need not be measured but can be corrected for assuming it accounts for about 15 % of the convective flux (Denmead, 1995). Thus the mass balance method requires the measurement of mean wind speed and mean concentration of the entrained property under consideration up to a height where the concentrations are not modified by the emission patch anymore, which is assumed to be about $z = 0.1\ x$ but depends strongly on the thermal stability. This method does not require such an extensive homogeneous surface and atmospheric condition as gradient methods, nor does the gas concentration need to be measured that accurately. However, in return it does not represent the exchange with a large area and its use is restricted to the measurements of emissions from spacially limited sources.

2.5.3 Chamber and throughfall measurements

The restriction of the representation of a small rather than a large area applies even stronger to gas chamber measurements which in addition are understood to modify the ecosystem and its meteorological conditions. A small surface area is enclosed by a chamber through which air is drawn. Measuring the ammonia concentrations of the air entering and leaving the chamber the atmosphere surface exchange can be calculated. Chamber measurements can be used to estimate the contribution of spatially small sources or to measure the exchange at the ground below the plant canopy. The magnitude of dry deposition can also be estimated by the difference of measured total and wet deposition.

2.6 THE RESISTANCE ANALOGUE OF POLLUTANT EXCHANGE

In order to parameterise the atmosphere surface exchange and to examine fluxes within the plant community it is convenient to introduce atmospheric resistances. In analogy to the electric resistance, which is defined as the potential drop ($V=\varphi_2-\varphi_1$) divided by the current (I), the diffusive resistance for momentum (R_M) can generally be defined as the concentration difference divided by the flux:

$$R_{el} = \frac{V}{I} = \frac{\varphi_2 - \varphi_1}{I} \qquad \text{eq 51}$$

$$R_M(z_1, z_2) = \frac{\chi(z_1) - \chi(z_2)}{\tau} \qquad \text{eq 52}$$

The dimensions of R_M are s m^{-1} thus it is the inverse of a characteristic velocity, called the deposition velocity (V_d), which is proportional to u, the factor of proportionality being the momentum transfer coefficient (C_M). C_M denotes the overall effectiveness with which vertically distributed elements of the community extract momentum. In addition to this Thom (1975) shows that R_M can also be written as the integral over the reciprocal of the eddy diffusivity between the heights.

$$R_M(z, z_o) = R_M(z) = \frac{1}{v_d(z)} = \frac{1}{\bar{u}(z) C_M} = \int_{z_0}^{z} K_H(z')^{-1} dz' \qquad \text{eq 53}$$

R_M is also given by the ratio of the mass flux of an incoming incident flow ($\rho\bar{u}$) and the drag force per unit area (F A^{-1}) or shear stress, which can be identified with the vertical momentum flux, τ, if the area is taken as horizontal. τ on the other hand can be substituted by the expression of equation 23. Thus the following dependencies are obtained:

$$R_M(z) = \rho\bar{u}(z)\frac{A}{F} = \frac{\rho\bar{u}(z)}{\tau} = \frac{\bar{u}(z)}{u_*^2} = \frac{\left(\ln[(z-d)/z_0]\right)^2}{\kappa^2 \bar{u}(z)} \qquad \text{eq 54}$$

It follows that R_M is smaller with rougher surfaces (high z_0) and large wind speeds, u.

A similar approach can be used for heat and entrained properties. Since they are not deposited at z_0 but have to penetrate the viscous sub-layer, additional resistances describing this diffusive process and the exchange with the canopy itself have to be added. The total effective diffusion resistance R_t is usually divided into three independent resistances in series, i.e. the aerodynamic resistance (R_a), the laminar boundary layer resistance (R_b), and the canopy resistance (R_c). The deposition velocity at a given height z is given by the reciprocal of $R_t(z)$ and, if the concentration at the surface can be assumed to be zero, by the flux divided by the concentration at height z. A minus sign has to be introduced as the flux is taken as positive for emission.

$$v_d(z) = \frac{1}{R_t(z)} = \frac{1}{R_a(z) + R_b + R_c} = -\frac{F_\chi}{\chi(z)} \qquad \text{eq 55}$$

From this equation in becomes obvious that the introduction of the concept of a deposition velocity and atmospheric resistances is only sensible if the flux remains constant with height. Thus this concept cannot be used for the analysis of gas-to-particle conversion processes.

2.6.1 The aerodynamic resistance

Like the atmospheric resistance for momentum, R_M, the aerodynamic resistance, R_a, describes the rate of transport by turbulent diffusion within the surface layer above the top of the laminar sub-layer, z_0. In stable and neutral conditions the result from equation 54 is not only valid for the transfer of momentum but also of entrained properties:

$$R_a(z) = \frac{\bar{u}\{z-d\}}{u_*^2} = \frac{\rho\bar{u}\{z-d\}}{\tau} \qquad \text{, for stable and neutral} \qquad \text{eq 56}$$

For unstable conditions, however, the integrated stability functions (eq. 45) must be used again in analogy to the use in equation 44.

$$R_a(z) = \frac{\left[\ln\left(\frac{z-d}{z_0}\right) - \Psi_M(\varsigma)\right]\left[\ln\left(\frac{z-d}{z_0}\right) - \Psi_H(\varsigma)\right]}{\kappa^2\bar{u}\{z\}} \qquad \text{, unstable cond} \qquad \text{eq 57}$$

By substitution with u_* which already contains the stability correction for momentum, we obtain:

$$R_a(z) = \frac{\ln\left(\frac{z-d}{z_0}\right) - \Psi_H(\varsigma)}{\kappa u_*} = \frac{\bar{u}(z)}{u_*^2} - \frac{\Psi_H(\varsigma) - \Psi_M(\varsigma)}{\kappa u_*} \qquad \text{eq 58}$$

The second equality is derived by Garland (1977) and also includes the neutral and stable case in which the second term vanishes.

2.6.2 Laminar boundary layer resistance

As briefly mentioned in section 2.1, all roughness elements at the surface are surrounded by a very shallow quasi-laminar layer. Here the transport of entrained entities and heat is driven by molecular or Brownian rather than turbulent diffusion. This mechanism is orders of magnitude slower and R_b can be of great importance despite of the small transport distance it accounts for. Whereas the bottom height of the turbulent surface layer, z_o, can be found according to section 2.5.2.1, the height of the bottom of the viscous sub-layer, z_o', is unknown. Although an analogue form to equation 58 can be found it is of no direct use:

$$R_b = \frac{\ln\left(\frac{z_0}{z_0'}\right) - \Psi_H\left(\frac{z_0}{L}\right)}{\kappa u_*} \qquad \text{eq 59}$$

Unfortunately, only semi-empirical approaches exist for how to determine R_b so that a great error may be induced if R_a is small, like in very unstable conditions or over very rough surfaces, e.g. forests, or if measurements are carried out near the mean plant height, h.

Owen and Thomson (1963) suggested the introduction of a sub-layer Stanton number (B) in order to calculate R_b:

$$R_b = \left(Bu_*\right)^{-1} \qquad \text{eq 60}$$

For vegetation Garland (1977) found that B^{-1} can be described by

$$B^{-1} = 1.45\,\mathrm{Re}_*^{0.24}\,Sc^{0.8} \qquad \text{eq 61}$$

where Re_* is the turbulent Reynolds number given as $Re_* =$ frictional/inertial force $= z_0 u_*/\nu$, ν being the kinematic viscosity of air, and Sc is the Schmidt number defined by $Sc=\nu/D$. This formula is often used in literature, e.g. by Sutton *et al.* (1993), Coe (1993). B is therefore a function of u_* and D, and thus different for different species. Hargreaves and Atkins (1987) revise literature values for D_{NH3} and use a value of $2.09*10^{-5}$ m^2 s^{-1} for NH_3. Seinfeld (1986) gives a Brownian diffusivity for sub-micron particles such as NH_4^+-aerosol of the order

$$3*10^{-11}m^2s^{-1} < D_{NH_4^+} < 7*10^{-10}m^2s^{-1}$$

However, as additional settling processes effect the speed aerosol particles overcome the laminar sub-layer, equation 60 underestimates the deposition velocity of aerosol. A more detailed description of the settling processes of particles is given in section 2.6.5.

2.6.3 Canopy resistance

Unlike the aerodynamic and the boundary layer resistances the canopy resistance does not depend on the micrometeorological situation but is determined by the exchange of the tracer by the soil and vegetation with the atmosphere. No uniform description can be found in literature for what contributes to R_c. *The canopy resistance can be modelled by a whole network of serial and parallel independent* resistances describing the uptake resistances of plant and soil.

Differences in R_c in day and night time conditions have led to the general assumption that uptake of gases like SO_2 or NO_x is governed by the pores of the leaves, the stomata, which are closed during the night or under heavy rain stress (Fowler and Unsworth, 1979; Coe, 1993) (R_s). Another transmission path is formed by deposition directly onto the leaf surfaces and uptake by the cuticulae (R_w). A wet leaf surface can enhance the uptake and store a certain quantity of gas. It might therefore be adequate to include the surface wetness as done by Kramm and Dlugi (1994) or to introduce a capacitance as demonstrated by Sutton *et al.* (1995) as most of the gas might be released again when the leaf dries. Moreover, an internal resistance, R_{int}, in series with R_s has often been introduced in order to describe the mesophyll transfer within the sub-stomatal cavity. Besides the foliage uptake, *the soil also contributes to the* deposition and a R_{soil} might be introduced. Again, the wetness might have an influence, which might be able to be quantified. Obviously, the system can be made infinitely complicated, e.g. by the introduction of several foliage layers connected by additional boundary layer resistances, and estimations need to be done as for *how to keep the system as simple and still as precise as* possible. Figure 3 gives an example for a simple resistance model.

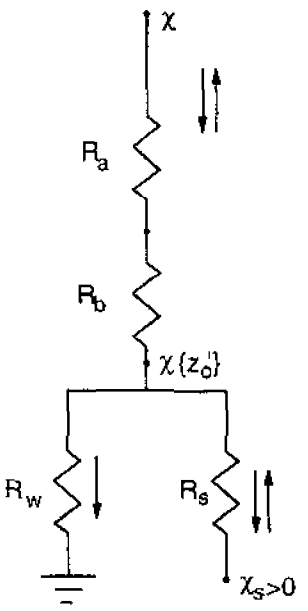

Figure 3: Resistance model after Sutton *et al.* (1995) including parallel deposition to leaf cuticles, R_w, and through stomata, R_s with a stomatal compensation point, $\chi(z_o')$.

When stomatal uptake has been identified as the mean contribution the canopy resistance, $R_c \approx R_s$, can be estimated by consideration of the R_s for latent heat transfer, which is defined as proportional to the difference in the water vapour pressure between the considered heights divided by the latent heat flux. As the latter originates from the intercellular spaces

the pressure at the lower level is given as the saturation value for the average ambient temperature at height z_0', $T(z_0')$, i.e. as $e_{sat}(T(z_0'))$, whereas at the upper level the water vapour pressure is a function of height rather than temperature:

$$R_s \approx \frac{\rho\lambda\varepsilon}{p}\,\frac{e_{sat}\left\{T\left(z_0'\right)\right\}-e\left(z_0'\right)}{\lambda E} \qquad \text{eq 62}$$

Thus, once the mean surface temperature and the water vapour pressure at the mean height of the uptaking elements has been found, the stomatal resistance can be estimated (Monteith and Unsworth, 1990). Other expressions for the stomatal resistance using meteorological and plant physiological data have been derived by Jarvis (1976) and Wesely (1989).

2.6.4 Surface concentrations

As the parameterisation of all plant physiological and meteorological Whereas the bottom up or inferential approach seems to be difficult R_c can easily be calculated if the total effective diffusion resistance R_t (or V_d) is known.

$$R_c = R_T - \left(R_a + R_b\right) = -\frac{\chi(z)}{F_\chi} - \left(R_a + R_b\right) \qquad \text{eq 63}$$

Instead of regarding R_c as another resistance it can be considered as caused by a non-zero NH_3 concentration at the bottom of the viscous sublayer, $\chi(z_0')$, which effectively diminishes the concentration difference driving the flux. This concept can account for the fact that in the case of emission the surface concentration can surely not expected to be zero. In this model the surface concentration could be obtained by

$$\chi(z_0') = \chi(z) + F_\chi\left(R_a(z) + R_b\right) \qquad \text{eq 64}$$

If the concentration profile has been corrected with respect to the stability conditions as described in section 2.5.2.1 the log-linear plot can be extrapolated to the height z_0', which might also be found by comparison of equations 59 and 60 as:

$$z_o' = z_0 \exp\left\{-\frac{\kappa}{B} - \Psi_H\left(\frac{z_0}{L}\right)\right\} \qquad \text{eq 65}$$

However, based on the semi-empirical derivation of R_b this relation must be treated with care.

In the case of NH_3 emission equation 63 would lead to a negative canopy resistance. Although this concept is mathematically coherent it does not reflect natural processes. A combination of describing the difference between R_t and the sum (R_a+R_b) by both an additional canopy resistance (R_c) and a

surface concentration at another notional height, z_o'', i.e. $\chi(z_o'')$, might be the physiologically most appropriate expression. Concentrating on stomatal uptake, R_c would consist only of R_s and $\chi(z_o'')$ would describe the NH_3 air concentration given by the partial pressure of gaseous NH_3 above the water film in the mesophyllic cell walls (apoplast). The Henry equilibrium relates the partial pressure to the apoplastic NH_4^+ concentration, which depends on the physiological state of the plant community. Methods have been developed to measure the apoplastic NH_4^+ concentration directly (e.g. Husted and Schjørring, 1995) and provide an independent means for the validation of the resistance descriptions.

Assuming the uptake is solely controlled by the stomata, $\chi(z_o'')$ could then be interpreted as a stomatal compensation point (χ_s), the air concentration at which no net exchange through the stomata takes place (e.g. Sutton *et al.*, 1995).

$$\chi_{st} = \chi\{z_0''\} = \chi\{z\} - F_\chi\left(R_a\{z\} + R_b + R_{st}\right) \qquad \text{eq 66}$$

However, even if other pathways exist alongside the stomatal exchange Sutton *et al.* (1995) suggest the introduction of a canopy compensation point ($\chi_c=\chi(z_o')$) at the height z_o' as the NH_3 air concentration at which no NH_3 net exchange with the canopy takes place. Unlike χ_s, χ_c is not determined by the physiological state of the plants alone, but also by meteorological factors as wetness, by the soil exchange and the NH_3 concentration within the canopy itself.

2.6.5 Estimating the deposition velocity of particles

Because of their different nature (size, density, inhomogeneity) aerosols undergo quite different dry deposition processes than gases. Here the main mechanisms governing the deposition velocity of particles, and in particular the transport through the quasi laminar sub-layer, are discussed. The first two mechanisms are controlled by the characteristics of the aerosol itself, whereas the other three largely depend on the properties of the collecting surface.

1. Brownian diffusion:

   Brownian diffusion is the domination process by which gases overcome the viscous sub-layer. Their transport is due to molecular bombardment. Very small aerosol particles behave very much like molecules whereas increasing inertia with increasing particle size limits this mechanism. A formula for the diffusivity of particles, D, can be found in Seinfeld (1986):

$$D = \frac{kTC_c}{3\pi\mu D_p} \qquad \text{eq 67}$$

   k being the Boltzman constant, T the temperature, μ the viscosity of air and C_c the Cunningham slip flow correction. C_c is close to unity for particles with diameters smaller than the mean free path length of air ($D_p > 0.065$ μm), but changes with D_p^{-1} for smaller particles; hence effectively $D \propto D_p^{-2}$ in the free molecule regime (see Figure 4) .

2. Gravitational settling:

The drag force on particles, on the other hand, increases with mass and helps penetrating the viscous sub-layer. Large particles reach a considerable settling speed, at which the friction force equals the gravitational force given by Stoke's law as:

$$V_g = \frac{\rho_p g D_p^{\,2} C_c}{18\mu} \qquad \text{eq 68}$$

where ρ_p is the particle density and g the acceleration due to gravity. Hence V_g strongly increases with the diameter, i.e. the mass of the particle.

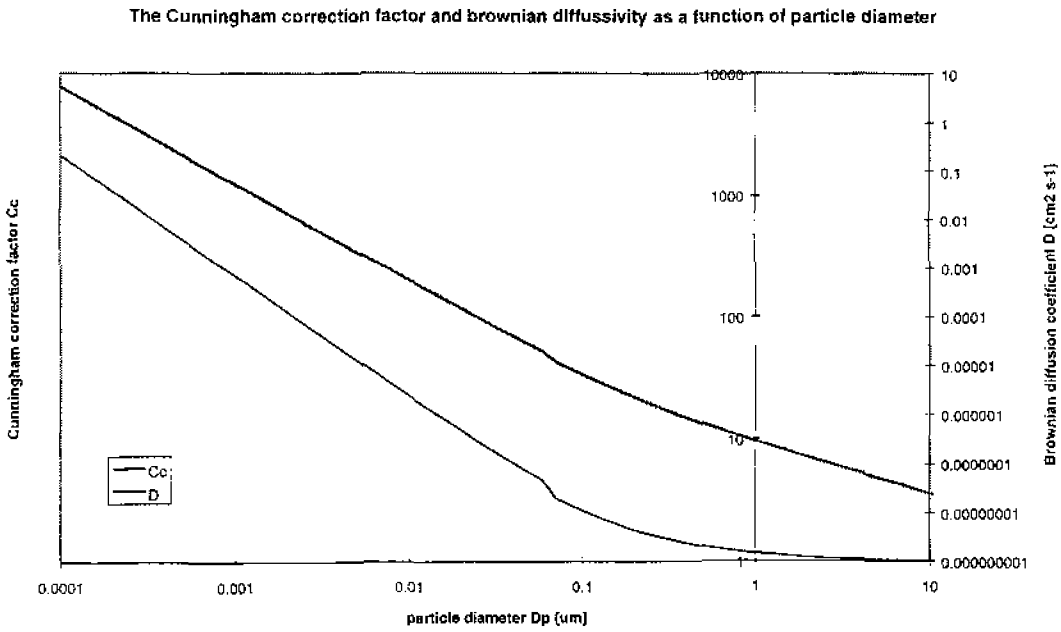

Figure 4: The Cunningham slip flow correction and the Brownian diffusivity as a function of particle diameter D_p (Seinfeld, 1986)

3. Impaction:

Impaction describes the disability of heavier particles to follow streamlines due to their inertia. As large particles are not able to follow the motion of small eddies and rapid curvature of streamlines around obstacles near the surface, this effect enhances their deposition. It describes the influence of *particle mass* on the deposition process.

4. Interception:

It occurs when the particle following the streamline around an obstacle is sufficiently large to come in contact with the obstacle and therefore deposits. It describes the influence of *particle size* on the deposition process.

5. Rebounce:

   Depending on the stickiness of the collecting surface a certain amount of particles will bounce off. This effect acts alongside the collection mechanisms 2.-4. and reduces the overall collection efficiency.

A number of different attempts of parameterizing and combining these collection processes can be found in literature. In his widely used model, Slinn (1982) derives separate collection efficiencies for Brownian diffusion, interception and impaction (E_B, E_{IN} and E_{IM}) and combines them to an overall efficiency (E) using a bounce-off factor (R):

$$\mathrm{E} = R\left(E_{IN} + E_{IM} + E_B\right) \qquad \text{eq 69}$$

The total deposition velocity is then given by

$$V_d = V_g + \frac{U_*^2}{U_{ref}}\left\{1 + \frac{U_h}{U_{ref}}\,\frac{1-\mathrm{E}}{\mathrm{E} + \left[\sqrt{\mathrm{E}}\tanh\left(\gamma\sqrt{\mathrm{E}}\right)\right]}\right\}^{-1} \qquad \text{eq 70}$$

where U_{ref} and U_h are the mean wind speeds at a reference and the canopy height, respectively, γ being a shape parameter for the concentration profile within the canopy.

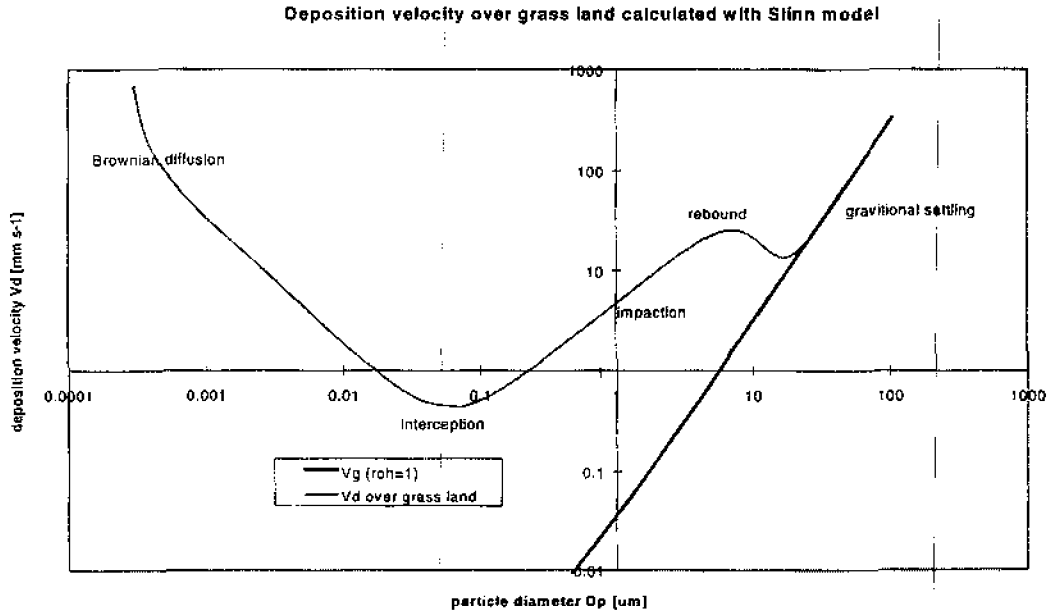

Figure 5: Particle deposition velocity for grass land after Slinn (1982).

Figure 5 shows the particle deposition over grassland according to the efficiency parameterisation of Slinn (1982). A variety of similar parameterisations exist partially taking the plant morphology in multilayer canopy models (Peters and Eiden, 1992) into account. A literature review of parameterisations based on theoretical models and measurement data can for example be found in

Gallagher *et al.* (1995). The important intermediate size region, in which most ammonium containing particles can be expected, is neither strongly effected by Brownian diffusion nor sedimentation and associated with the largest uncertainties. Although the plots show the deposition velocity to be small for particles with 0.1 $\mu m < D_p < 1$ μm field measurements have consistently shown higher deposition rates (e.g. Slinn, 1983; Hummelshøj, 1992). This indicates that the mechanisms of surface/atmosphere exchange of particles are not yet fully understood.

3. THE CHEMISTRY OF AMMONIA AND AMMONIUM AEROSOL

Ammonia reciprocates with the atmospheric acids, nitric acid (HNO_3) and hydrochloric acid (HCl), forming NH_4^+ salts. It can also be partially or fully neutralised by sulphuric acid (H_2SO_4) in a virtually irreversible two stage process:

$$NH_3 + HNO_3 \leftrightarrow NH_4NO_3 \qquad \text{R 1}$$

$$NH_3 + HCl \leftrightarrow NH_4Cl \qquad \text{R 2}$$

$$\begin{aligned} NH_3 + H_2SO_4 &\rightarrow NH_4HSO_4 \\ NH_3 + NH_4HSO_4 &\rightarrow (NH_4)_2SO_4 \end{aligned} \qquad \text{R 3}$$

Since H_2SO_4 is known to be highly reactive, it neutralises any present NH_3 instantly and thus does not travel far from its source if any atmospheric NH_3 is present. It has been suggested to include H_2SO_4 in reaction models of NH_3 by allowing all H_2SO_4 to react first and calculating the reaction rates with HNO_3 and HCl according to the remaining NH_3 concentration (Seinfeld, 1986).

3.1 THE NITRATE TRIAD

In contrast to H_2SO_4, HNO_3 forms a genuine equilibrium with NH_3 and NH_4NO_3. As it is the predominant of the three atmospheric acids under consideration, most work has been done to describe the equilibrium product of this process. The reaction rate coefficients k_1 and k_2 are introduced for both processes, sociation and dissociation:

$$NH_3 + HNO_3 \xrightarrow{k_1} NH_4NO_3 \qquad \text{R 4}$$

$$NH_4NO_3 \xrightarrow{k_2} NH_3 + HNO_3 \qquad \text{R 5}$$

These reaction rate coefficients are not well determined. However, there are expressions for the chemical time scale, i.e. the time for gas and particle phase to obtain equilibrium. Seidl *et al.* (1995) derive the expression

$$\tau_{c,\infty} = 3D\int_0^\infty \frac{m(r_p)dr_p}{\left(1+\frac{\lambda}{\alpha r_p}\right)r_p^2\rho_p} \qquad \text{eq. 71}$$

where D is the gas phase diffusion coefficient, r_p the particle radius, $m(r_p)$ the mass concentration function, λ the mean free path of gas molecules in air (0.065 μm) and α the accommodation coefficeint (0.1). Hence measurements of the size distribution of the NH_4NO_3 aerosol are necessary to estimate the chemical time scale. Unfortunately, τ cannot be directly related to the reaction rate coefficients, k_i. Nevertheless, a relationship between the two reaction rate coefficients can be yield if we introduce the equilibrium dissociation constant (k_{p,NO_3^-}) for NH_4NO_3 aerosol.

3.1.1 The dissociation constant of NH_4NO_3 aerosol

According to thermodynamic theory, the equilibrium constant is given by the product of the partial pressure of the gases above the aerosol. It can also be written in terms of the standard Gibbs free energy change for the reaction:

$$\ln(k_{p,NH_4NO_3}) = \ln(p_{NH_3} p_{HNO_3}) = -\frac{\Delta G_T^0}{RT} \qquad \text{eq 72}$$

In conditions, for which the Gibbs free energy is tabulated, the dissociation product can easily be calculated. For modelling purposes, however, it is desirable to obtain an expression as a function of temperature and relative humidity in order to account for gradients. This can be achieved by integrating the van't Hoff equation, also called *reaction isochore,*

$$\left(\frac{\partial \ln(k_p)}{\partial T}\right)_p = \frac{\Delta H^0}{RT^2} \qquad \text{eq 73}$$

yielding an expression for the dissociation product under the assumption that the temperature dependence of the specific heat capacity is negligible as:

$$\ln(k_p) = -\frac{\Delta S^0}{R} - \frac{\Delta c_p}{R} + \left\{\frac{298\Delta c_p}{R} - \frac{\Delta H^0}{R}\right\}\frac{1}{T} + \frac{\Delta c_p}{R}\ln\left(\frac{T}{298}\right) \qquad \text{eq 74}$$

where ΔS^0, Δc_p and ΔH^0 are the changes in entropy, specific heat capacity and enthalpy during the reaction, respectively; R is the universal gas constant.

This equation can readily be used to calculate the equilibrium constant for relative humidities below the relative humidity of deliquescence (RHD), i.e. for solid NH_4NO_3 aerosol. Unfortunately, considering the nature of the logarithm the dissociation constant is very sensitive to the accuracy of the thermodynamical data used. Hence equations found in literature differ considerably from each other. Stelson and Seinfeld (1982) found

$$\ln(k_{ps,NH_4NO_3}) = 84.6 - \frac{24220}{T} - 6.1\ln\left(\frac{T}{298}\right) \qquad \text{eq 75}$$

whereas Mozurkewich (1993) claims his solution

$$\ln(k_{ps,NH_4NO_3}) = 91.27 - \frac{24084}{T} - 6.025\ln\left(\frac{T}{298}\right) \qquad \text{eq 76}$$

based on reviewed thermodynamical data to be accurate within 12 %. Here k_p is given in units of ppb^2.

Aerosol formation is known to be favoured under cold and humid conditions; hence, for relative humidities above the deliquescence point the concentration of the solution of the aqueous aerosol and thus the humidity need to be considered. For a saturated solution the aqueous phase is in equilibrium with the solid, therefore the solution for aqueous aerosol must be expected to approach the solution for solid aerosol at the RHD. For more diluted solutions, however, the activity coefficients must be taken into account:

$$K_p = a\left(NH_4^+\right)a\left(NO_3^-\right)\frac{K_{p,id}}{K_{sp}} = \left(\gamma_{\pm}m\right)^2\frac{K_{p,id}}{K_{sp}} \qquad \text{eq 77}$$

where a is the activity coefficient, $K_{p,id}$ the ideal solution obtained by using equation 74 with the value of the specific heat capacity of a saturated ammonium nitrate solution, K_{sp} the solubility product constant, $\gamma_{\pm}$ the mean activity coefficient and m the molality of the NH_4NO_3 solution. Using temperature dependent expressions for $\gamma_{\pm}$ and m Mozurkewich (1993) approximates his findings by a curve described by

$$\begin{aligned} k_p &= (P_1 - P_2(1-a_w) + P_3(1-a_w)^2) \times (1-a_w)^{1.75} k_{p,id} \\ \ln(P_1) &= -135.94 + \frac{8763}{T} + 19.12\ln(T) \\ \ln(P_2) &= -122.65 + \frac{9969}{T} + 16.22\ln(T) \\ \ln(P_3) &= -182.61 + \frac{13875}{T} + 24.46\ln(T) \end{aligned} \qquad \text{eq 78}$$

Where a_w, the activity coefficient of water, itself depends on temperature. Stelson and Seinfeld (1983) use an iterative algorithm to calculate the inter-dependent values of $\gamma_{\pm}$ and m using the thermodynamic data of Hamer and Wu (1972) and Roux *et al.* (1978). Figure 6 shows the result.

3.1.2 The reaction rates

Once the equilibrium constant has been found, the relationship

$$k_{p,NH_4NO_3} = [HNO_3]_{eq}[NH_3]_{eq} \qquad \text{eq 79}$$

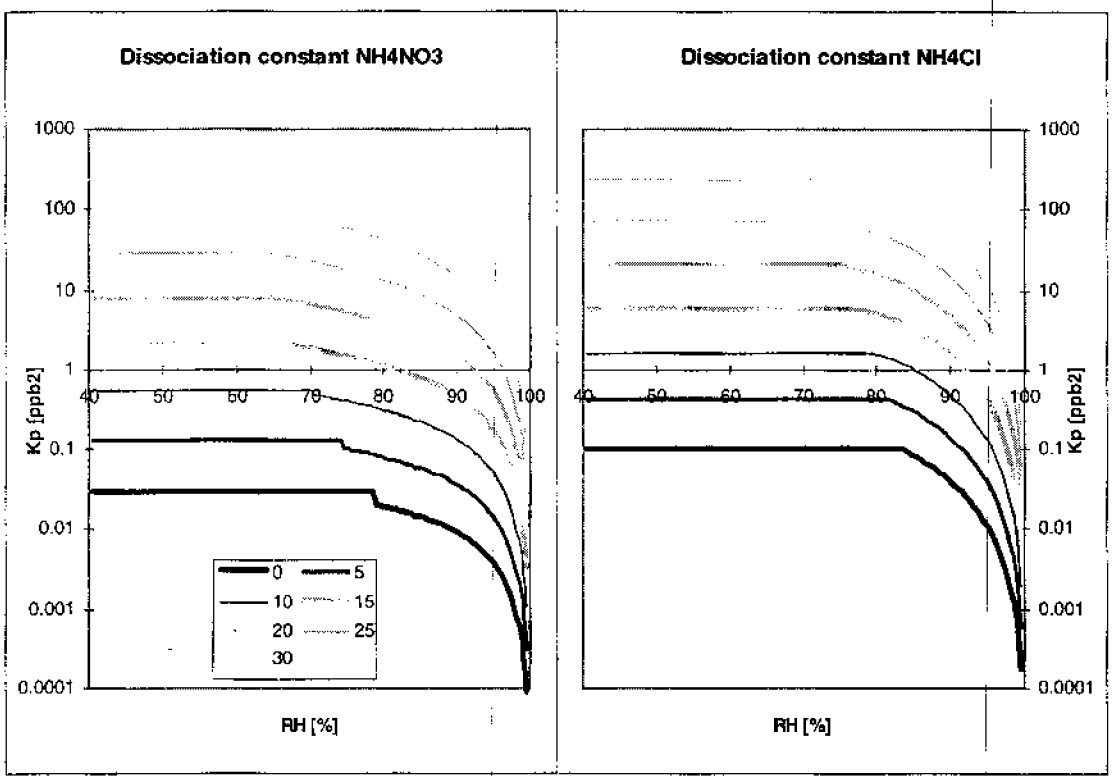

Figure 6: The dissociation constant of ammonium nitrate and ammonium chloride as a function of temperature and relative humidity according to Stelson and Seinfeld (1983) and Pio and Harrison (1987).

can be used to calculate the equilibrium concentrations. The equilibrium concentration refer to an equilibrium state which is reached if the two reaction rates

$$R_1 = k_1[NH_3][HNO_3] \qquad \text{eq 80}$$

$$R_2 = k_2[NH_4NO_3] \qquad \text{eq 81}$$

equal each other. Substitution of k_p from equation 79 into equation 80 and using $R_1=R_2$ leads to a relationship between k_1 and k_2:

$$k_2 = k_1 \frac{k_{p,NH_4NO_3}}{[NH_4NO_3]_{eq}} \qquad \text{eq 82}$$

It will be shown that the total nitrate concentration

$$TN = [HNO_3] + [NH_4NO_3] \equiv c_{g1} \qquad \text{eq 83}$$

and the total ammonia concentration

$$TA = [NH_4] + [NH_4NO_3] \equiv c_{g2} \qquad \text{eq 84}$$

and therefore the difference

$$TD = [HNO_3] - [NH_3] \equiv c_{g3}, \qquad \text{eq 85}$$

are time invariant, no matter whether equilibrium is obtained or not, and that the constant flux assumption consequently holds for these so called group concentrations. Equations 79 to 84 applied to equilibrium conditions lead to a system of three equations which can be solved for $[NH_4NO_3]_{eq}$ giving:

$$[NH_4NO_3]_{eq} = \frac{TN + TA}{2} \pm \sqrt{\frac{(TN + TA)^2}{4} - TNTA + k_p} \qquad \text{eq 86}$$

Here the +-sign cannot represent a valid solution as (TN+TA)/2 is the upper possible limit of the ammonium nitrate equilibrium concentration. The other equilibrium concentrations can easily be obtained as:

$$[HNO_3]_{eq} = TN - [NH_4NO_3]_{eq} \qquad \text{eq 87}$$

$$[NH_4]_{eq} = TA - [NH_4NO_3]_{eq} \qquad \text{eq 88}$$

3.1.3 Comparison of the dissociation constant with measurements

The theoretically obtained equilibrium product of NH_3 and HNO_3 was tested against measured data in several studies. Harrison and Pio (1983) found good agreement of their measurements, performed in north-west England under mainly high humidity conditions, with the theory presented by Stelson and Seinfeld (1983) (see Figure 6). Erisman *et al.* (1988) report good agreement for not too high relative humidities (RH < 80 %) and temperatures above 0 °C, but measured higher concentration products of the gas phase than predicted by theory for high humidities. Allen *et al.* (1989) limit the range, in which good agreement can be found, to RH < 80 % and T > 5 °C (an example of measurements at Essex, UK, is given in Figure 7).

The following explanations for the difference in the concentration products can be assumed of:

1. The inhomogeneity of the aerosol, which does not exist of only ammonium chloride or nitrate, leads to a depression of the gas phase products.
2. Meteorological situations with insufficient mixing (during the measurements often coinciding with temperatures below 5 °C) could lead to higher concentration products than expected.
3. Low temperatures might also be correlated to low concentrations leading to bigger uncertainties in the measurements.

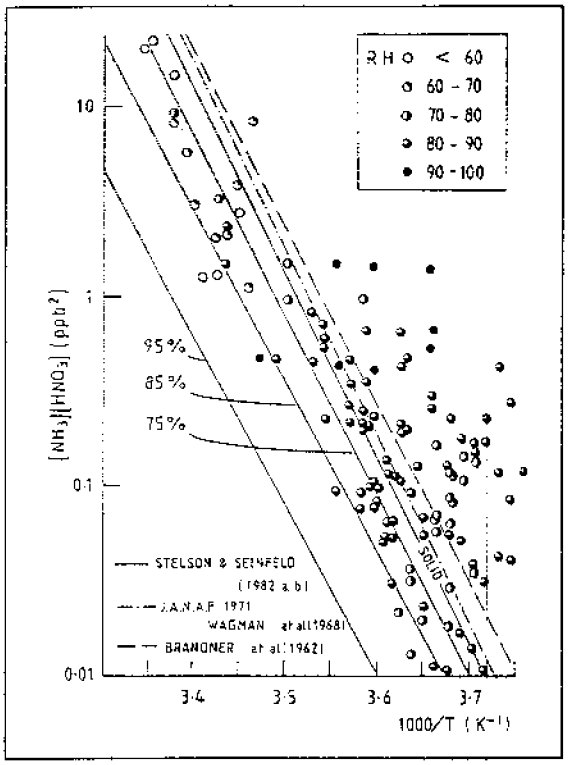

Figure 7: Concentration products of $[HNO_3][NH_3]$ as a function of temperature and relative humidity measured at Essex by Allen *et al.* (1989).

4. Local sources of NH_3 and acids, which might be higher at day-time (e.g. due to higher temperatures, stomatal activity), can lead to kinetic constraints upon the attainment of the equilibrium. In fact, modelling the chemistry of ammonia shows that equilibrium can only be obtained at one single height for each triad. Zhang *et al.* (1995) find best agreement with theoretical values for low relative humidity at about 15 °C during studies at Leende, NL. They state that in this dataset the divergence from the theoretical value (often expressed as the ratio of measured, k_m, to expected value, k_e) is neither directly related to relative humidity nor temperature, but shows a strong diurnal cycle of k_m/k_e. As this ratio seems to be correlated to changes in the NH_3 concentration, local emission and deposition of NH_3 must be assumed as the main cause for dis-equilibria.

3.2 THE CHLORIDE TRIAD

The third major inorganic atmospheric acid reacting with ammonia is hydrochloric acid (HCl). Again, under steady state conditions an equilibrium would be found. Less work has been done to establish reaction rate coefficients k_3 and k_4 or to calculate the equilibrium constant.

$$NH_3 + HCl \xrightarrow{k_3} NH_4Cl \qquad \text{R 6}$$

$$NH_4Cl \xrightarrow{k_4} NH_3 + HCl \qquad \text{R 7}$$

3.2.1 The dissociation constant of NH_4Cl

Pio and Harrison (1987a) derive the equilibrium constant for solid NH_4Cl using temperature dependent relationships for the specific heat capacities as

$$k_{p.s.,NH_4Cl} = 78.176135 + 2.2358\ln\left(\frac{T}{298}\right) - \frac{0.000213204}{T} - 0.008167T + 4.64383\times10^{-7}T^2 - 1.10475\times10^{-10}T^3 \qquad \text{eq 89}$$

which compares well with the semi empirical equation by Wagner and Neumann (1961)

$$k_{p,s,NH_4Cl} = 78.581686 + 1.812\ln\left(\frac{T}{298}\right) - \frac{0.0002138641}{T} - 7.4604\times10^{-3}T^3$$

eq 90

Using the integrated van't Hoff equation and neglecting the temperature dependence of the specific heat capacities the thermodynamic data by Wagmann *et al.* (1968) and Roux *et al.* (1978), which was also used by Stelson and Seinfeld (1983) to derive equation 75, the following expression can be obtained:

$$k_{p,s,NH_4Cl} = 78.23 + 1.812 - 2.35\ln(T) - \frac{21980}{T}. \qquad \text{eq 91}$$

Here the temperature and humidity dependence of the vapour pressure of NH_4Cl aerosol derived by Pio and Harrison (1987b) in analogue form to the formula of the equilibrium constant of NH_4NO_3 by (Stelson and Seinfeld) and was re-decoded (see Figure 6).

4. MODELLING GAS-TO-PARTICLE CONVERSION

4.1 INTRODUCTION AND EQUILIBRIUM CONSIDERATIONS

The constant flux assumption discussed in chapter 2.4 requires no atmospheric sinks or sources to be present. As soon as chemical transformations become significant this requirement is violated. Ammonia reacts with HNO_3 and HCl forming NH_4^+ salt aerosols. The chemical source and sink terms can be written as the difference of the reaction rates of sociation and dissociation:

$$Q_i = \begin{cases} -k_1[HNO_3][NH_3] + k_2[NH_4NO_3] = -k_1 c_1 c_2 + k_2 c & ,i = 1,2 \\ -Q_1 & ,i = 3 \end{cases} \qquad \text{eq 92}$$

for the nitrate triad and

$$\tilde{Q}_i = \begin{cases} -k_1[HCl][NH_3] + k_2[NH_4Cl] = -k_1 c_4 c_2 + k_2 c_5 & ,i = 2,4 \\ -\tilde{Q}_4 & ,i = 5 \end{cases} \qquad \text{eq 93}$$

for the chloride triad. Here indices have been introduced in order to simplify the equations. The index i is defined as follows: i = 1: HNO_3, 2: NH_3, 3: NH_4NO_3, 4: HCl, 5: NH_4Cl. c_i and F_i can be identified with the concentration and the flux of species i. The reaction rate coefficients are used as introduced in the reaction schemes above. From these terms it can be seen that sources and sinks would vanish were there equilibrium at all heights and vice versa. However, several facts counteract the formation of equilibria:

1. The chemical species differ in R_b, R_c and therefore V_d:

   The deposition velocities of the dry deposition for the different compounds are quite different. The aerosol experiences a large R_b due to the small molecular diffusivity. The NH_3 flux is largely determined by the canopy concentration, expressed in terms of R_c and / or $c_2(z_o)$, and can be both up- and downwards. In addition to this it has been assumed that any canopy acts as a perfect sink (R_c=0) for gaseous acid (e.g. Huebert *et al.*, 1988). As a simplified model, one can imagine parcels of the different gases not travelling alongside each other, but at different speeds or even in opposite directions and consequently having only a limited time to achieve equilibrium. Even if the chemistry of NH_3 is accounted for, models would predict height invariant fluxes if equilibrium was achieved at a reference height and if the deposition velocities were assumed to be the same for all species.

2. The equilibrium needs time to develop:

   The equilibrium is not reached instantaneously but needs time to develop. The characteristic chemical time constant (τ_c) is given by equation 71 but other estimates exist in literature: according to Brost *et al.* (1988), Schwartz (1986) theoretically derived a time scale of less than 1 s whereas data from Larson and Taylor (1983) indicate a time scale of about 100 s. In addition to the

size spectrum, which has been considered in equation 71, the composition of the NH_4NO_3 containing aerosol might have a great effect. Kramm and Dlugi (1994) point out that chemical conversion is only to be considered if the chemical time scale is of the same order of magnitude as the time scale of the vertical diffusive transfer (τ_t): for $\tau_c << \tau_t$ the equilibrium approaches the instantaneous, reaction whereas for $\tau_c >> \tau_t$ the system can be regarded as chemically inert. Hence, in the first case the two terms in equation 92 cancel each other, in the latter the reaction rate coefficients are small and so are the source/sink terms. For neutral conditions Brost and Wyngaard (1978) expressed τ_t by

$$\tau_t = \frac{\kappa z}{1.75 u_*} \qquad \text{eq 94}$$

The comparison of chemical and diffusive time scale for a given NH_4NO_3 concentration and meteorological situation can therefore provide a first means for the estimation of the importance of GPC.

3. Disequilibrium caused by advection:

   Advection from adjacent sources (of any of the three chemical species) can lead to significant dis-equilibrium at the top of the layer which is normally expected to be in equilibrium with the surface, ie. the constant flux layer. This dis-equilibrium can then propagate through this layer to the surface if surface exchange and chemical reactions take place. In this case the expression 'constant flux layer' is not appropriate.

4. Gradients of temperature and relative humidity:

   As the theoretical equilibrium product is a strong function of temperature and relative humidity, the dissociation constant becomes height dependent in the presence of gradients of temperature and relative humidity. This dependence becomes more significant above the RHD and causes the equilibrium concentration product to change with height. Hence, even in the absence of surface/ atmosphere exchange concentration gradients and therefore flux gradients would form. The different values of V_d of the different species and the time constraints prevent the equilibrium to be obtained at all heights. In this case flux divergence can also be found if the deposition velocities of all species are considered the same and there is equilibrium at a reference height.

The conditions at the surface are controversely discussed in literature. One could argue that with vanishing z $\tau_c >> \tau_t \cong 0$ and thus the second condition for equilibrium are fulfilled. However, equation 94 is only valid above the height of the quasi-laminar sub-layer (z_0) and the transfer through this sub-layer is considerably slow, while concentration gradients are in general large. Kramm and Dlugi (1994) state that there must be equilibrium at the surface, as it follows from the fact that the flux divergence, $\partial F / \partial z$, vanishes at the surface. The total derivative wrt. time is given by

$$\frac{dc_i}{dt} = \underline{u} . \nabla c_i + \frac{\partial c_i}{\partial t} \qquad \text{eq 95}$$

where $\underline{u}$ is the vector of the mean wind speed. Assuming horizontal homogeneity and writing the local change of the concentration as

$$\frac{\partial c_i}{\partial t} = -\frac{\partial F_i}{\partial z} + Q_i \qquad \text{eq 96}$$

it becomes indeed obvious that under steady state conditions ($\partial c_i/\partial t = 0$) the source/sink terms (Q_i) have to vanish as the flux divergence approaches zero. The authors argue that the flux divergence must be zero if the description of R_b according to the equations 59 and 60 shall be applied. Although this a mathematically coherent requirement, it might not actually represent the physical processes. As the transport velocities of the different species within the viscous sub-layer are different and the concentration gradients potentially very large, it must be assumed that the chemical transformation processes are indeed substantial. Whereas a hight dependent relationship can be given for R_a (equation 57), it is for most purposes sufficient to calculate a bulk value for R_b. In order to validly extent the models to the range of the viscous sub-layer a hight dependent expression for R_b must be found that forms a mathematically continous extension of R_a.

The models of Brost *et al.* (1988) and Gao *et al.* (1991) are also based on the assumption that the flux divergence has to vanish at the surface but their concentrations are not in equilibrium. This is certainly a contradiction to equation 96. Fitzjarrald and Lenschow (1983) overcome the problem by using the concentrations at two heights above z_o as boundary conditions so that no assumptions about the surface conditions have to be made. In section 4.2.1.3 this concept is extended by a method to extrapolate the profiles to the surface so that the surface conditions can be examined.

Lenshow and Delany (1987) consider the reactive system of NO_2, NO and O_3, which can be treated similarly to the nitrate triad, although here the reaction rates are determined by photolysis of NO_2. Assuming the concentration of O_3 to be virtually constant (which is justifiable as its absolute concentration largely exceeds the concentrations of NO_2 and NO), they derive an analytical expression for the concentrations as a function of height. Their solution shows the flux divergence to be *highest* closest to the ground. This result was also obtained from global chemistry models used by Duyzer *et al.* (1995).

According to the different factors that contribute to the formation of dis-equilibrium the source of the dis-equilibrium can be either at the surface or at higher levels in the atmosphere. If the fetch is big enough and if no advection occurs, chemical equilibrium of the nitrate triad can be expected well above the surface ($\tau_t >> \tau_c$). Nevertheless, the different deposition rates are controlled by transport and exchange mechanisms at the surface, which can either be depletion or emission. Hence the dis-equilibrium is induced at the surface, which becomes obvious if we consider NH_3 emission caused by a surface concentration. This dis-equilibrium propagates upwards but becomes less significant with height. In the case of NH_3 emission there might be particle production which decreases with height. In the case of NH_3 deposition one might find stronger aerosol evaporation close to the surface. Kramm and Dlugi (1994) extend their model for NH_3 emission by introducing of a NH_3 surface concentration without revising the surface equilibrium requirement.

As discribed before advection of single species can lead to high deviation from the equilibrium just above the layer which would, neglecting chemistry, be expected to be in equilibrium with the surface. This equilibrium 'diffuses' downwards and becomes decreasingly significant. This situation has been modelled by Fitzjarrald and Lenschow (1983), and Kramm and Dlugi (1994). If these reference concentrations were chosen to be in equilibrium then the second equilibrium condition at the surface would lead to constant fluxes as explained under (1) above. Hence the model of Kramm and Dlugi (1994) cannot be applied to situations where the equilibrium is driven from the surface; the equilibrium condition is associated with difficulties.

In an advection situation the influence from above is dominant. However, at the same time different deposition processes at the surface take place as well. This might lead to the fact that equilibrium is not achieved at any height (if surface exchange and advection act in the same way) or that equilibrium is fulfilled at a height between the top concentration and z_o (if surface exchange and advection act in opposite ways). Presumably, the equilibrium height decreases with increasing dis-equilibrium at the top height. If temperature and humidity gradients influence the equilibrium at the same time, the net effect is difficult to estimate.

4.2 THE DIFFERENT CONCEPTS FOR MODELLING EQUILIBRIUM CHEMISTRY

As mentioned earlier on, GPC can often be identified by looking at the divergence of the measured deposition velocities from the expected values. Since the atmosphere/surface exchange of NH_3 is bi-directional and governed by a generally unknown value of R_c, V_d of NH_3 is difficult to estimate. The deposition velocity of particles is size dependent and the different deposition processes not yet well understood. Hence the comparison of the measured fluxes of HCl and HNO_3, which are assumed to deposit with V_{max} (e.g. Huebert *et al.* 1988) must be expected to give the best indication for GPC. If the gradients of HNO_3 and NH_3 are obtained in the same way as the one for NH_3, i.e. if the concentrations are measured at the same heights, the error due to GPC on the flux measurements of both species should be expected to be similar (assuming the effect of HCl is negligible). Since the error in the HNO_3 flux can be estimated using the expected value for $V_d=V_{max}$ a first order correction of the NH_3 flux is given by:

$$F_{NH_3,real}(z_o') = F_{NH_3,meas}(1m) + \Delta F_{NH_3} \qquad \text{eq 97}$$

with

$$\Delta F_{NH_3} = \left[HNO_3\right]_{meas}(1m) \times \left(V_{d,HNO_3}(1m) - V_{max,HNO_3}(1m)\right) \qquad \text{eq 98}$$

Similar expressions can be derived for the correction for the reaction with HCl, if appropriate. However, a potentially more accurate correction can be obtained by modelling the profiles of the concentrations and fluxes of the different chemical species including the values at the surface. Generally the following assumptions are made:

1. Chemical conversion processes are the only sources and sinks within the atmosphere.

2. The concentrations are horizontally homogenous, i.e.

$$\left(\frac{\partial c_i}{\partial x}\right)^2 + \left(\frac{\partial c_i}{\partial y}\right)^2 = 0 \qquad \text{eq 99}$$

In this case equation 96 has to be solved:

$$\frac{\partial c_i}{\partial t} = -\frac{\partial F_i}{\partial z} + Q_i \qquad \text{eq 100}$$

This is a set of partial differential equations containing too many variables to be solved without any further information. Two different approaches, first- and second-order-closure, can be found in literature. Models also differ in the expression of the source and sink terms used. Alongside the reaction rate expressions of equations 92 and 93 a relaxation approach is used considering the chemical conversion as a reaction towards equilibrium with the chemical time scale (τ_c). The formula for first-order-relaxation for the species i is given by:

$$Q_i = -\frac{c_i - c_{i,eq}}{\tau_c} \qquad \text{eq 101}$$

whereas for second-order-relaxation Q_1 would be written as

$$Q_1 = -\frac{c_1 c_2 - c_{1,eq} c_{2,eq}}{\tau_c} \qquad \text{eq 102}$$

Brost *et al.*(1988) claim that second-order-relaxation is to be preferred if the neutralising gases react in the gas phase producing new aerosol nuclei, whereas first-order-relaxation describes the chemistry in liquid aerosol where both gases undergo independent first-order-relaxation to equilibrium values determined by their Henry's law coefficients. In the latter case the pH presents the only coupling between the two equilibria.

4.2.1 First-order-closure

One way to close the set of differential equations is to assume that K-theory stays valid for chemical reaction so that at each height

$$F_i(z) = -K_{h,eff}\left(\frac{z-d}{L}\right)\frac{\partial c_i}{\partial z} \qquad \text{eq 103}$$

where the flux has become a function of height unlike in equation 17 and where the eddy diffusivity has been changed by the presence of chemical reactions. Brost *et al.* (1988) derive the relationship

$$K_{h,eff} = \frac{\tau_c}{\tau_c + \tau_t} K_h \qquad \text{eq 104}$$

which allows the effective diffusivity to approach the normal turbulence diffusivity for $\tau_c >> \tau_t$.

Fitzjarrald and Lenschow (1983) develop a formula including a chemical reactivity length scale λ_i as

$$K_{h,eff} = \left(0.74\left(1 - z/\lambda_i\right)\right)^{-1} K_h \qquad \text{eq 105}$$

for near neutral conditions and find only negligible deviation from using the uncorrected eddy diffusivity. Thus the normal turbulent eddy diffusivity (eq 23) seems to be a sufficiently accurate approximation making the application of this model in all stability conditions easy. Solving the system of differential equations can be limited to an integration in height leading to fast algorithms.

4.2.1.1 Coding of a first-order-closure model

Equations 96 and 103 together with the formulation for the chemical sources and sinks according to equations 92 and 93 form a system of six coupled non-linear first order differential equations which can be transformed into a system of three coupled non-linear second order differential equations in height. This system can then be solved according to the boundary conditions given. Kramm and Dlugi (1994) use concentrations at a reference height of 20 m as the only input. The concentrations at the height of the laminar sub-layer are derived using the inferential approach described in the next section. In their model for NO_2, NO and O_3, Fitzjarrald and Lenschow (1983) also apply first-order-closure to calculate profiles but they use two reference heights above z_o, thus avoiding the discussion about the surface conditions. Both models were decoded within this work. As an example, the equations for NH_3 (c_2) shall be looked at in detail. From equations 92 and 96 it follows that:

$$\frac{\partial F_2}{\partial z} = -k_1 c_1 c_2 + k_2 c_3 \qquad \text{eq 106}$$

where c_1 can be eliminated by using the more meaningful group concentrations, c_{gi}, to yield a second order polynomial expression

$$\frac{\partial F_2}{\partial z} = -\alpha_2 c_c^2 - \beta_2 c_2 - \tau_2 \qquad \text{eq 107}$$
$$\alpha_2 = k_1; \quad \beta = k_2 - k_1 c_{g3}; \quad \tau_2 = -k_2 c_{g1}$$

as e.g. done by Kramm and Dlugi (1994). From equation 103 the second derivative of the concentration wrt. to height is given by:

$$\frac{\partial^2 c_2}{\partial z^2} = \frac{\partial}{\partial z}\left(-\frac{F_i}{K_h}\right) = -\frac{1}{K_h}\left(-\alpha_2 c_2^2 - \beta_2 c_2 - \tau_2 + \frac{\partial c_2}{\partial z}\frac{\partial K_h}{\partial z}\right) \qquad \text{eq 108}$$

The equations for the other concentrations can be derived analogously. These differential equations are obviously coupled through the factors α_i, β_i and τ_i. These coefficients and K_h have to be calculated for each height and after each iteration step of the solving algorithm. Before integrating a logarithmic height co-ordinate h(z) was introduced deviding the height z_{max} into stepcount-1 equidistant intervals:

$$\begin{aligned} h(z) &= b\ln(z) + a \\ b &= \frac{\ln(z_{max}) - \ln(z_0)}{stepcount - 1} \\ a &= 1 - b\ln(z_0) \end{aligned} \qquad \text{eq 109}$$

The two point boundary problem was solved using a generalised shooting algorithm outlined by Keller (1968) allowing fluxes or concentrations as input. Also, a finite difference algorithm (Burden and Faires, 1993) was implemented, which, in some cases, shows better convergence behaviour.

4.2.1.2 An analytical expression for the lower boundary conditions for the case of surface equilibrium

Kramm and Dlugi (1994) assume that the flux divergence vanishes at the surfaces and that there is equilibrium. They use an iterative algorithm to calculate the lower boundary conditions (both fluxes and concentrations) from the concentrations at the upper reference height and the atmospheric resistances. A first approximation for the fluxes neglecting chemistry is derived as $F_i = -c_i(z_{ref})\ R_{t,i}^{-1}$, then the group fluxes are calculated and a first approximations for the group concentrations at z_o as $c_{gi}(z_o) = c_{gi}(z_{ref}) + R_i(z_{ref})\ F_{gi}$ using the height invariance of the group fluxes, is derived. Assuming equilibrium at z_o the concentrations of the single species can be obtained from equations 86 to 88. A new approximation for the single fluxes can be derived from the surface resistances as $F_i(z_o) = -c_i(z_o)\ (R_{b,i}+R_{c,i})^{-1}$. After calculating the second approximation for the group fluxes, a second approximation for the group species can be found etc..

Obviously, the iteratively obtained solution obeys the following equations:

$$c_{gi}(z_0) = c_{gi}(z_{ref}) + R_t(z_{ref})F_{gj}$$
$$F_i(z_0) = -\frac{c_i(z_0)}{R_{b,i} + R_{c,i}} \qquad \text{eq. 110}$$

Kramm and Dlugi (1994) fail to recognise that this algorithm can be solved analytically. Substituting the group flux in the first equation by the sum of the single fluxes according to the second equation for both TA and TN the following system of equations is obtained:

$$TA(z_0) = c_2(z_0) + c_3(z_0) = c_2(z_{ref}) + c_3(z_{ref}) + R_t\left\{-\frac{c_2(z_0)}{R_{b,2} + R_{c,2}} - \frac{c_3(z_0)}{R_{b,2} + R_{c,2}}\right\}$$
$$TN(z_0) = c_1(z_0) + c_3(z_0) = c_1(z_{ref}) + c_3(z_{ref}) + R_t\left\{-\frac{c_1(z_0)}{R_{b,1} + R_{c,1}} - \frac{c_3(z_0)}{R_{b,2} + R_{c,2}}\right\}$$
$$k_{p,NH_4NO_3} = c_1(z_0)c_2(z_0)$$

eq 111

which is readily solveable for the surface concentrations:

$$c_1(z_0) = \frac{c_1(z_{ref}) - c_2(z_{ref})}{2\alpha_1} \pm \sqrt{\left(\frac{c_1(z_{ref}) - c_2(z_{ref})}{2\alpha_1}\right)^2 + k_{p,NH_4NO_3}\frac{\alpha_2}{\alpha_1}}$$
$$c_2(z_0) = \frac{k_{p,NH_4NO_3}}{c_1(z_0)}$$
$$c_3(z_0) = \frac{c_1(z_{ref}) + c_2(z_{ref}) - c_1(z_0)\alpha_1}{\alpha_3} \qquad \text{eq 112}$$
$$\alpha_i = 1 + \frac{R_t}{R_{b,i} + R_{c,i}}$$

The fluxes can be calculated from the concentrations using equation 111. This analytical calculation of the boundary conditions overcomes problems with the numerical algorithm, which shows poor convergence properties. However, as discussed before the equilibrium condition does not seem to be physically appropriate.

4.2.1.3 Extrapolation down to the surface

As the validity of the equilibrium condition at the surface has to be questioned, the concentrations at z_o cannot be calculated; therefore one of the boundary conditions must be given up. In order to base the model assessment mainly on field data, it seems advisable to use the measured concentrations at two different heights above z_o as an input and to extrapolate the profile down to z_o - an approach which does not seem to have been done elsewhere. A common 4th order Runge Kutta algorithm for solving initial value problems of 2nd order differential equations (e.g. Burden and Faires, 1993; Press *et al*, 1992) was used to extrapolate the fluxes and concentrations from the values found at the lower reference height by

the calculation described above. For the discussion of the results it must be kept in mind that small deviations in the boundary conditions lead to great deviations at the surface and that boundary value algorithms require a significantly smaller vertical step size than two point boundary problem. A sensitivity analysis would be necessary to estimate the accuracy of this extrapolation. However, first results show that the algorithms allow the profiles to be smoothly and continuously extended beyond the lower input height.

4.2.1.4 Extension of the first-order-closure model by adding the chloride triad

Whereas different models for the nitrate triad can be found in literature the chloride triad has not yet been dealt with let alone a system of both. The adoption for chloride is easily done replacing k_{p,NH_4NO_3} by k_{p,NH_4Cl} the combination of both, however, makes it necessary to re-formulate the source/sink terms. Equation 92 becomes:

$$Q_i = \begin{cases} -k_1[HNO_3][NH_3] + k_2[NH_4NO_3] = -k_1c_1c_2 + k_2c_3 & for\ i = 1 \\ Q_1 + Q_4 & 2 \\ -Q_1 & 3 \\ -k_3[HCl\ ][NH_3] + k_4[NH_4Cl\ ] = -k_3c_4c_2 + k_4c_5 & 4 \\ -Q_4 & 5 \end{cases} \quad \text{eq 113}$$

The group concentrations here are total nitrate, total ammonium and total chloride:

$$\begin{aligned} TN = c_{g1} &= [HNO_3] + [NH_4NO_3] \\ TA = c_{g2} &= [NH_3] + [NH_4NO_3] + [NH_4Cl] \\ TC = c_{g3} &= [HCl] + [NH_4Cl] \end{aligned} \quad \text{eq 114}$$

These three equations are not sufficient to determine the five equilibrium concentrations. As NH_3 is involved in both reaction cycles it can be eliminated in the expression of the two equilibrium constants

$$\begin{aligned} k_{p,NH_4NO_3} &= [HNO_3]_{eq}[NH_3]_{eq} \\ k_{p,NH_4Cl} &= [HCl]_{eq}[NH_3]_{eq} \end{aligned} \quad \text{eq 115}$$

to yield an relationship between the equilibrium concentrations of the acids:

$$[HNO_3]_{eq} = \frac{k_{p,NO_3^-}}{k_{p,Cl^-}}[HCl]_{eq} \qquad \text{eq 116}$$

which can be used alongside equation 114 to calculate the equilibrium concentrations as

$$\begin{aligned}
[NH_4NO_3]_{eq} &= \frac{1}{2}\left\{\frac{\alpha}{\beta} + TN - \left(\left(\frac{\alpha}{\beta} + TN\right)^2 - 4\left(\frac{\alpha}{\beta}TN - \frac{k_{p,NH_4NO_3}}{\beta}\right)\right)^{1/2}\right\} \\
[NH_3]_{eq} &= \alpha - \beta[NH_4NO_3]_{eq} \\
[HNO_3]_{eq} &= TN - [NH_4NO_3]_{eq} \\
[NH_4Cl]_{eq} &= TA - [NH_3]_{eq} - [NH_4NO_3]_{eq} \\
[HCl]_{eq} &= TC - [NH_4Cl]_{eq} \\
\alpha &= TA - TC + \frac{k_{p,NH_4Cl}}{k_{p,NH_4NO_3}}TN \\
\beta &= 1 + \frac{k_{p,NH_4Cl}}{k_{p,NH_4NO_3}}
\end{aligned} \qquad \text{eq 117}$$

As a fourth relationship can only be found for the equilibrium situation, the source/sink terms cannot be expressed by the group concentrations as it was done for the nitrate triad in equation 107 . Using directly the terms of equation 113 a system of five differential equation can be derived and solved using the technique explained before.

4.2.2 Second order closure

A second way to develop a closure expression for the flux equation is to look at the second order flux budget equation. Analogously to scalar entities such as temperature, Fitzjarrald and Lenschow (1983) derive a 2nd order equation for the fluxes directly from the combination of the fluctuation equations for vertical velocity and chemical concentrations for the photochemical nitrogen cycle. However, it can easily be adopted for the nitrate triad (here written for $HNO_3=c_1$):

$$\underbrace{\frac{\partial \overline{w'c_1'}}{\partial t}}_{(1)} = \underbrace{-\overline{w'^2}\frac{\partial \overline{c_1}}{\partial z}}_{(2)} + \underbrace{\frac{g}{\overline{q}}\overline{q'c_1'}}_{(3)} - \underbrace{\frac{1}{\overline{\rho}}\overline{c_1'\frac{\partial p'}{\partial z}}}_{(4)} - \underbrace{\frac{\partial \overline{w'^2c_1'}}{\partial z}}_{(5)} \qquad \text{eq 118}$$

$$\underbrace{-k_1\left(\overline{c_1}\,\overline{w'c_2'} + \overline{c_2}\,\overline{w'c_1'} + \overline{w'c_1'c_2'}\right) + k_2\overline{w'c_3'}}_{(6)}$$

with similar expressions for i = 2 and 3. Term 1 represents the local flux change in time, term 2 the flux production due to vertical turbulent transport and concentration gradients, term 3 the effect of buoyancy, term 4 the destruction of flux by pressure variation, term 5 the vertical mechanical transport of the flux and the last term the production and destruction by chemical interchange. This equation can be simplified by the following assumptions:

1) The last constituent of the first factor of the chemical reaction term 6 ($\overline{w'Q_i'}$) can be neglected as a product of three small quantities.

2) The pressure term 4 represents the tendency to return to an isotrop situation and can be parameterised by

$$\frac{1}{\rho} c_i' \frac{\partial p'}{\partial z} = \frac{\overline{w'c_i'}}{\tau_t} \qquad \text{eq 119}$$

as suggested by Fitzjarrald and Lenschow (1983), Brost *et al* (1988) and Gao *et al* (1991). Here τ_t represents the turbulent time scale.

3) Unfortunately, this approach has only been used under neutral conditions in which case three other simplifications can be made:

- The gravity term in equation (term 3) can be ignored as small for constant virtual temperature.
- The turbulent time scale is given by $\tau_t = (\kappa z) / (1.75 u_*^2)$ (Brost and Wyngaard, 1978).
- $\overline{w'^2}$ can be parameterised by $\overline{w'^2} = 1.75 u_*^2$ (*dito*).

A generalisation for all stability classes seems to be difficult.

For the 1st order relaxation approach term 6 in equation 118 is to be substituted by

$$\overline{w'Q_i'} = -\frac{\overline{w'c_i'} - \overline{w'c_{i,eq}'}}{\tau_t} \qquad \text{eq 120}$$

as used by Brost *et al* (1988) who also give explicit expressions for the equilibrium fluxes ($\overline{w'c_{i,eq}'}$).

4.2.2.1 Implementation of a second-order-closure model

A second-order-closure model was de-coded according to the descriptions of Gao *et al.* (1991) and Coe (1993). Boundary conditions are prescribed by the concentrations at a reference height, the surface resistances $R_{c,i}$ and the surface concentration of NH_3. Both flux and concentration profiles are calculated using equation 118 with the simplifications described above, where the differentials are substituted by finite differences (i.e. δt and δz). The distance between the reference height and z_0 was divided into heightstepno=30 logarithmically spaced layers and 0.001 seconds were used as the time step.

4.2.2.2 Extension by the chloride triad

For the reaction rate expressions of the chemical source and sink terms according to equation 113 the co-variance with the vertical wind component can be written as:

$$\overline{w'Q_i'} = \begin{cases} -k_1\left(\overline{c_1 w' c_2'} + \overline{c_2 w' c_1'} + \overline{w' c_1' c_2'}\right) + k_2 \overline{w' c_3'} & for\ i = 1 \\ \overline{w'Q_1'} + \overline{w'Q_4'} & 2 \\ -\overline{w'Q_1'} & 3 \\ -k_3\left(\overline{c_4 w' c_2'} + \overline{c_2 w' c_4'} + \overline{w' c_{41}' c_2'}\right) + k_2 \overline{w' c_5'} & 4 \\ -\overline{w'Q_4'} & 5 \end{cases} \qquad \text{eq 121}$$

The reaction rate coefficients for the sociation (k_1 and k_3) were given as input values and kept constant with height. Frome these the reaction rate coefficient for the dissociations (k_2 and k_4) were calculated using the height dependent equilibrium concentrations (see equation 117). The integration was carried out in the same way as for the nitrate triad described in the section before.

4.2.3 Semi empirical models

The techniques for calculating the 'true' concentration and flux profiles presented so far, dealt with the numerical solution of theoretically derived coupled differential equations, and were limited by the insufficient knowledge of the reaction kinetics involved. Duyzer *et al.* (1995) criticise numerical approaches for the nitrogen cycle as they ignore other competing chemical processes and thus lead to results, which might differ more from the 'true flux' than results obtained by standard techniques neglecting chemical conversion processes altogether. They do not use measurement data but generate 'real' concentration profiles using the multi-layer air chemistry model (base model) by Hough and Derwent (1987), which includes 85 reactions of 43 chemical species. From these modelled profiles, input data are extracted and used for different models calculating surface fluxes. The results can then be compared to the surface fluxes obtained by the base model, and this way the different models can be assessed. They also calculate fluxes from the base model data neglecting chemistry and compare the results to the 'true' surface fluxes. From this comparison they derive correction functions, which, despite being derived semi-empirically, are claimed to be both more accurate and more practically applicable than numerical models. Based on the results of the base model Duyzer *et al.* (1995) assume the flux divergence to be a logarithmical function of height - quite in contrast to the statement of Kramm and Dlugi (1995) that the flux divergence vanishes near the ground:

$$\frac{\partial F(z)}{\partial z} = a \ln(z) + b \qquad \text{eq 122}$$

from which the flux at height z can be calculated as the sum of the surface flux, $F(z_o)$, and the integral over the flux divergence from z_o to z:

$$F(z) = F(z_o) + \int_{z_o}^{z} \frac{\partial F(z)}{\partial z} dz$$
$$= F(z_o) + (a-b)(z-z_o) - b\left[z_o \ln(z_o) - z\ln(z)\right] \qquad \text{eq 123}$$

Using the flux gradient relationship equation 103, a_{HNO3} is for example given by

$$a_1 = z\frac{\partial^2 F_1}{\partial z^2} = z\frac{\partial Q_1}{\partial z} = z\left[-k_1\left(\frac{\partial c_1}{\partial z}c_2 + \frac{\partial c_2}{\partial z}c_1\right) + k_2\frac{\partial c_3}{\partial z}\right]$$
$$= \frac{\Phi_H\left(\frac{z}{L}\right)}{ku_*}\left[-k_1\left(c_2F_1 + c_1F_2\right) + k_2F_3\right] \qquad \text{eq 124}$$

where the fluxes are the fluxes derived using the constant flux assumption. Assuming the flux divergence to vanish at the highest measuring point, b can be evaluated as $b=a\ln(z_{wp})$.

This approach is easy to use, but it is based on the logarithmic shape of the flux divergence, which has to be tested for the chemistry of NH_3, and also on the validity of the base model. Moreover, it still requires the knowledge of the reaction rate coefficients.

4.2.4 Analytical solution of the concentration as a function of height

An analytical solution for the photochemical nitrogen cycle is presented by Lenshow and Delany (1987). Ignoring stability effects and assuming the concentration of ozone to be constant with height ,they solve the set of coupled differential equations to obtain an analytical expression for the NO flux with height containing two Bessel functions. Although analytical solutions are to be preferred over numerical because of the completeness of the description and the speed of their application, an adoption of this solution to the chemistry of NH_3 might not be feasible as no flux can be set to zero.

4.2.5 Sample run - intercomparison between first- and second-order-closure

Both first- and second-order-closure models have their specific advantages and disadvantages. The first-order-closure can be solved by faster algorithms than the second-order-closure, which has to be integrated wrt. both height and time. The first-order-closure is based on the assumption that the flux gradient relationship remains unaffected and although this is a simplification Fitzjarrald and Lenschow (1983) show that the effect of chemistry on the eddy diffusivity is negligible. The second-order-closure is correct in this respect but here second order approximations have to be used, like the parameterisations of the pressure term and the variance of the vertical wind component described in section 4.2.2. These parameterisations have not been expanded for non-neutral conditions. Whereas the second-order-closure has only been applied when the boundary conditions were given by a reference concentration and the surface resistances, first-order-closure can be more flexibly solved for arbitrary two point boundary or initial value problems.

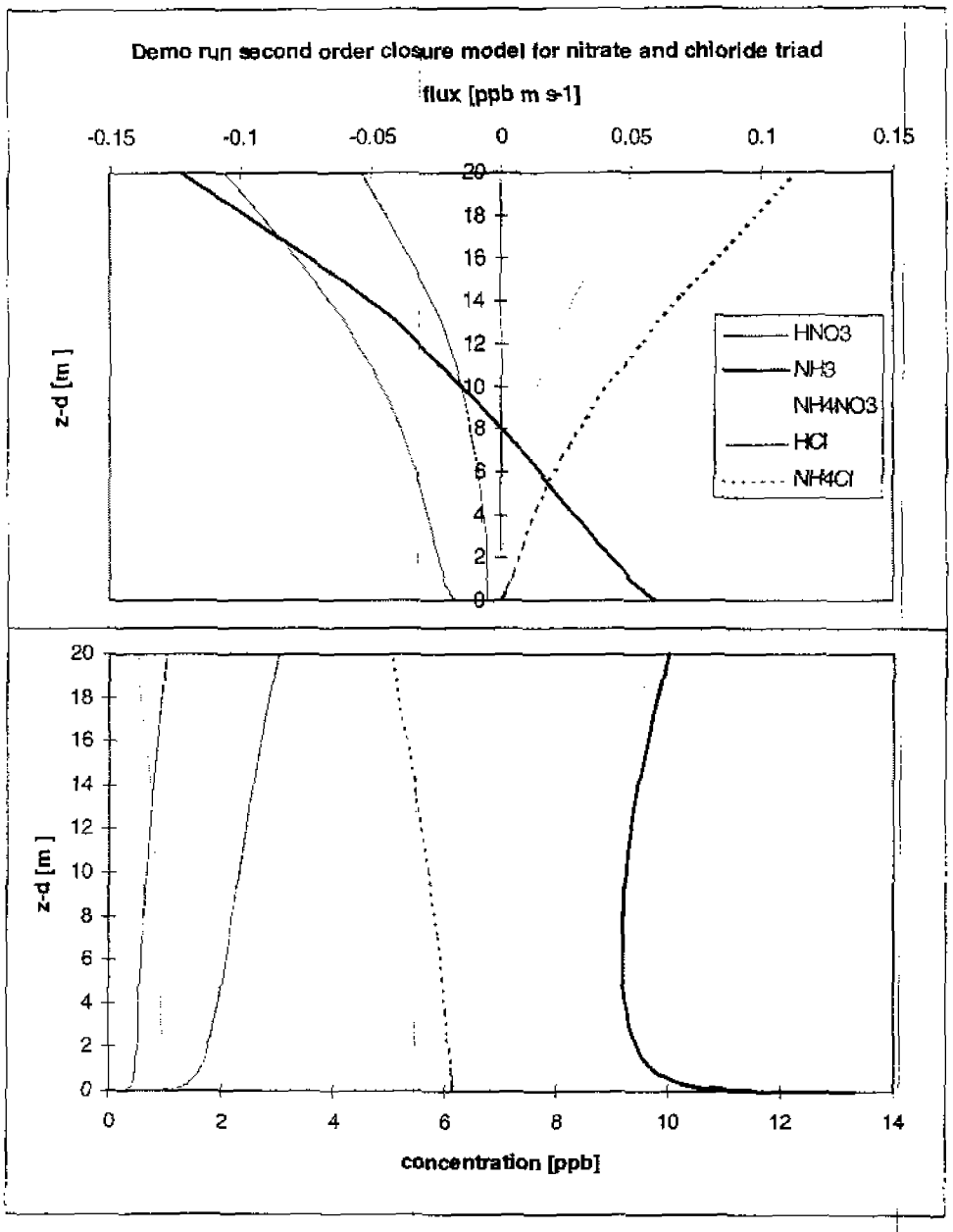

Figure 8: Demo run of the second-order-closure model showing how a NH_3 emission flux at the surface can theoretically be changed to an apparent deposition flux (here above 8 m) by the presence of GPC. Aerosol shows an increasingly higher apparent emission flux away from the surface whereas the acids would seem to be deposited faster than possible by turbulence.

Figure 8 shows a demo run of the second-order-closure using as arbitrary input values: $u_* = 0.22$ m, $L = \infty$, $T = 15$ °C, $RH = 40\%$, $z_0 = 1$ mm, $z_{ref} = 20$ m, $R_{b,HNO3} = R_{b,NH3} = R_{b,HCl} = 25$ s m^{-1}, $R_{b,NH4NO3} = R_{b,NH4Cl} = 300{,}000$ s m^{-1}, $k_1 = 50$ ppb s^{-1}, $k_3 = 20$ ppb s^{-1}, $[NH_3]_{20m} = 10$ ppb, $[HNO_3]_{20m} = 1$ ppb, $[HCl]_{20m} = 3$ ppb, $[NH_4NO_3]_{20m} = 0.5$ ppb, $[NH_4Cl]_{20m} = 5$ ppb, $[NH_3]_{cp} = 15$ ppb. The NH_3 flux changes from the 'true' emission at the surface (due to the high canopy concentration) to an apparent deposition flux higher up in the atmosphere. Where its flux changes sign, the ammonia concentration shows a *maximum, a feature which was also reported by Kramm and Dlugi (1994)* using a first-order-closure model. In agreement with their large R_b, the aerosol species show slow deposition at the surface, which appears as emission further up. In contrast, the gaseous acids seem to be deposited faster than possible

by turbulence, if measured well above the surface, but actually deposit with the velocity determined by their R_b. HCl shows a higher flux than HNO_3 reflecting the difference in their concentrations. This first look shows that chemical reactions can

a) lead to **apparent emission of aerosol,**

b) cause **HCl and HNO_3 to seem to be deposited faster than permitted by turbulence,**

c) have a *significant* ***effect on the quantity and even direction of NH_3 fluxes,***

and are thus a likely explanation for some of the unusual observations mention in the introductory section 1.4.

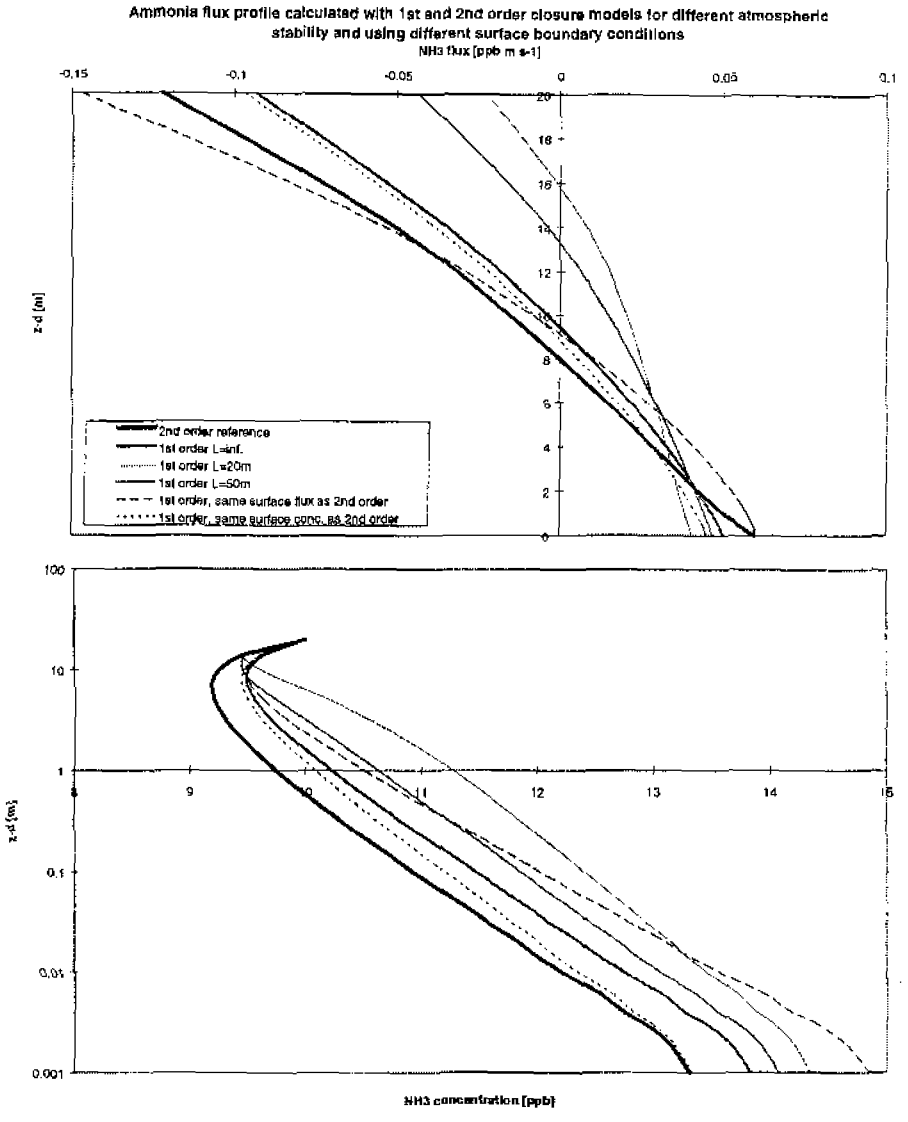

Figure 9: Intercomparison between first order closure and second order closure models for the chemistry of NH_3, HCl and HNO_3 showing significant increasing differences for non-neutral conditions as atmospheric stability is neglected in the second order closure model.

Using the same input data Figure 9 shows the NH_3 concentration and flux gradients calculated by a second-order-closure and by first-order-closure model for different values of L. The different ways of calculating the surface boundary conditions (unlike the second-order-model, the first-order-model ensures equilibrium at the surface) lead to different results at the surface. The difference between the models becomes more significant with increasing non-neutrality showing that for these conditions the second-order-closure model cannot be applied. Also plotted in Figure 9 are the gradients calculated with first-order-closure using the surface flux or concentration calculated with the second-order-closure approach as the lower boundary condition rather than calculating them using the resistance model.

4.3 APPLYING NUMERICAL MODELS TO EXPERIMENTAL DATA

4.3.1 The Halvergate experiment

Unpublished data from measurements carried out in a joint field campaign in September 1989 as a part of the BIATEX project near Halvergate, Norfolk, UK, show unexpected surface exchange rates of gaseous HNO_3 and HCl as well as particulate NH_4^+. A site description of the experiment has been provided by Hargreaves *et al.* (1992) and Dollard *et al.* (1990). The data of four out of twelve runs are shown in Figure 10.

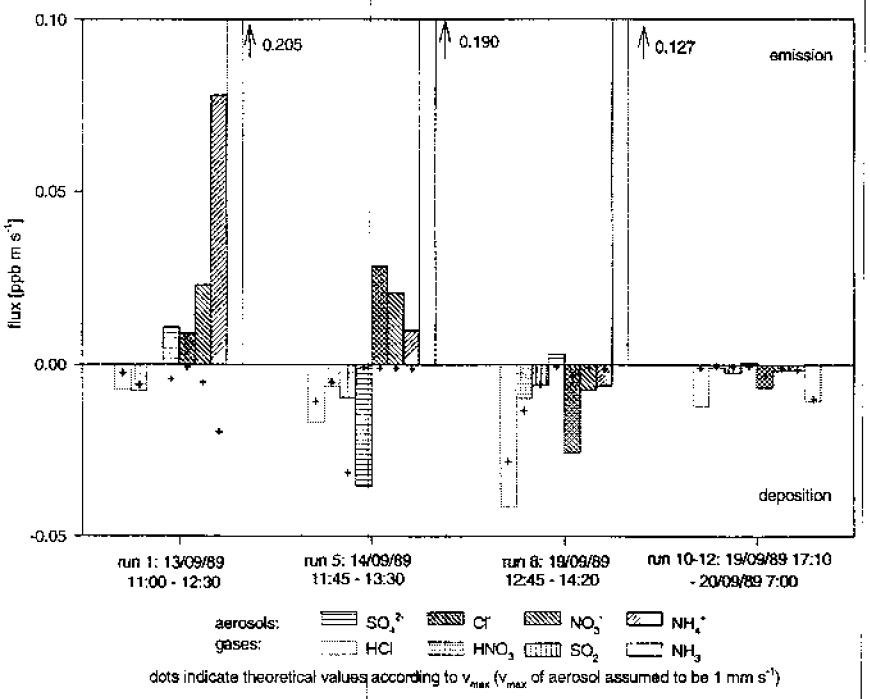

Figure 10. Fluxes of four out of twelve runs during the Halveragate '89 campaign as calculated with the aerodynamic gradient method. Fluxes of both aerosol and acids show high deviation from the expected values.

The average of the night time runs 10 - 12 shows expected deposition fluxes for NH_4NO_3 and HNO_3 which indicate that GPC did not effect the measurements. In contrast, runs 1 and 5 show high apparent emission of NH_4^+ aerosol and deposition of HNO_3 and HCl faster than permitted by turbulence (V_{max}) indicating aerosol formation or growth close to the surface. The opposite process, enhanced evaporation of aerosol near the surface, may be the cause of the slow acid and too rapid NH_4^+ deposition in Run 8.

As the measurements included simultaneous gradients of NH_3, HNO_3, HCl, NH_4NO_3 and NH_4Cl they provide a unique dataset for model assessment. However, some other runs (data not included in Figure 10) show inconsistent data, e.g. deposition of all chemical species faster than permitted by turbulence, observation which cannot be explained in terms of GPC. A large contribution of SO_4^{2-} to the NH_4^+ concentration was also found during some runs requiring the inclusion of H_2SO_4 into the modelling which was beyond the scope of the first model tests presented here.

The model described is applied to two different measurement examples as presented in Figure 11 and Figure 12. Figure 11 shows a case in which the concentration product $[NH_3][HNO_3]$ does not obtain its theoretical value (k_p) at any height. This leads to aerosol evaporation which is highest close to the ground where the HNO_3 concentration is smallest. The magnitude of the dis-equilibrium is governed by the concentration of HNO_3 rather than NH_3.

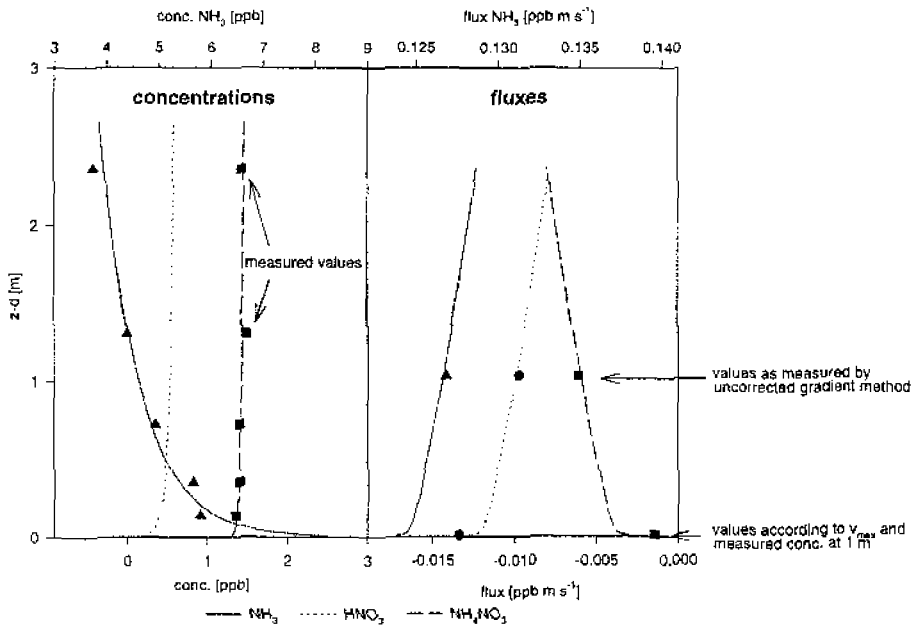

Figure 11. Model application to data from Halvergate, Run 8, when aerosol production or growth occurred close to the surface. The reaction with HCl is neglected as NH_4^+ and NO_3^- concentrations balance.

A comparison of the concentrations of the aerosol species suggested that for Run 8 the NH_4^+ presents mainly NH_4NO_3. Consequently the reaction with HCl was ignored. The high deposition velocity of the Cl^- aerosol could be explained by the chloride mainly consisting of sea salt which usually shows a larger mass median diameter than NH_4^+ aerosol leading to deposition faster than $V_d = 1$ mm s^{-1}.

In contrast to Run 8, Figure 12 demonstrates the case of aerosol formation which was more frequently observed during the Halvergate experiment, as shown for Run 5. The relative humidity approaches 100% near the ground which leads to a small value of k_p. Because of the high emission of NH_3, the equilibrium product exceeds its theoretical value ($[NH_3][HNO_3]>k_p$) leading to aerosol formation to be highest close to the surface, where the smallest value for k_p and the highest for $[NH_3]$ can be found. In order to balance the NH_4^+ concentration measured, the reaction with HCl has to be included in the model. As the NO_3^- and Cl^- gradient measurements show high scatter, the NH_4^+ gradients were used as input and arbitrarily split into NO_3^- and Cl^-.

In modelling both runs 8 and 5 the reaction rate coefficients, k_1 (and in Run 5 also k_2), was altered for the surface flux of HNO_3 (or HCl) to match the predicted value, i.e. $-[HNO_3](z_0)/R_b$, R_b being the resistance of the laminar boundary layer (see Figure 11). A value of $k_1 = 8$ ppb^{-1} s^{-1} was found for Run 8 which results in a mean NH_4^+ formation rate of about 0.32 ng m^{-3} s^{-1}. The good match of the surface flux of the aerosol indicates data consistency (see Figure 11). However, matching the fluxes at z_o assumes no flux divergence to occur within the laminar boundary-layer. This assumption was also made by Kramm and Dlugi (1994), but becomes doubtful considering that in Run 8 the dis-equilibrium was highest near the ground.

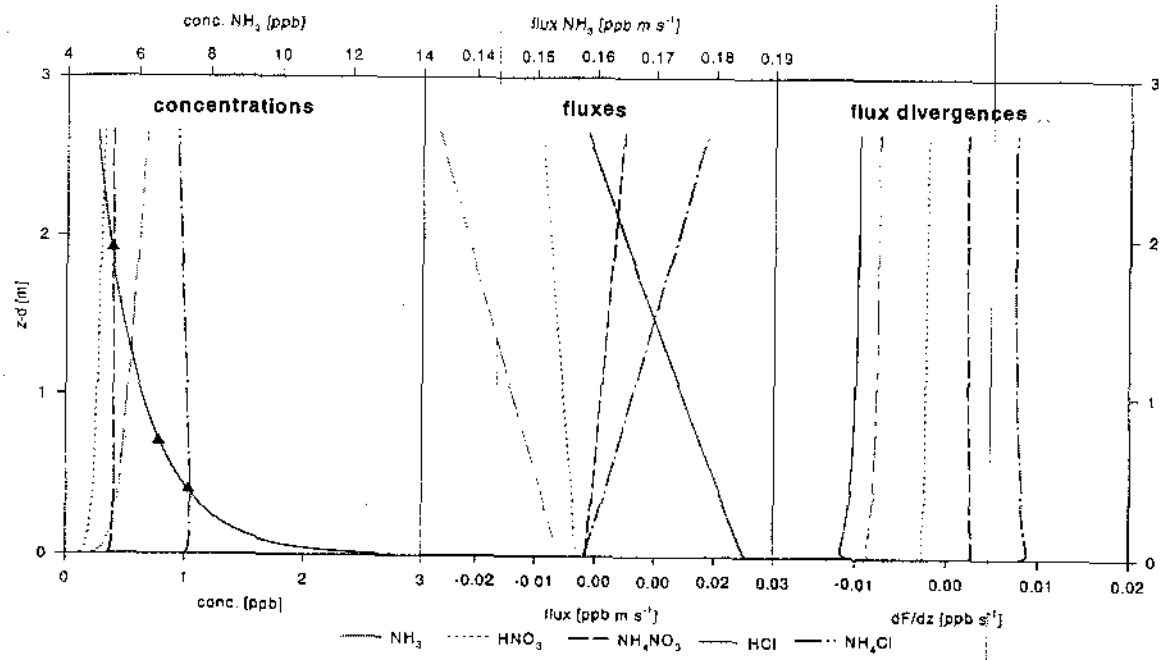

Figure 12. Model application to data from Halvergate, Run 5, showing aerosol evaporation close to the surface, including the reaction with HCl. The flux divergence is highest near the ground.

The numerical model can quantitatively simulate GPC for both aerosol production and evaporation. However, not enough runs are available to enable a full model assessment. The profiles of Cl^- and NO_3^- showed too much scatter to be useful. These uncertainties give room for interpretation which was used to fit the models. Moreover, the values for the reaction rate coefficients have been chosen so as to fit the model results to the data.

4.3.2 Requirements and plans for further data acquisition

For further model assessments it would be desirable to acquire more data of increased accuracy for the aerosol specication (i.e. NH_4NO_3, NH_4Cl). Recent developments of automated sampling techniques for all species under consideration (e.g. Wyers *et al.*, 1993; Khlystov *et al.*, 1995) will lead to statistically valid input data. Temperature and relative humidity gradients have to be measured exactly in order to account for changes in k_p with height. The measurement of aerosol size spectra at different heights could also provide a means to detect aerosol production and growth due to GPC and measurements of the size spectrum of NH_4^+ aerosol would enable the estimation of the chemical time scale according to equation 71.

5. MEASUREMENT OF THE CONCENTRATION AND FLUX OF AMMONIA AND OTHER GASES

5.1 TECHNIQUES

5.1.1 Annular batch denuder

Automated wet annular denuder systems have been developed over the last ten years allowing unattended long term measurements of trace gases with time resolutions of 1 hour. The systems employed here were designed by Netherlands Energy Research Foundation (ECN) and are described in Keuken *et al.* (1988). An air sample is sucked through the annulus between two concentric glass cylinders, which is kept small (1.5 mm) in order to obtain a laminar flow that allows gaseous but prevents particle diffusion perpendicular to the air flow. Collection solution is pumped into the gap, cotes the rotating denuder tubes with a water layer of 0.5 mm thickness, is extracted after a sampling time of 40min. and pumped into test tubes, which can then be analysed. The sampling efficiency for different chemical species depends on the collection solution used. An overview is given in Table 2. The addition of a formaldehyde preservative is recommended to prevent bacterial nitrification during storage.

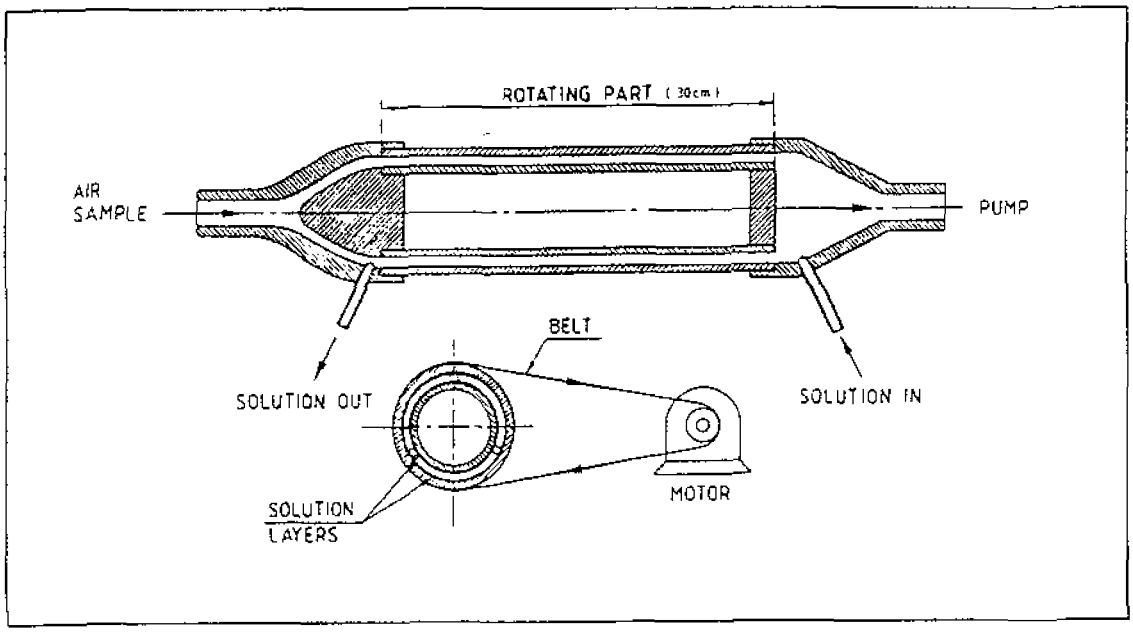

Figure 13: The wet annular denuder tube (taken from Keuken *et al.*, 1988)

Table 2: Overview of the sampling properties of some collection solution used in annular batch denuders

coating solution	captured NH_3	species: SO_2	HNO_3	HONO	HCl	H_2O_2
potassium carbonate, K_2CO_3		✓	✓	✓	✓	
sodium phosphate, Na_3PO_4		✓				✓
formic acid, HCHO	✓		✓	✓	✓	

Experience in running annular batch denuders was gained by operating the denuder at a measuring site in Midlothian, some seven miles south of ITE, for the LIFE project one day every week.

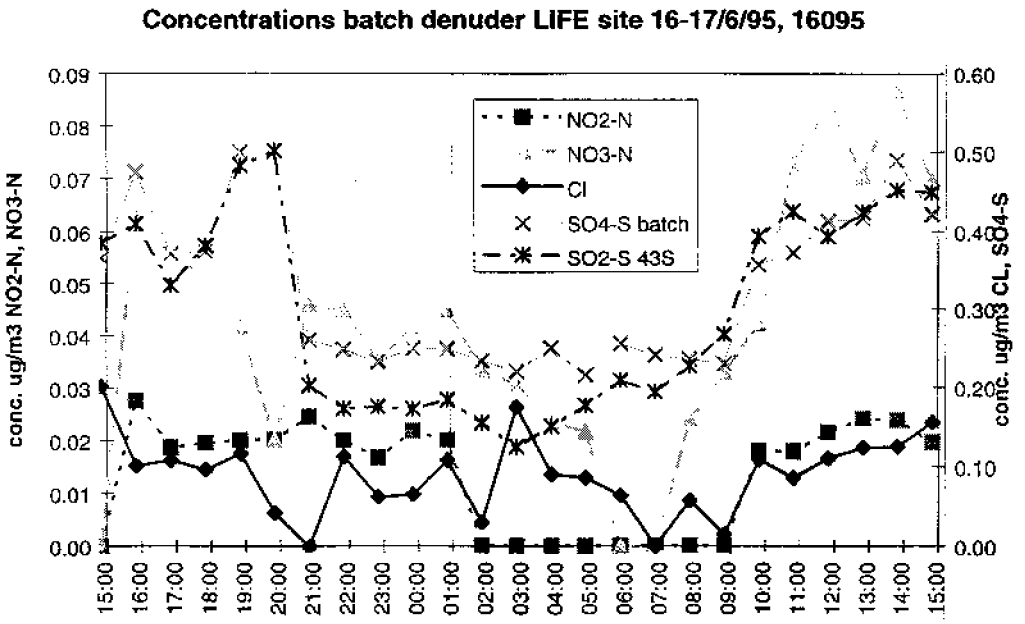

Figure 14: Diurnal cycle of HNO_3, HONO, HCl and SO_2 from 16-17/6/95 at the LIFE site as measured with a wet annular batch denuder showing the low concentrations typical for this site. The SO_2 concentration measured independently by a TECO 43S gas analyser is plotted as a comparison and shows reasonable agreement with the SO_4^{2-} concentration measured with the batch denuder.

5.1.2 Continuous annular NH_3 denuder

Ammonia gradients were measured using automated continuous NH_3 denuders with on-line conductivity NH_4^+ analysis (AMANDAs) also designed by ECN (e.g. Wyers *et al.*, 1993). They consist of three annular denuders (see Figure 13), through which an acidic coating solution (3.6 mM $NaHSO_4$ with formaldehyde preservative) is continuously pumped. Switching valves alternately connect the outlets of the different denuders to a conductivity cell where the stripping solution is mixed with a 0.5 M NaOH solution forcing the NH_3 into its gaseous state so that it can diffuse through a PTFE membrane into de-ionised water whose conductivity is than analysed.

5.1.3 Filter Packs

Filter packs are common practice to measure the concentrations of particles and different gases simultaneously. Here 90 mm filter packs according to the design described in Sutton (1990) were used (see Figure 15) to simultaneously measure concentrations of NH_3, HNO_3 and particulate NH_4^+. As a high pressure drop over particle filters is known to enhance aerosol evaporation, which would effectively lead to sampling of e.g. NH_4NO_3 aerosol as gaseous HNO_3 and NH_3, the bigger diameter was preferred to the more common 47 mm to reduce the resistance and allow higher flow rates and thus higher loadings.

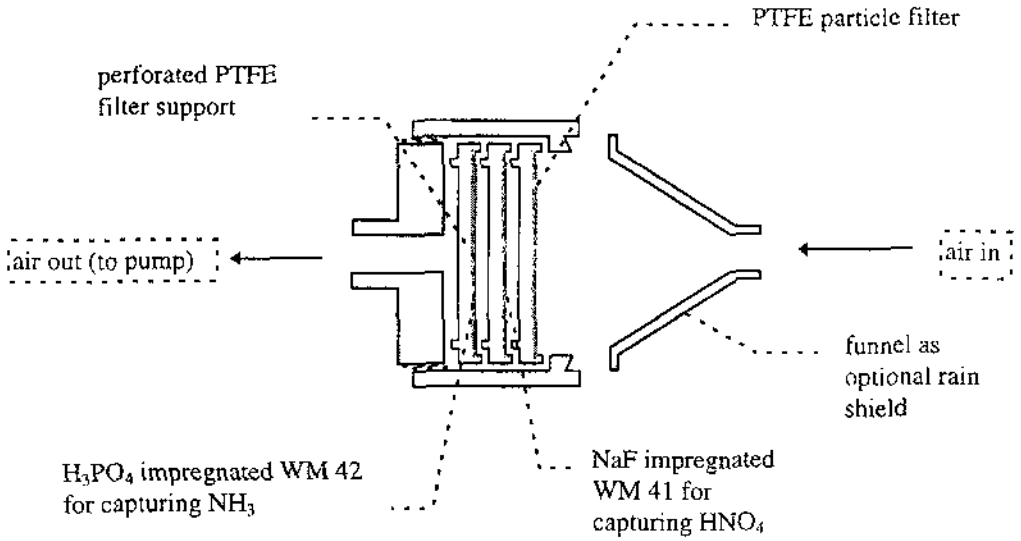

Figure 15: Outline of the filter packs used for sampling of aerosol and gaseous nitric acid and ammonia.

Three filters were used in series which were:

1. PTFE particle filter:

   PTFE membranes with 1 µm pore size by Micro Filtration Systems (MFS) and Cole Parmer (CP) were used to capture particles. Because of their high price the Teflon filters were cleaned and reused according to Sutton (1990). Extraction was performed by wetting the hydrophobic filters with 0.5 ml iso-propanol followed by 20 min. extraction in further 9.5 ml de-ionised water on a wrist shaker. The extract could then be analysed by anion chromatography for Cl^-, NO_3^- and SO_4^{2-}. Analysis for NH_4^+ was performed using an ammonia flow injection analyser with conductivity cell (AMFIA) designed by the Netherlands Energy Research Foundation (ECN). As GPC is likely to form new NH_4^+ particles it has to be shown that the filters are, despite their relatively large poor size, capable of efficiently collecting even small particles. A test was carried out using two optical particle counters (OPCs) (see section 6.3) connected with each other by a filter pack containing only the particle filter. Whereas all particles with diameters greater then 1 µm were captured, the sampling efficiency for smaller particles (down to 0.1 µm) was shown to decrease for smaller particles and higher flow rates. Although the MFS filters consistently showed a slightly better performance than the CP filters (average collection efficiencies for a flow rate of 26.8 l min^{-1} were measured as 99.9% for the MFS and 99.7% for the CP filter) the error introduced even for the smallest particles detectable by the OPCs (D_p=0.1µm) was negligibly small. Considerably damaged MFS filters, which had been excluded from use by Sutton (1990), showed still a satisfying but significantly size dependent collection efficiency of more than 96% (see Figure 16).

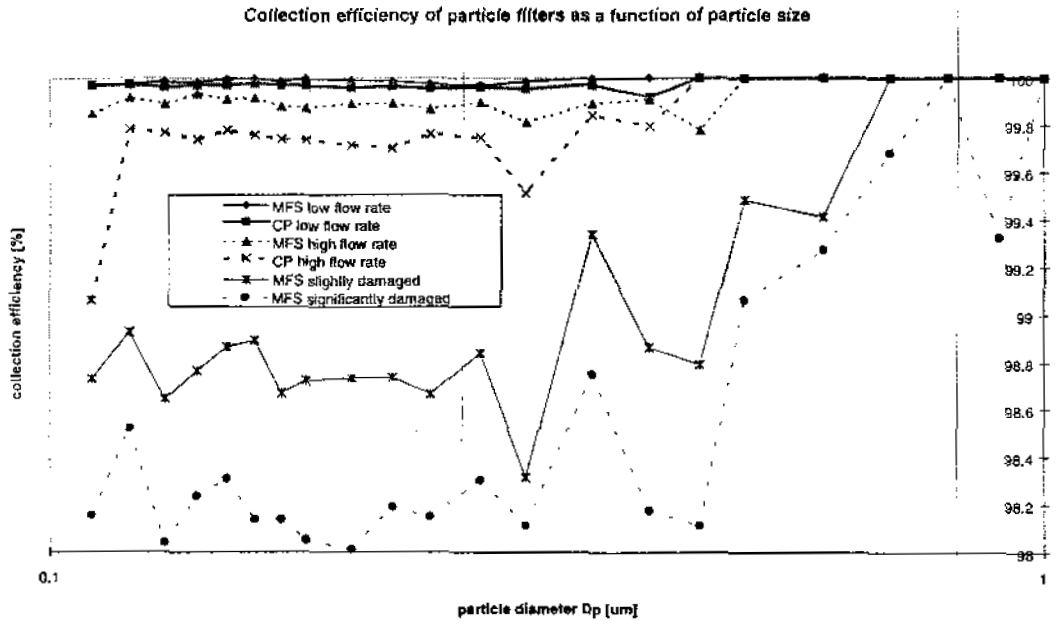

Figure 16: The size dependent collection efficiency of PTFE particle filters by Micro Filtration Systems (MFS) and Cole Parmer (CP) for the air flow rates of 6.5 and 26.8 l min^{-1} also showing the effect of holes in the membrane as measured using two optical particle counters in series.

2. *Nitric acid filter:*

   For capturing HNO_3 Whatman 41 paper filters impregnated with 0.7% m/v NaF in an ultrasonic bath following Andersen and Hovmand (1994) were placed between the particle- and the NH_3 filter. The filters were analysed for NO_3^- using anion chromatography and also NH_4^+ to estimate the collection of NH_3 by the alkaline NaF filter.

3. Ammonia filter

   For capturing gaseous NH_3 Whatman 42 paper filters were impregnated with 1% m/v ortho-phosphoric acid in an ultrasonic bath. Analysis was carried out only for NH_4^+ using the flow injection system.

Whereas the PTFE filters were dried in an oven (as any adsorbed gas can be expected to evaporate immediately due to the high temperature) both impregnated particle filters were dried at room temperature in a clean chamber described by Sutton (1990).

6. EXAMINE '95

6.1 INTRODUCTION

A joint field campaign with participants from five European research institutes took place in June 1995 near North Berwick in East Lothian, UK. The objective was to measure ammonia exchange over a field of winter oil seed rape. Two ECN continuous wet denuder systems (AMANDA) were operated by the university of MADRID and the Institute of Terrestrial Ecology (ITE) to measure six point NH_3 profiles above and within the canopy. Three ECN batch denuders were operated to measure the concentration profiles of the gaseous species HNO_3, HCl and HONO. ECN was also running two newly developed steam jet aerosol collectors (described by Khlystov *et al.*, 1995), which were measuring NH_4^+ aerosol concentrations. Two combinations of optical particle counters (ASASP-X designed by Particle Measurement Systems, MFS) and sonic anemometers (asymmetric Solent sonic anemometers) were meant to measure size dependent particle fluxes at 2.27 and 4.74 m above the ground. The size dependent chemical composition of the atmospheric aerosol was measured by a six stage Sierra Andersen cascade impactor. Furthermore, surface and horizontal fluxes of NH_4^+ were measured using passive samplers; while up to ten filter packs were used to obtain more detailed gradients of particles, HNO_3 and NH_3 within and above the canopy and to present an independent means for quality control of the AMANDA measurements. SO_2 and CO_2 fluxes were detected by three point gradient systems using a TECON 42S analyser. The micrometeorological conditions were established by the means of a five point wind profile (Vector Instruments), a Campbell bowen ratio system and a combination of a symmetric Solent sonic anemometer and a Campbell krypton hygrometer (KH_2O) operating at a hight of 3.08 m.

During the hole campaign the meteorology was dominated by the centre of a strong high pressure system above the UK, which at its east side brought clean northerly polar air over the sea into East Lothian. During the first half of the campaign the wind veered briefly to the South and then to the West causing periods of slightly higher aerosol loadings and SO_2 concentrations towards the end of the measurements.

Until now, the chemical and numerical analyses have only partially been carried out. The steam jet ammonium samplers gave a first indication that no considerable particle gradient occurred - neither within nor above the canopy. The expected deposition velocity of about 1mm s^{-1} together with the low concentration of below 0.7 µg m^{-3} might have led to concentration gradients below the resolution of the equipment. However, a significant influence of GPC during the measurements can be ruled out, since the clean polar air led to a low background concentration of HNO_3 so that its concentration product with NH_3 probably hardly ever approached the equilibrium value necessary for particle production. As the detailed HNO_3 concentration data are not yet available, dissociation products could not be calculated for this report.

6.2 AMMONIA MEASUREMENTS

6.2.1 Example for diurnal cycles of NH_3 concentrations and fluxes obtained by annular denuders

Although the data have not yet completely been analysed, first results of both denuder and filter pack measurements of NH_3 are available. A typical diurnal cycle is presented for June 23rd 1995 in Figure 18, the micrometeorological data given in Figure 17. The wind direction was veering from the West in the morning to the East in the afternoon with the wind speed too low to measure the wind direction in the morning, but gradually increasing to up to a moderate 2.5 m s^{-1} in the late afternoon. As the remarkably smooth net radiation curve indicates, the sky was clear leading to very stable conditions during night and unstable conditions during day time. A negative latent heat flux (λE) during the early morning hours (4:30-6:00 GMT) indicates dew fall at this time followed by a relative sudden evaporation peaking at 7:50 GMT. The fact that at z_0' the water vapour pressure approaches its saturation value suggests that this peak really presents evaporation, although it cannot be decided whether this took place in the canopy or within the air chamber of the bowen ratio system. Poor agreement was found between the sensible heat flux as measured by the bowen ratio system and the values given by the sonic anemometer for this day. The agreement of the values for the wind speed at 1 m and u_* of the two systems (not presented in Figure 17) was much better.

On the other hand, reasonably good agreement was found between the two independent NH_3 denuder systems. The NH_3 concentration shows a diurnal cycle with lowest concentrations at night. Whereas the plume at 2:40 GMT might be due to a change in wind speed or direction the plume of up to 10 µg m-3 at 6 am (leading to a peak in the deposition flux of about 40 ng m^{-3}) was probably due to agricultural activities on farms located SW of the measuring site. Just after the dew fall the NH_3 flux changes from deposition to emission - possibly first enhanced by evaporation of the dew, later dominated by the stomatal activity. The highest emission values of up to 100 ng m^{-3} just before noon exceed the highest numbers of 40 ng m^{-3} found by Sutton (1990) over agricultural crop land by far. Although they also represent the maximum emission found during the campaign, fluxes of +60 to +80 ng m^{-3} were regularly observed under sunny conditions. With decreasing concentrations in the evening the uncertainties in the fluxes and thus the difference between the systems become larger, resulting in the ITE system showing emission and the MADRID system showing deposition at 21:00 GMT. After 22:30 GMT, however, both systems detect a deposition flux of about 20 ng m^{-3}. During the plumes the values of V_d are close to V_{max}, the maximum deposition velocity possible by turbulence, the ITE values being slightly above, the MADRID value slightly below V_{max}. Deposition to water films, i.e. dew, might be the dominating process leading to small canopy resistances.

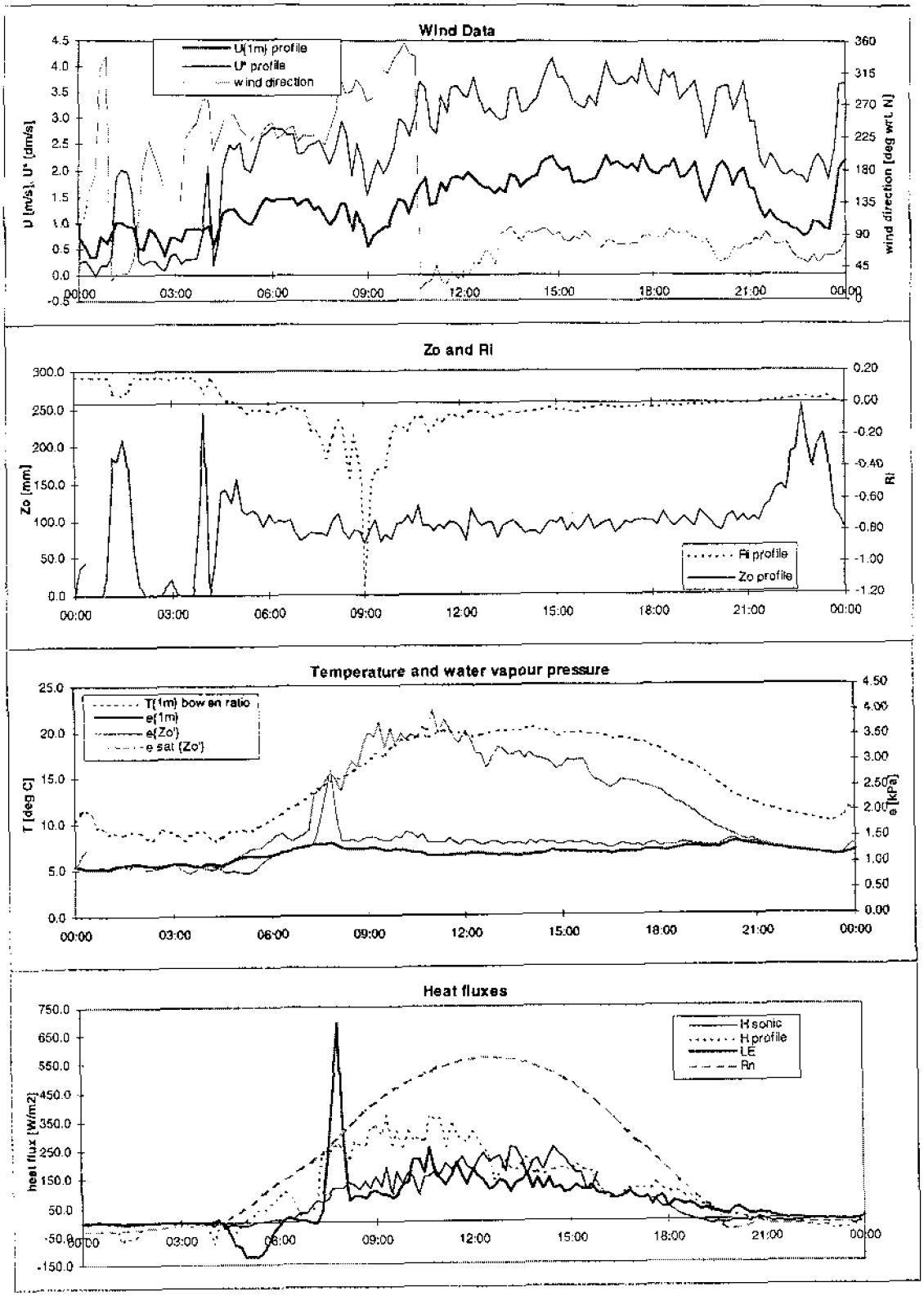

Figure 17: Micrometeorological data for the oilseed rape site of EXAMINE '95 for 23/6/1995

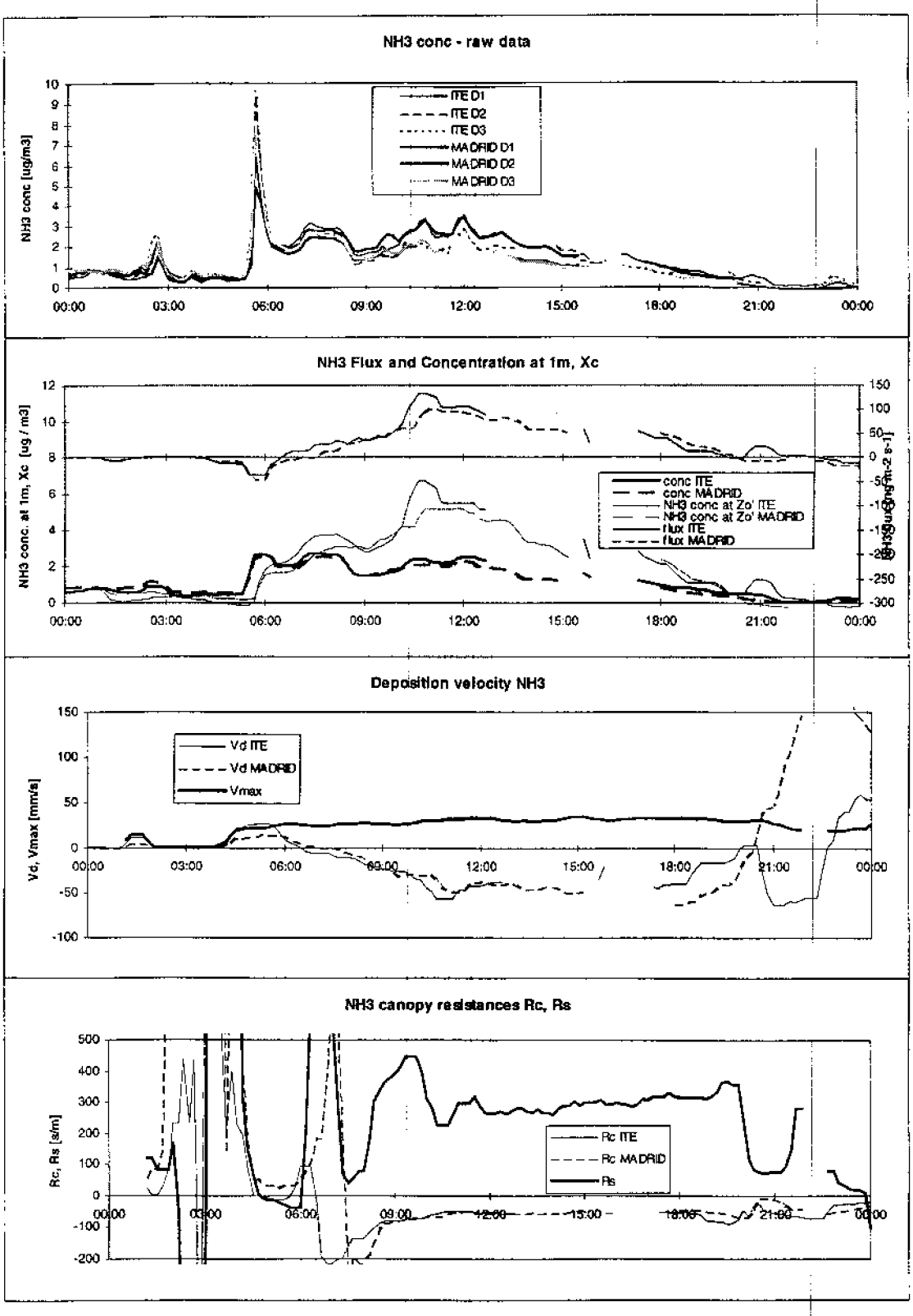

Figure 18: Ammonia concentrations, fluxes, deposition velocities and canopy resistances measured with two independent continuous wet annular denuder systems, here specified by "MADRID" and "ITE". The raw concentrations are presented as 10 min averages whereas all calculated values are presented as hourly running means of 10 min values.

6.2.2 NH_3 gradients obtained by filter packs

Filter pack measurements were carried out to assess the quality of the denuder and steam jet collector measurements by independent measurements of the gradients of NH3, HNO_3 and the aerosol species. Whereas the particle and nitric acid filters have not yet been analysed. Table 3 shows preliminary NH_3 concentrations and fluxes which will have to be corrected by the amount of NH_3 adsorbed to the HNO_3 filter. Some runs show significantly lower concentrations obtained with filter pack measurements (Runs 2, 3, 6, 7) which might be due to the high variability of the blanks of the batch of filters used for capturing NH_3 during the runs 1 to 7. The MADRID denuder system tended to show deposition when both other techniques and the micrometeorological situation indicated emission (e.g. Run 5, 16). More work needs to be done to compare the data of the different systems.

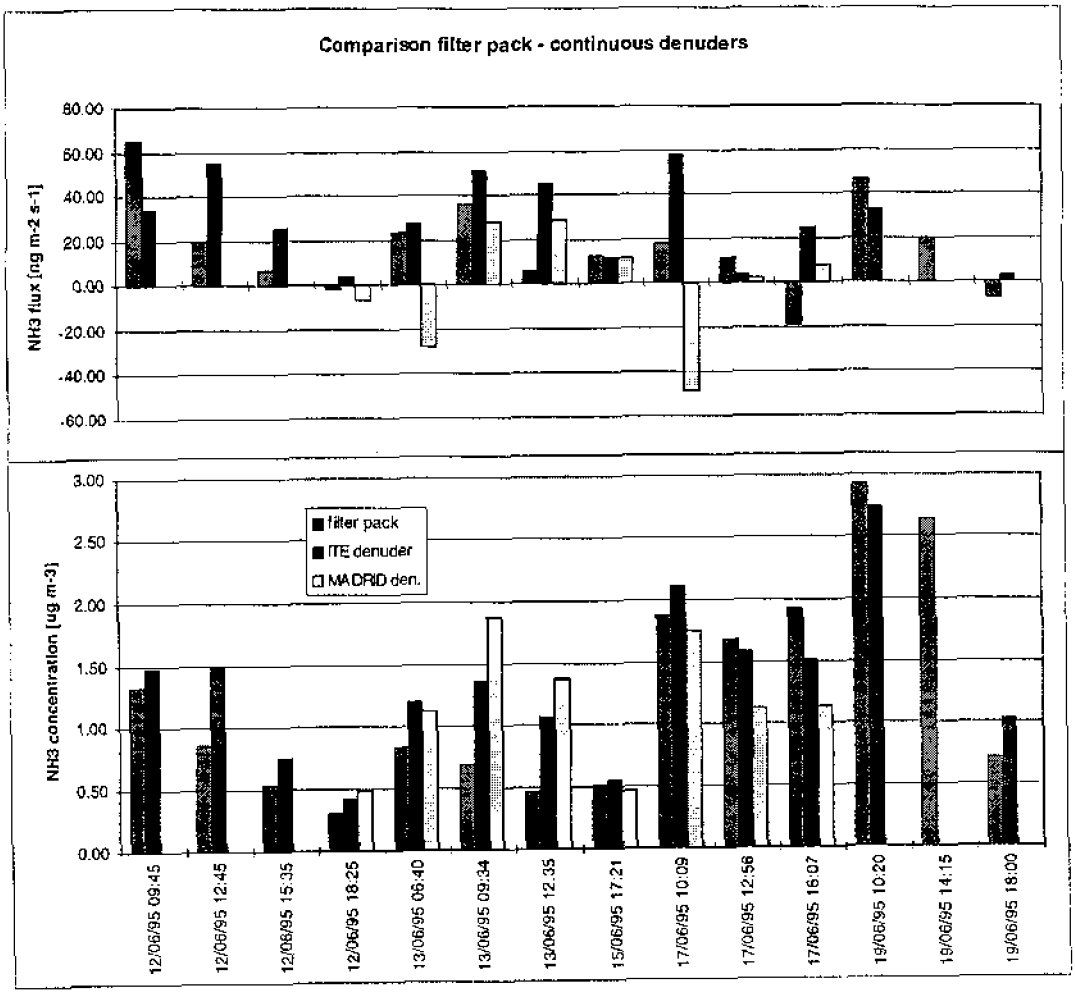

Figure 19. Comparison of NH_3 concentrations and fluxes as measured with filter packs and continuous denuder systems

Table 3: Comparison of NH_3 concentrations and fluxes as measured with filter packs and two independent annular denuder systems, here labelled 'ITE' and 'MADRID'. Brackets signify figures obtained by averaging only over a part of the period as the denuder system was not working continuously.

			NH_3 conc. (1m) ($\mu g\ m^{-3}$)			NH_3 flux (1m) ($ng\ m^{-2}\ s^{-1}$)			$V_d\ NH_3$ (1m) ($mm\ s^{-1}$)		
run no.	start time	end time	filter pack	ITE denuder	Madrid denuder	filter pack	ITE denuder	Madrid denuder	filter pack	ITE denuder	Madrid denuder
1	12/06/95 09:45	11:45	1.33	(1.47)		64.81	(34.05)		-48.82	(-23.22)	
2	12/06/95 12:45	14:45	0.85	1.50		19.84	55.10		-23.21	-36.85	
3	12/06/95 15:35	17:45	0.53	0.76		6.64	25.06		-12.54	-33.18	
4	12/06/95 18:25	20:41	0.30	0.41	0.49	-1.77	3.78	-6.37	5.79	-9.26	13.00
5	13/06/95 06:40	08:48	0.83	1.19	1.12	23.10	26.99	-27.85	-27.82	-22.61	24.76
6	13/06/95 09:34	11:39	0.68	1.37	(1.88)	36.31	50.64	(27.62)	-53.10	-37.05	(-14.68)
7	13/06/95 12:35	14:43	0.46	1.07	1.38	5.34	45.08	28.90	-11.52	-42.23	-20.96
15	15/06/95 17:21	20:18	0.51	0.55	0.46	12.68	11.58	11.54	-24.94	-21.18	-25.25
16	17/06/95 10:09	12:13	1.88	2.11	1.76	17.81	58.01	-48.21	-9.47	-27.53	27.39
17	17/06/95 12:56	15:19	1.68	1.59	1.12	10.81	3.35	2.24	-6.44	-2.11	-1.99
18	17/06/95 16:07	18:30	1.93	1.51	1.13		24.35	7.68		-16.10	-6.78
19	19/06/95 10:20	12:49	2.92	2.73		45.91	32.67		-15.70	-11.95	
20	19/06/95 14:15	16:33	2.64			19.58			-7.43		
21	19/06/95 18:00	20:28	0.71	1.03		-6.91	2.78		9.68	-2.71	

6.2.3 Within canopy profiles of NH_3

As to estimate the source contribution of NH_3 both the continuous annular denuders and filter packs were temporarily operated within the canopy to obtain profiles of up to 12 measuring heights. The Lagrangian method developed by Raupach (1989a, 1989b) can be used to derive source distributions from concentration profiles. This method also requires a parameterisation of the Lagrangian time scale and the variance of the vertical wind speed component, σ_w, as functions of height proving to be more sensitive to the latter. Measurements of σ_w within the canopy were carried out using a sonic anemometer. The sonic was logged at frequencies of 10 and 22.8 Hz; here the curve obtained using the higher frequency shows less scatter and a more consistent shape. As the mean eddy size within the canopy must be expected to be very small even the higher sampling rate might not have resolved them all. Above the canopy the ratio σ_w/u_* approaches a value of 0.98 which is in disagreement with the value of 1.25 reported in literature (e.g. Raupach 1989b).

The NH_3 concentration profiles show consistently high concentrations at the ground due to decomposing leaves which is positively correlated to the surface wetness. In general three distinct pattern, shown in Figure 21, can be identified. During measurements at the 14th and 15th of June the

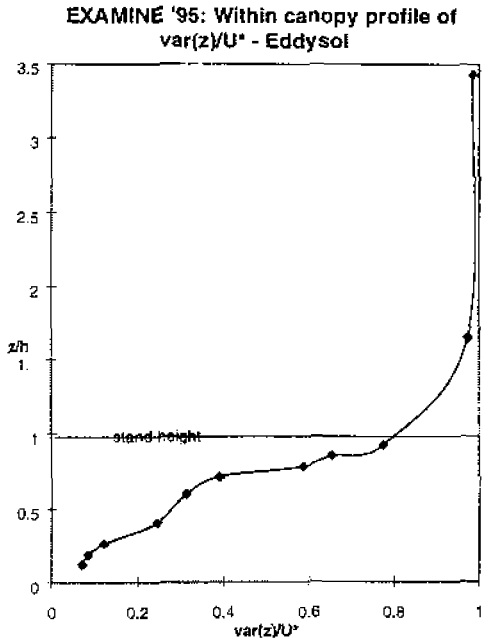

Figure 20: Profile of σ_w/u as measured within the oilseed rape canopy at the EXAMINE '95 campaign.

surface wetness was high and the rotting leaves were the major source (a) and the canopy acted as a sink still leaving some NH_3 pass so that a net emission flux can be observed. The source/sink analysis and the analysis of the apoplastic NH_4^+ concentration will show whether the stomatal compensation point was high enough to still control the net exchange.

Day measurements at the 21st and 22nd of June indicate a second strong narrow source at the top height of the canopy where the pods are (b). During night time conditions deposition occurs and, as the soil is wet (c) high emission, originates from the ground level. The upper layers of the canopy act as an efficient sink for the NH_3 both depositing from the atmosphere and being emitted from the soil. In case (d) a high NH_3 plume of 50 µg m^{-3} passed the site during the averaging period leading to a strong gradient above the canopy which subsequently propagated into the top layers of the canopy.

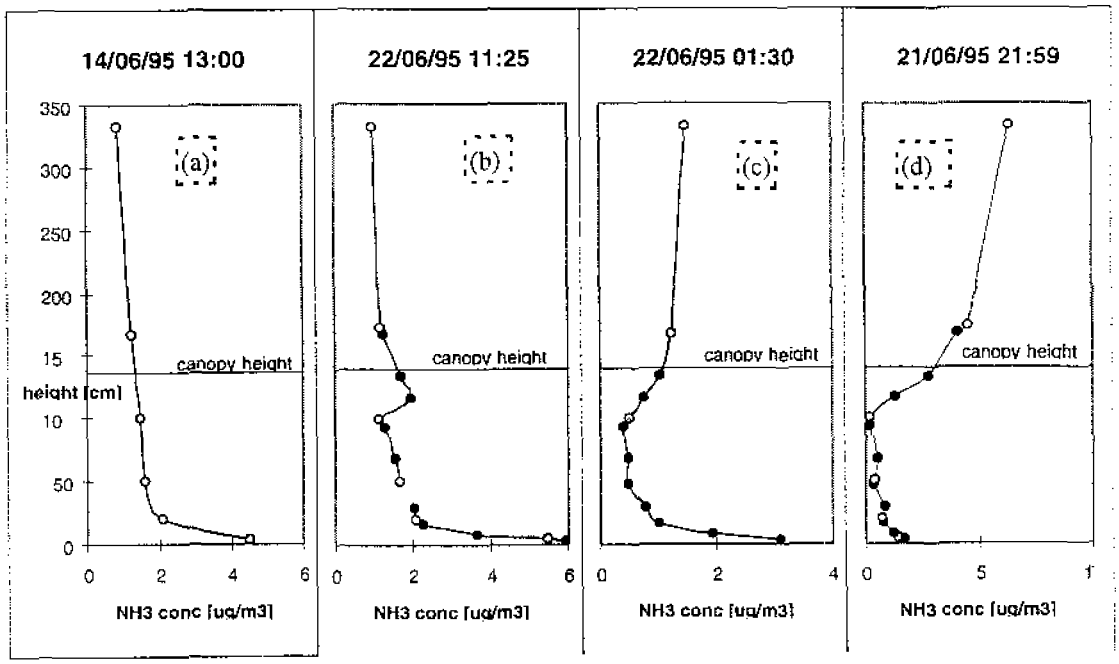

Figure 21: Within canopy profiles of NH_3 concentration measured with filter packs (black dots), ITE denuder (white dots) and MADRID denuder (grey dots). At the beginning of the campaign the only major source of NH_3 were de-composing leaves at the soil surface (a) the canopy acting as a sink still enabling net emission. Later on, however, a second source was found in the pods at the top height of the canopy (b). At night time conditions both deposition flux and ground emission flux are deposited in the canopy (c). (d) shows a night time period including a short plume of 50 µg m^3 leading to a high deposition profile with subsequent propagation of the high concentration into the canopy.

6.3 PARTICLE FLUX MEASUREMENTS

6.3.1 Introduction

Two combinations of optical particle counters (OPC), ASASP-Xs designed by Particle Measurement Systems (MFS), and ultrasonic anemometers were employed to measure the size dependent particle flux above the oil seed rape. The idea was to check whether any flux divergence occurred which could be attributed to gas-to-particle conversion of NH_3 to NH_4^+ salts. Some systematic errors in the set-up, however, made it impossible for fluxes to be calculated. The absence of NH_4^+ gradients indicated by the steam jet collectors and the low HNO_3 back ground concentration suggest that no flux divergence would have been found. Nevertheless, a closer look at the particle data obtained is worth in the light of improvements for future measurements.

6.3.2 Set-up

The asymmetric Solent sonic anemometers were mounted to poles of a height of 2.27 and 4.73 m facing west into the predominant wind direction. The attempt was made to keep the particle counters themselves sheltered in a cabin; this made an inlet tube of 13 m necessary. The set-up had to fulfil two requirements: Both particle losses and time delay by the sampling tube had to be kept as small as possible. The latter demands high gas flow rates, a fact which contradicts the small sampling flow of the OPCs used, i.e. 2 ml/s. Although this has been done by connecting the inlet of the OPC to a high air stream by a T piece (e.g. Neumann and den Hartog, 1985) iso-kinetic sampling is to be preferred, especially if larger particles are to be sampled. Here an iso-kinetic inlet as described and designed by Hummelshøj (1993) was used (see Figure 22). It consists of a stainless steal cylinder, tapered at both ends, through which a high air stream can be drawn. The particle counter is connected to a small tube that is centred in the cylinder and points upstream. The diameters of this tube and the cylinder were chosen so that sampling could be expected to be sufficiently iso-kinetic for a sample flow of 2 ml s^{-1} at air flow rates of 30 to 60 l min^{-1}. An additional inlet further downstream acting as an underpressure valve had to be added since the well balanced air flow system within the OPC proved having difficulties drawing the sample against too low pressure: In order to guarantee that a very narrow sample beam crosses the laser of the OPC vertically and to prevent particles from entering the optical system, the ASASP-Xs make use of a clean sheath flow focusing the sample flow. The well functioning of the OPCs largely depends on the ratio of these two flows and any disturbance leads to immediate contamination of the optical parts which can be seen in a drop of the reference voltage V_{ref} indicating power loss of the laser beam.

Another means to minimise losses of fluctuations of the particle concentration is to keep the air stream turbulent (Lenschow and Raupach, 1991). This can be checked by considering the turbulent Reynolds number $Re=VD_i/\nu$, V being the velocity of the air stream, D_i the inner diameter of the tube and ν the kinematic viscosity of air, which should exceed the critical value of 3000. A laminar flow leads to smoothing of the signal and large residence times enhancing deposition of larger particles to the tube walls. This is especially important for plastic tubes which tend to charge up and capture larger particles.

For the EXAMINE campaign PVC tubing with a 10 mm bore was chosen. In order to maintain a sufficiently high flow rate despite the considerable resistance of the tube a strong pump had to be employed. This high resistance also dropped the pressure in the iso-kinetic inlet which resulted in a high flow rate through the underpressure valve. The flow rate through the valve was risen to 28.6 l min^{-1} compared to 34.3 l min^{-1} for the sample air stream.

Using these flow rates the Reynolds number was greater than 5500 and the time lag could be estimated as about 2 s. The inlet tube was connected to the rear pole of the sonic cage facing downwards.

All 32 size channels (logarithmically spaced between 0.1 and 3 µm diameter plus oversize channel) of the OPCs were logged at 10 Hz using a data logger built by UMIST. The analogue outputs of the sonic anemometers were also connected to the ADCs of the same data logger but 40 Hz signals were averaged to 10 Hz as to filter out high frequency noise and reduce aliasing from higher frequencies. The 10 Hz data was then stored on adequately large hard disk drives.

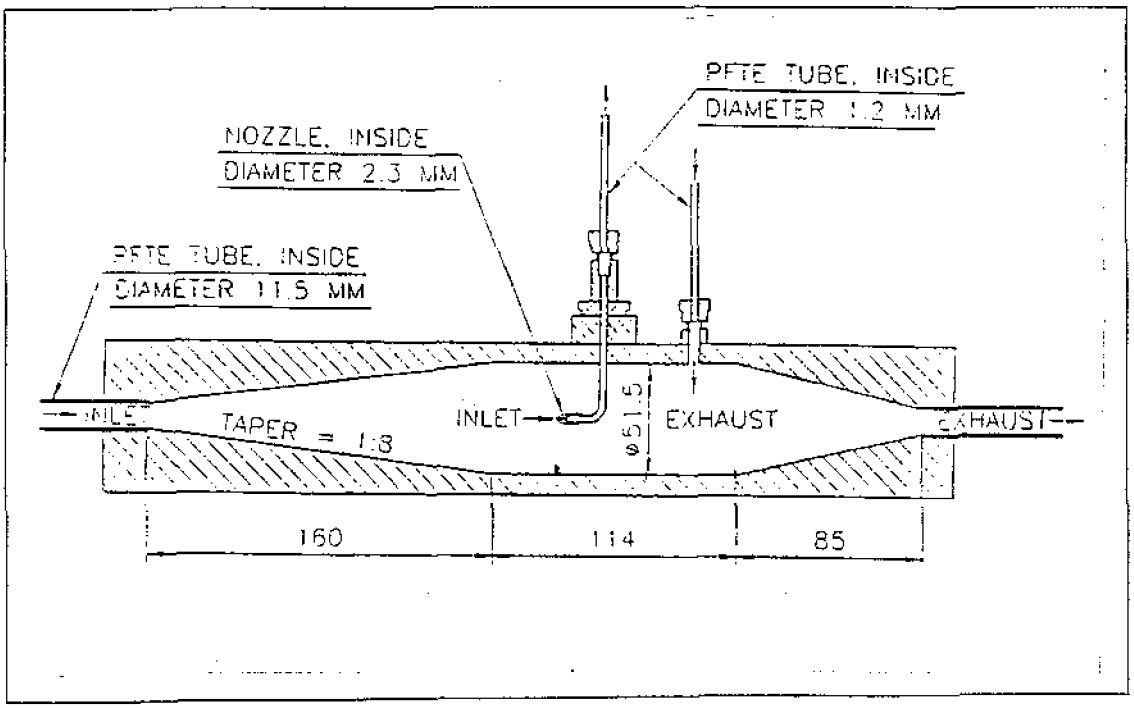

Figure 22: Outline of the iso-kinetic inlet designed by Hummelshøj (1993).

6.3.3 Problems with the set-up

1) Zero drift of the analogue to digital converters (ADC)

Already during the setting-up it became obvious that the two sonic anemometers connected to the same ADC system, and thus using the same ground, interfered with each other leading to independent zero drifts of the ADC channels. Mainly the logging of the vertical wind component was effected. Here a small offset showed a great effect on small values and in the data analysis the vertical wind component was used to detect deviations of the sonic from the vertical and to rotate the wind components accordingly. Afterwards it was not possible to distinguish between a contribution to a mean vertical wind component caused by misalignment from the z axis or by the ADC offset. The drift was too strong for regular zero checks to be used for correction. This problem could in future be overcome by logging

the digital data from the sonic anemometers directly instead of converting them into an analogue signal in between.

2) Charging up of the PVC tubing

Over the time the PVC tubing showed visible amounts of particles which had settled to its walls. The use of metal tubing (copper or stainless steal) would prevent these losses of bigger particles due to electrostatic forces. The quantification of the losses due to the tubes needs further examination of collected data and laboratory tests.

3) Sampling of the iso-kinetic inlets through the valves

The greatest problem, however, was caused by the choice of the flow rates for the iso-kinetic inlets. Although the underpressure valve was placed downstream and the flow rate through the valve was less than half of the total rate sucked out of the inlet by the pump the OPCs were measuring air entering the iso-kinetic inlets through the valve as well as the sample tubes. Hence the measured fluctuation in particle concentration was only partially related to the change in concentration at the site of the anemometers partially related to changes at the surroundings of the OPCs themselves. This effect was detected and examined using both OPC probes, the inlet of one (measured by probe 1) connected to the valve of the other (measured by probe 2) so that the particle concentration of the flow entering the valve and its effect on the reading of the concentration in the iso-kinetic inlet could be established at the same time. Now particle plumes were generated at the inlet of the iso-kinetic inlet no. 1. As there are differences between the two probes in both sizing and sensitivity one has to be corrected to the other which was done by sampling lab air and comparing the numbers of particles detected over a period of 10 min. The generated particle plumes contained a great number of bigger particles whereas their concentration of the lab air was very small giving a low background concentration of about 6 particles ml^{-1} for particles with a diameter $D_p > 0.35$ µm. Unfortunately the small numbers of counts in this size range led to an inaccurate comparison of the probes in this size range. As it will become obvious from the results more calibration work is necessary in order to be able to interpret the ratio of the plumes measured as an absolute number. Until now it is only an indication of the magnitude of contamination caused by the valve.

Figure 23 shows a typical response in the iso-kinetic inlet no. 2 using the flow rates used during EXAMINE '95.

For the comparison of the magnitude of the plumes the area under the peaks was used rather than the peak height. This was done by subtracting the mean background concentration and integrating over the peak. Comparison of the background concentrations showed probe 2 was overestimating the concentration by less than 10%. However, using higher flow rates probe 2 was detecting up to three times as many particles as were introduced through the valve. Thus although the calibration of the probes seems appropriate for low concentrations it is not valid for high concentrations. Figure 23 shows a clear response of probe 2 and a comparison suggests that probe 2 is reading 93% of probe 1. This test was done using different flow rates and manipulations of the iso-kinetic inlet. The results are summarised in Table 4.

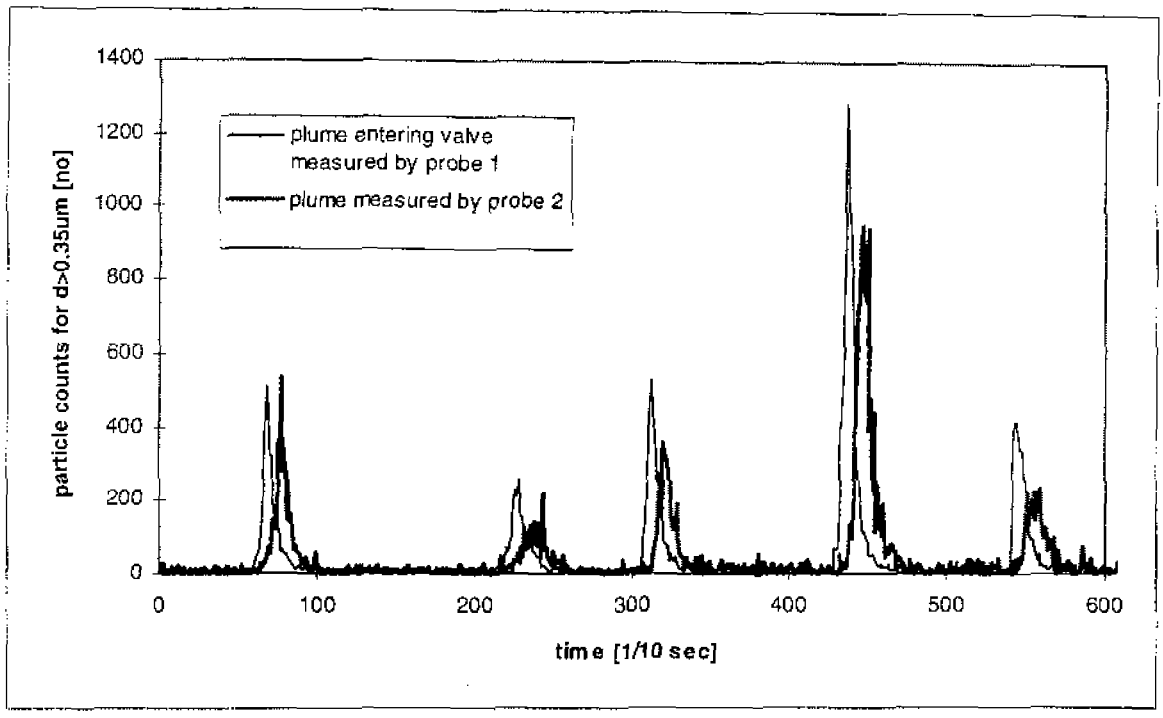

Figure 23: Sample of the contamination caused by the valve of the iso-kinetic inlets for flow rates as used during EXAMINE '95

Table 4: The magnitude of the response to contamination through the valve for different flow rates and set-ups.

description	valve flow [l/min]	sample flow [l/min]	ratio sample/valve flow	response (not to be interpreted as absolute percentage)
as used at EXAMINE '95, inlet tube 13m	28.6	34.3	1.2	93 %
higher flow rate	59	61	1.03	287 %
lower flow rate	11	9.4	0.85	8.1 %
valve narrower	5.7	56	9.9	below detection limit
valve inlet bent downstream, 10 cm long	28.6	34.3	1.2	2.8 %
no inlet tube	5.7	56	9.2	below detection limit
3m inlet tube	11	45	4.2	6.5 %

The tests lead to the following results:

a) The contamination increases with the valve flow rate rather than with the ratio of valve to sample flow rate. Although the valve flow rate exceeded that of the sample when a smaller pump was used it caused a lower contamination. In order to establish the accurate reason the stream line pattern

within the iso-kinetic inlet would have to be modelled. Obviously, more backward turbulence is generated by higher valve flow rates.

b) Using the pump and the tube material used during EXAMINE '95 even an inlet tube of 3 m length leads to a resistance sufficiently high to increase the valve flow rate to 23% of the sample flow and causing a contamination response of 6.5%.

c) Without modifying the iso-kinetic inlet either the sample flow rate or the resistance of the sampling tube has to be decreased. Since the latter would mean the use of a wider or shorter inlet tubes both demands contradict the purpose of iso-kinetic sampling, which is to enable the use of long inlets with high flow rates thus short transport times.

d) Two modifications of the iso-kinetic inlet have been tried: Firstly, the valve was extended into the iso-kinetic inlet and the tube bend approximately 10 cm downstream. Surprisingly, this still led to a detectable contamination using the flow rates of the EXAMINE '95 campaign. Secondly, the valve was partially blocked decreasing the valve flow from 85% to 10% of the sample flow. Here no contamination could be found anymore. However, the pressure in the iso-kinetic and inlet dropped and, as expected, the reference voltage of probe 2 decreased by 0.4 V. A long term run is necessary to show whether the probe still performs sufficiently well under these conditions or whether the disturbed flow pattern causes contamination of the optics of the OPC especially if operated in dirty surroundings.

Finally it should be mentioned that both iso-kinetic inlets used showed the same features. Iso-kinetic inlet 1 showed a response of 93% where inlet 2 showed 91% contamination. Hummelshøj (1992) used an identical iso-kinetic inlet connecting the valve to the exhaust of the OPC. This way the whole system of the OPC operates under low pressure and the pump does not have to overcome the big pressure difference. Moreover, the air flow through the valve equals the small sampling flow of the OPC (about 2 ml s^{-1}) and its concentration that of the air sampled. This set-up was tried in the field during EXAMINE '95 but led to a considerable drop in the reference voltage although Hummelshøj (1992) used a similar set-up (15 m Teflon tubes, 11.5 mm bore, flow rate 30 l min^{-1}). A possible reason might be the use of a diaphragm pump during EXAMINE '95 causing a pulsing air stream not only through the iso-kinetic inlet but also within the OPC.

4) High frequency contamination by the use of a diaphragm pump

The effect of the diaphragm pump became obvious while measuring the time lag caused by the inlet tubes with a set-up where both iso-kinetic inlets were connected by one of the inlet tubes and the time for particles travelling from one sensor to the other was measured. Figure 24 shows such a response curve. The signal measured by probe 2 seems to be superposed by a 5 Hz oscillation. As inlet 2 was directly connected to the pump (tube length about 1.5 m) here the vibrations were not damped as they were at inlet 1 connected by the 13 m tube. Moreover, inlet 1 being open to the ambient air enabled rapid reactions to pressure changes again damping the oscillation.

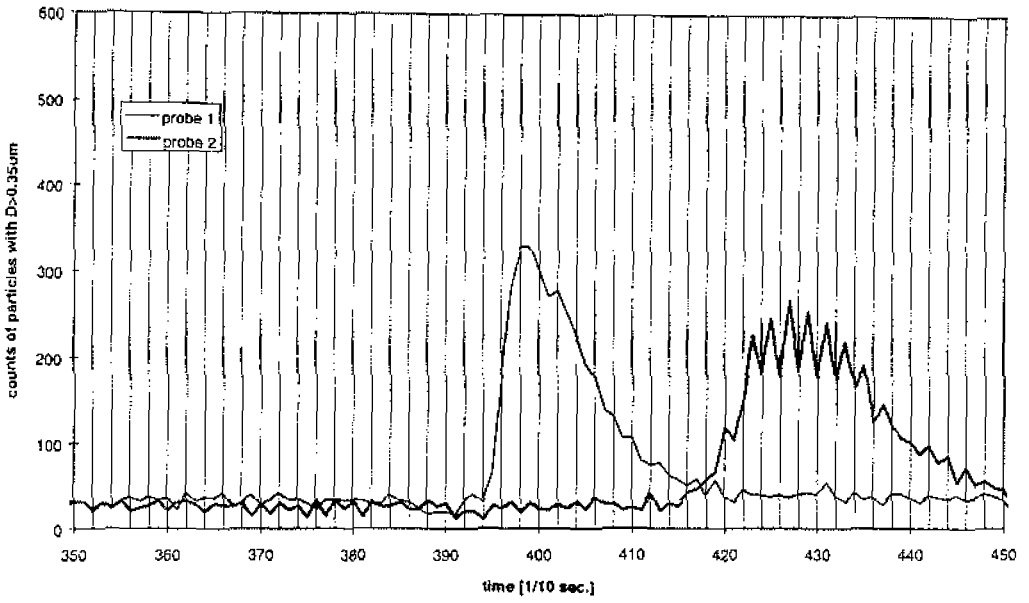

Figure 24: Measurement of a particle plume passing through both iso-kinetic inlets connected by inlet tube 2 in order to measure the time lag. Probe 2 shows contamination by superposed 5 Hz oscillation of the pump.

This 5 Hz frequency should also appear in the power spectrum of the particle concentration. Figure 25 shows the spectrum for the vertical wind component, w, temperature and particle concentration for diameters below 0.7 µm calculated by the application of a fast Fourier transform routine to 32,768 data points representing approximately 55 min. The power of the frequencies was then averaged over 60 intervals equally spaced on the logarithmic ordinate leading to high scattering for low frequencies (few values per interval) and a smooth curve for high frequencies. For additional smoothing several subsequent 55 min periods were averaged. The curves for w and T show the features found by other authors (e.g. Fontan *et al.*, 1995; Neumann and Hartog, 1985) apart from relatively high low frequency contributions for the variance of temperature. But both authors do not consider such low frequencies and the change in temperature within an hour can be significant. The power spectrum of the particle concentration is expected to have a higher low frequency contribution than the one of w and T but to approach their shape at higher frequencies. The measured spectrum, however, shows a very high contribution of high frequencies, especially of a frequency of about 4.7 Hz matching the shape of the response curve in Figure 24. Usually frequencies are normalised by multiplication with z/U in order to enable intercomparison of data acquired at different meteorological conditions. This leads to a shift along the ordinate by ln(z/U). This was, however, not done for the representation of Figure 25 as to show that the particle concentration spectra match accurately for higher frequencies which should, neglecting the shift, not be the case. The high frequency contribution could represent white noise due to the measuring probe or just the statistical distribution of the particles (see Neumann and den Hartog, 1985) but the peak at 4.7 Hz is certainly due to the set-up. In contrast, the curves for the power spectra of w and T as measured at 2.27 m do not match the curves of 4.73 m (not shown in Figure 25).

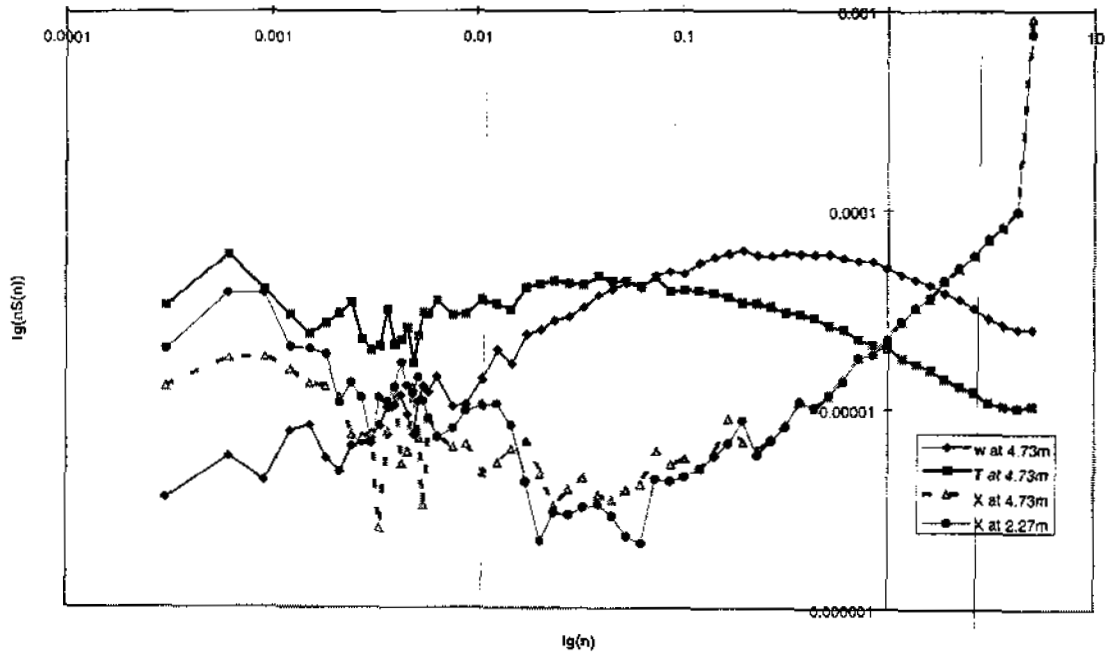

Figure 25: Power spectra of vertical wind component, temperature and particle concentrations for diam. D_p<0.7 μm for probe 2 at 4.74 m for the 22/6/95. The power spectrum of the particle concentration shows a high contribution of both low and high frequencies which is independent of the measuring height, hence the meteorological situation.

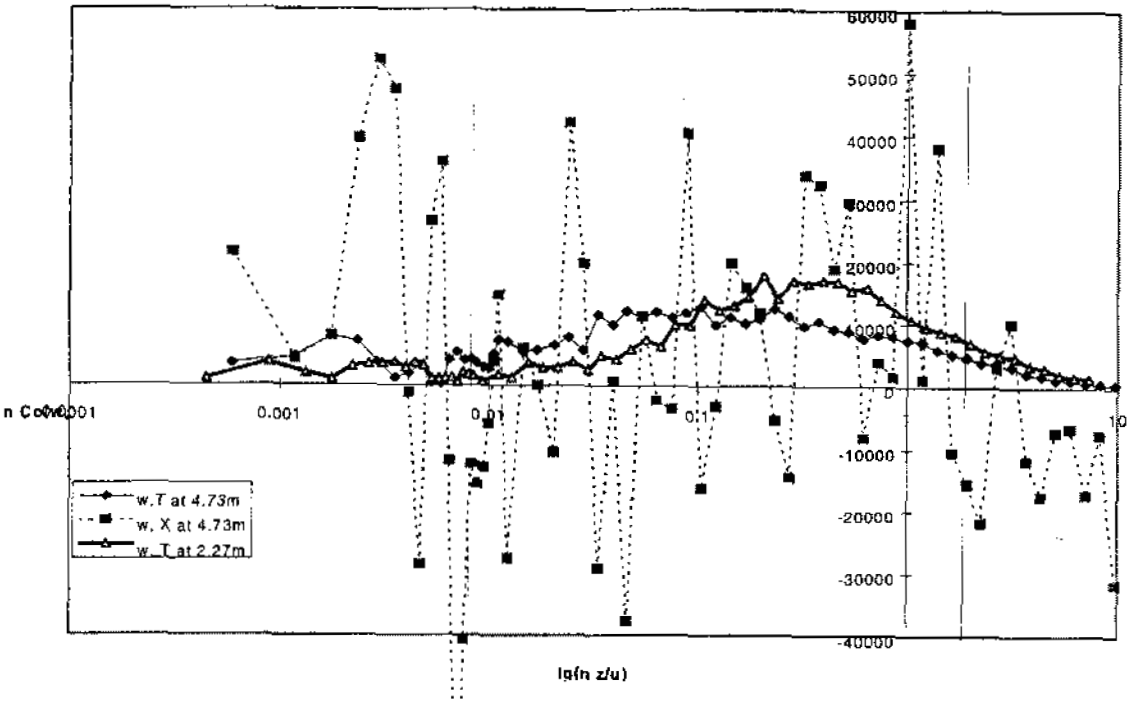

Figure 26: Co-spectra of wT and wχ for both heights. Whereas the co-spectra for wT show expected shapes w and χ do not seem to be correlated. Note that the contribution of the frequencies to the flux is shifted towards higher frequencies closer to the canopy reflecting the small mean eddy size

From the considerations so far it is questionable that the measurements are good enough to calculate particle fluxes and deposition velocities. A better indication, however, can be given by looking at the

co-spectrum of vertical wind component, w, and the particle concentration, χ. Again a fast Fourier transform was used taking the time lag into account. Once more the co-spectrum of w and T shows the expected shape. Despite the correction for height and mean horizontal wind speed by rescaling the ordinate the curve for the lower measuring height (2.27 m) is moved towards higher frequencies with respect to the curve for the higher height (4.73 m). Closer to the crop height we can expect the mean eddy size to be smaller. Vertical wind speed, w, and the particle concentration, χ, do not seem to be correlated whatsoever, the chart shows random scatter. This is the most significant sign for the particle data to be too contaminated to obtain reliable fluxes. Hence it does not seem reasonable to look at the data in more detail..

6.3.4 Suggestions for further measurements

The following alterations for further measurements seem advisable:

1. If two Solent sonic anemometers are to be logged at the same time the digital signal should be used to avoid interference of the two ground potentials.
2. Taking the OPCs out into the field and placing them into boxes close to the sonic anemometers and using thin metal pipes and only the sample flow of the pumps of the OPCs would solve all the other problems at the same time. Metal pipes do not charge up and attract the particles. Drawing the sample from the sonic height to the OPC using the built in pump of the OPCs leads to bigger time lags which have to be corrected for but does not demand the use of iso-kinetic inlets at all.
3. Alternatively, the valve has to be partially blocked reducing the air flow passing it. It has to be checked, however, whether this effects the flow within the OPCs. The use of a pump producing a smooth air flow instead of the diaphragm pump or damping of the oscillation by connecting the pump to the iso-kinetic inlet via a large air volume might enable the exhaust of the OPC to be connected to the valve which would overcome the contamination problem. Still it seems advisable to use metal pipes which would neither be easy to handle nor cheap if in the dimensions of the inlets used.

6.3.5 Estimation of the time lag caused by the inlet tubes

In order to calculate the particle flux by eddy correlation methods it is necessary to synchronise the reading of the sonic anemometers and the OPCs. A phase shift of a few seconds has been estimated to lead to an underestimation of the flux. The time lag caused by the travel time of the air through the inlet pipe was estimated in three different ways:

1. The dimensions of the tube and the iso-kinetic inlets were measured together with the flow rates. The mean residence time could be calculated. This method is referred to as the 'theoretical method'.
2. Two iso-kinetic inlets were used in series, connected by the inlet tube under consideration. Particle plumes were send through the tube and the time delay detected by the OPCs (see Figure 24). As the travelling volume was increased by the part of the first iso-kinetic inlet behind the OPC sample tube

the time had to be corrected using the flow rate and the volume of the rear part of the iso-kinetic inlet. This method is thus been called the 'semi experimental method'.

3. And finally the time lag was tried to be calculated from the data. This was done by calculating the cross-correlation coefficients for a range of time lags (1.2-2.5 s) by spectral analysis methods. 4096 data points were used. In order to condition the data it was de-trended, the first and last 2.5 s were replaced by zeros (zero padding) and data windowing using a Hanning window (e.g. Press *et al.*, 1992) was applied to the rest of the data. The Fourier transform was calculated for both the data for the vertical wind component and the particle concentration. Now one transform was multiplied by the complex conjugation of the other and an inverse transform was applied to the result giving the correlation factors for the different time lags. The greatest modulus of the values within the time range under consideration was chosen as the time lag. However, since the correlation between w and χ was too poor this method leads to random scattering, the average time lag of 1.83 s being close to the mean of the interval taken into account (1.85 s), whereas the cross correlation of w and χ shows a clear maximum for zero time lag. This is shown in Figure 27.

Despite the systematic errors in the set-up Figure 28 shows particle concentration and calculated deposition velocity for June 22nd. The particle concentration represents 10 min values of the measured concentration of particles with a diameter less than 0.8 µm (channels 1-20). The deposition velocity is presented as an running hourly mean of 10 min values with positive values indicating deposition and shows a fluctuation around zero which is neither correlated to the time lag automatically calculated nor the friction velocity u_* again proving the inadequacy of the set-up. The particle concentration shows a smooth curve with higher concentrations during day time. Here it must be suspected that not only the particle concentration at the inlet height but also in the cabin around the iso-kinetic inlet is reflected.

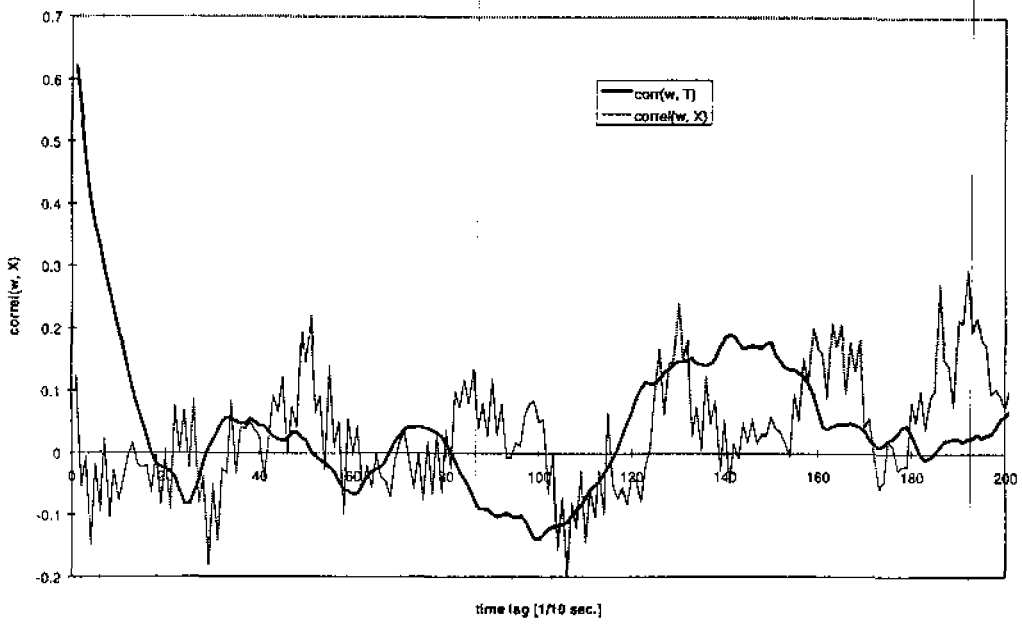

Figure 27: The cross correlation for wT and wχ for different time lags calculated by spectral analysis. A clear maximum for the correlation of w and T can be seen for zero time lag whereas w and χ do not show a significant extremum in the region of 1.5 to 2.5 s the time lag caused by the sampling tube.

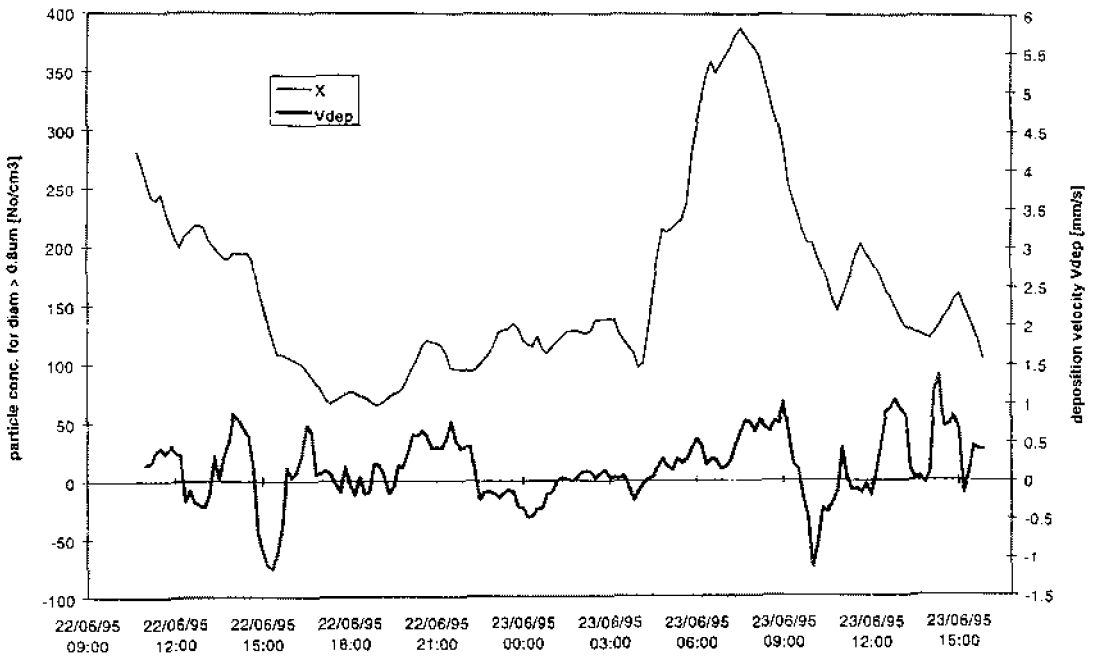

Figure 28: Example of the calculation and deposition velocity of particles with a diameter of less than 0.8 μm measured at 4.73 m. The concentration is plotted as 10 min averages, the deposition velocity as 1 hour running means.

7. SUGGESTIONS FOR FURTHER WORK

7.1 DATA ACQUISITION

7.1.1 Simultaneous measurements of the gradients of NH_3, gaseous acids and aerosol

The GPC models require either the input of concentrations at two heights or the input of concentrations at one height and a description of the surface conditions including the values for R_b and R_c as well as the surface concentrations of the tracers, especially NH_3. If the first method is used the concentrations have to be measured very accurately and the fluxes have to be extrapolated to the surface whereas the second approach requires good knowledge of the processes of the atmosphere/surface exchange and the physiological state of the plant community.

The measurements carried out during the EXAMINE '95 campaign, ie.

- automated concentration measurements of NH_3, NH_4^+, HNO_3, HCl and H_2SO_4 together with
- filter pack gradient measurements of Cl^-, NO_3^- and SO_4^{2-} and
- measurements of both the flux and chemical composition of particle of different sizes and
- explicit determination of the canopy compensation point by analysis of the intercellular liquid

would potentially have provided good input data for the models if GPC had taken place at this site. Although this site might be representative for Scotland and GPC might eventually be found to have a negligible effect in this area, it seems advisable to make measurements in extreme situations. High background concentrations of HNO_3 and HCl and strong NH_3 gradients would enable examination of GPC processes and reaction kinetics without being too much restricted by the detection limits of the analysers. From the experiences gained during EXAMINE '95 and treating the Halvergate '89 data the following conclusions and suggestions for further data acquisition must be drawn:

1. The concentration of the different chemical species should be **measured at the same height** in order to provide good input data.
2. Recent developments in measurement techniques of measuring particle fluxes of different chemical composition enable **continuous automated aerosol measurements** alongside automated measurements of NH_3 and HNO_3 and HCl using AMANDAs and batch denuders, respectively. Attempts are being made by ECN to connect a ion-chromatography system to the steam jet aerosol collectors. This would be a major improvement for measurements in situations where both equilibria with HNO_3 and HCl have to be taken into account since in this case modelling requires the input of the concentrations of both particulate NO_3^- and Cl^- so that bulk NH_4^+ concentrations are not sufficient.
3. Although fluxes of **nitrate and chloride aerosol** might be estimated by **filter pack measurements** the results are **not accurate enough** to use the concentrations detected at two single heights as model input.

4. A **high background concentration of the acids** is desirable so that the effect of GPC becomes *more significant.*
5. Measurements should be carried out for **both strong ammonia deposition and emission situations**. Equilibrium considerations have indicated that the processes are quite different depending on whether the in-equilibrium is driven from the ammonia release at the surface or from insufficient mixing in the atmosphere.
6. **Temperature and humidity** have shown to have a great impact on the reaction rates and kinetic constraints. Measurements should be carried out over a big range of both variables and their values has to be established as accurately as possible (see problems with Halvergate data).
7. ***Direct measurements of the canopy compensation point*** *can increase the applicability of the* inferential models.
8. ***Particle size spectra of*** NH_4NO_3 ***and*** NH_4Cl *and the* aerosol composition are important as to estimate the chemical time scale and thus the importance of GPC.

Plans are being set up to make measurements over grazed grass land in the Netherlands in spring 1996 as a part of the EXAMINE project. Measurements at the site under consideration have shown average NH_3 concentrations of 5 $\mu g\ m^{-3}$ and equally high HNO_3 concentrations can frequently be found during the summer months. It should be possible to consider all the issues mentioned above.

7.1.2 Particle fluxes

Size dependent particle flux measurements can give indications of quality and quantity of the formation and evaporation processes of NH_4NO_3 and NH_4Cl aerosol if done at different heights. Thorough investigations in possible set-ups have been described in section 6.2 and during a short field campaign in October 1995 at Connah's Quay, UK, the suggestions will be tested. It is planned to log the digital signal of the sonics and to test two different set-ups.

1. The OPCs will sample the air using their own flow rates of 2 ml sec through a short copper pipe.
2. The iso-kinetic inlets will be operated in a set-up where the under pressure valve is connected to the exhaust of the OPC.

The aim is to find an adequate set-up which can then be used during further field measurements in summer. The quality of the set-ups can now quickly be established as computer programs for both examination and flux analysis programmes are ready for use. However, the lowest size range the ASASP-Xs can detect, 0.1 µm, might be to large to detect particle formation and growth. Thus differential mobility analyser (DMAs), which often can scan the size range from 1 nm to 1 µm, might be more suitable. However, their time resolution is limited to a few minutes so that fluxes cannot be measured by eddy correlation methods.

7.2 MODELLING

7.2.1 Assessment of the models by measured data

1. HALVERGATE:

   First conclusions obtained by applying GPC models to data collected in 1989 at Halvergate have been reported. A poster on this subject has been presented at a conference on NH_3 and a paper version is being submitted to the conference organisation team and will be published in a 'poster book'. As some HNO_3 data have not yet been included the analysis of the Halvergate data will be extended and and an expanded paper, also outlining the model changes described above, will be submitted to a refereed journal.

2. EXAMINE:

   As this work is founded as part of the EC EXAMINE project some time will be spent on the chemical and numerical analysis of the EXAMINE '95 campaign. Although it is unlikely to extract useful model input data, experience in NH_3 flux measurements will be gained. Further insight in the processes of the surface/atmosphere exchange of NH_3 will improve the formulation of the lower boundary conditions if GPC models are run with the input of concentrations at only one height. Furthermore, the concentration products of NH_3 and the HNO_3 (or HCl) will be calculated and tested against theory.

   Work will include setting up an ion-chromatography system at ITE for analyse the particle and HNO_3 filters, the analysis itself (anion-chromatograph, NH_4^+ flow injection), calculation of NH_3, SO_2 and CO_2 fluxes, derivation of the source/sink distribution of NH_3 in the oilseed rape canopy and the development of models describing the exchange process.

3. LIFE:

   Again this site might not have produced adequate input data but the calculation of the concentrations products can give further insight into restrictions of the equilibrium formation.

4. ADEPT:

   During the ADEPT campaign in May / June 1995 in Devon, UK, the NH_3 emission from slurry stripes and its dispersion have been examined by measuring horizontal gradients downwind and vertical fluxes at different distances from the source. As NH_4^+ and HNO_3 concentrations were measured at the same time this data might include some information about the reaction rates. First results have shown that HNO_3 was not depleted by the large emission of NH_3 as expected from equilibrium consideration, but was emitted by the slurry itself. The specific chemical production process is still unclear. Furthermore, here two time scales associated with great uncertainties interact with each other: the time scale of the diffusion and that of the chemical reactions. Since the time scale of horizontal diffusion is much smaller than the time scale of vertical diffusive transfer, changes in NH_4^+ aerosol and HNO_3 concentrations might be below the detection limit. Nevertheless, this data set is worth looking at.

5. LEENDE:

   Similar to the Halvergate experiment, simultaneous measurements of NH_4^+ (unfortunately not NO_3^- and Cl^- seperately), NH_3, HNO_3 and HCl were carried out in 1982 at a site at Leende, NL. As countergradients of NH_4^+ and high deposition rates of atmospheric acids was found this dataset is likely to include further input data which will be looked.

6. Simulated data:

   Duyzer *et al.* (1995) used modelled data as input for NO_x models. This way problems of data acquisition can be overcome. However, it has to be checked whether accurate enough NH_3 data can be produced this way (since NH_3 is governed by small scale transport) and whether the transfer from model data to the 'real world' and the application of the results to measurement data would be valid. Without putting too much emphasis on this approach simulated data might be used for inter-comparisons.

7. Further data:

   Literature will be searched for further adequate input data. Field campaigns especially aimed to provide model input data will be set up during the next year.

7.2.2 Specification of the reaction rates

More work is necessary as to establish the magnitude of the equilibrium constants and the reaction rates. Measurements of the concentration product $[NH_3][HNO_3]$ have shown too high values for high relative humidities and low temperatures. If this is due to GPC it should be possible to see the same effect in the model results. Particle flux measurements could give indications for how the aerosol size and composition effect the dissociation constant. Some more information can still be drawn from literature on this issue.

If consistent input data were used and if the models were correct the reaction rates would remain the only unknown. Changing the reaction rate coefficients k_1 and k_3 until the interpolated concentration profiles at the surface match the values calculated from inferential data the reaction rate coefficients can be determined. So far the sociation coefficients have been kept constant and k_2 and k_4 have been calculated according to the value of k_p and the equilibrium aerosol concentration (as suggested by Kramm and Dlugi, 1994). However, this approach might not be correct as k_1 and k_3 could change with height as well. New parameterisations need to be found.

7.2.3 Inclusion of reactions with H_2SO_4 and possibly SO_2

The description of the chemistry of gaseous NH_3 is not yet complete. The criticism of Duyzer *et al.* (1995) that models for the reaction cycle of NO_x introduce a bigger error than the application of the uncorrected gradient method probably also applies to NH_3 in many situations. The Halvergate dataset shows situations (e.g. run 1 and 2) where the NH_4^+ on the particle filters exceeds the sum of NO^-, Cl^- and SO_4^{2-} significantly. The relatively high levels of SO_4^{2-} also indicate that the reaction with H_2SO_4,

probably formed as a secondary product in situ, needs to be considered - not as an equilibrium process but as a further sink for NH_3. As mentioned before high NH_x concentrations rise the pH enhancing the oxidation of SO_2. This process needs to be looked at in detail.

7.2.4 Further model intercomparison, determination of the surface conditions

As discussed in detail before, the conditions of the concentrations at the surface are not well understood. The theory that there must be equilibrium at the surface has to be looked at and in this process it is worth including the transport through the quasi laminar sub-layer into the models. Though shallow, transport mechanisms differ immensely in this height region and in the case of NH_3 emission high surface concentrations might give rise to high deviation from equilibrium. It might be worth considering multi-layer models and the effect of locally high humidity gradients in the vicinity of the stomata.

As soon as appropriate input data are available the inferential approach has to be tested against the two point boundary approach which might give further information about the surface conditions.

7.3 Examination of the processes governing the formation of aerosol in gas-to-particle conversion

The formation of NH_4NO_3 by the reaction of NH_3 and HNO_3 can happen in the gaseous phase, at the surface of solid or in the aqueous phase within liquid aerosol. Depending on the mechanism new aerosol is either formed which might be in the size range of tenth of nm and could rapidly coagulate forming bigger aerosol or present aerosol must be expected to grow. Measurements of the size dependent particle flux at different heights could decide on which process dominates in which conditions.

This information is important as to help estimating the reaction rates because Mozurkewich (1993) found the equilibrium constant to depend on the aerosol size. Gas-to-particle conversion might also be one of the most important sources of new aerosol within the atmosphere and its magnitude is interesting for estimating the effect on the production of cloud condensation nuclei.

7.4 Formulation of correction procedures for ammonia fluxes measured by gradient methods

In the presence of GPC the NH_3 surface flux cannot be measured by common gradient methods. Direct methods (e.g. eddy correlation methods) require fast sensors which have not yet been developed for NH_3. Therefore, it must be one of the final aims to formulate recipes for correcting NH_3 fluxes for the effect of GPC so that the 'true' surface flux can be estimated by gradient methods.

In the best case this correction would be an analytical expression. Although such a solution has been found for the NO_x cycle it has been reported not to be very accurate by Duyzer *et al.* (1995) it is unlikely that an analytical solution can be found for the concentration profiles of NH_3.

The second alternative is a model of the form presented in this report which takes all major factors (chemical species, effects on the equilibrium and reaction rate constants etc.) into account and is implemented in as fast an algorithm as possible to make it applicable.

From a analytical and mathematical point of view a semi-empirical correction as also presented by Duyzer *et al.* (1995) for NO_x is least satisfactory. However, because of the complex nature of the equilibria it might be the most accurate way to correct for GPC. Derived from artificially generated data and for the NO_x cycle the validity and adoption of such an approach needs to be tested. Whereas the flux divergence was expressed by a logarithmic function in the case of NO_x the shape of the flux divergence of the NH_3 flux largely depends on the surface conditions and gradients of temperature and relative humidity which has not yet been sufficiently established.

7.5 Estimation of the quantitative influence of gas-to-particle-conversion on the exchange budget of NH_3 in the UK

Work is being done to map NH_3 sources at an increasingly finer grid resolution and to model the transport and deposition of NH_3 in the UK. As in the case of gradient methods the effect of gas-to-particle conversion has so far been neglected. Depending on the correction expression found according to the section before this model has to be overlaid with the necessary data to include GPC correction. This could mean that concentration data for NH_4^+ as well as HNO_3 and HCl or even their fluxes have to be mapped and that daily and yearly temperature and humidity cycles have to be estimated.

As the influence of GPC might lead to an underestimation of deposition fluxes of 10% and more this correction is important to correctly evaluate the exceedance of critical loads of N into different ecosystems.

8. LITERATURE

Allen A.G., Harrison R.M. and Erisman J.-W. (1989): Field measurements of the dissociation of ammonium nitrate and ammonium chloride aerosols. *Atmos. Environ.* **23** no. 7. pp 1591-1599.

Allen A.G., Harrison R.M. and Wake M.T. (1988): A meso-scale study of the behaviour of atmospheric ammonia and ammonium. *Atmos. Environ.* **22.** pp 1347-1353.

Andersen H.V. and Hovmand M.F. (1994): Measurements of ammonia and ammonium by denuder and filter pack. *Atmos. Environ.* **28** no. 21. pp 3495-3512.

Asman W.A.H (1992): Ammonia emission in Europe: updated emission and emission variations. *RIVM report.* 228471008. RIVM, Bilthoven, The Netherlands.

Behra P., Sigg L. and Stumm W. (1989): Dominating influence of NH_3 on the oxidation of aqueous SO_2: The coupling of NH_3 and SO_2 in atmospheric water. *Atmos. Environ.* **23** no. 12, pp 2691-2707

Brost and Wyngaard (1978): A model study of the stable stratfied planetary boundary layer. *J. Atmos. Sci.* **35.** pp 378-380.

Brost R.A., Delany A.C. and Huebert B.J. (1988): Numerical modeling of concentrations and fluxes of HNO_3, NH_3 and NH_4NO_3 near the surface. *J. Geophys. Res.* **93.** pp 7137-7152.

Burden R.L. and Faires J.D. (1993): Numerical analysis. 5th edition. PWS Publishing Company. Boston.

Businger J.A. and Oncley S.P. (1990): Flux measurement with conditional sampling. *J. Atmos. Ocean. Tech.* **7.** pp 349-352.

Businger J.A. (1966): Transfer of momentum and heat in the planetary boundary layer. In: *Arctic heat budget and atmospheric circulation* (Symposium proceedings) pp 305-332. The Rand Corporation.

Coe H. (1993): The exchange of nitrogen dioxide and ozone between the vegetation and the atmosphere. PhD thesis University of Manchester Institute of Science and Technology, UMIST.

Denmead O.T. (1983): Micrometeorological methods for measuring gaseous losses of nitrogen in the field. In: *Gaseous loss of nitrogen from plant-soil systems* (Edts.: J.R. Freney and J.R. Simpson). pp 133-157. Martinus Nijhoff and Dr. W. Junk. The Hague.

Denmead O.T. (1995): Novel meteorological methods for measuring trace gas fluxes. *Phil. Trans. R. Soc. Lond.* **351A.** pp 383-396.

Dentener F.J. and Crutzen P.J. (1994): A three-dimensional model of the global ammonia cycle. *J. Atmos. Chem.* **19.** pp 331-369.

Duyzer J.H., Deinum G. and Baak J. (1995): The interpretation of measurements of surface exchange of nitrogen oxides: Correction for chemical reactions. *Phil. Trans. R. Soc. Lond.* **A 351**. pp 231-248.

Dyer A.J. and Hicks B.B. (1970): Flux-gradient relationships in the constant flux layer. *Quart. J. Roy. Meteor. Soc* **96**. pp 715-721.

Erisman J.-W., Vermetten A.W.M., Asman W.A.H., Waijers-Ijeplaan A. and Slanina J. (1988): Vertical distribution of gases and aerosols: The behaviour of ammonia and related components in the lower atmosphere. *Atmos. Environ.* **22** no. 6. pp 1153-1160.

Erisman J.W. and Wyers G.P. (1993): Continuous measurements of surface exchange of SO_2 and NH_3; Implications for their possible interaction in the deposition process. *Atmos. Environ.* **27A**. no. 13. pp 1937-1949

Fitzjarrald D.R. and Lenschow D.H. (1983): Mean concentration and flux profiles for chemically reactive species in the atmospheric surface layer. *Atmos. Environ.* **17** no. 12. pp 2505-2512.

Fontan J., Lopez A., Lamaud E. and Druilhet A. (1995): Vertical flux measurements of the submicron aerosol particles and parameterization of the dry deposition velocity. *Not yet published.*

Fowler D. and Unsworth M.H. (1979): Turbulent transfer of sulphur dioxide to a wheat crop. *Quart. J. Roy. Meteor. Soc.* **105**, pp 767-783

Gallagher M., Fontan J., Wyers P.G., Ruijgrok W., Duyzer J. and Hummelshoj P. (1995): Atmospheric particles and their interaction with natural surfaces. A review paper for Biatex: A Eurotrac sub-programme.

Gao W. (1995): The vertical change of coefficient b, used in the relaxed eddy accumulation method for flux measurement above and within a forest canopy. *Atmos. Environ.* **29**. no. 17. pp 2339-2347

Gao W., Wesely M.L. and Lee I.Y. (1991): A numerical study of the effects of air chemistry on fluxes of NO, NO_2 and O_3 near the surface. *J. Geophys. Res.* **96** no. D10. pp 18,761-18,769.

Garland J.A. (1977): The dry deposition of sulphur dioxide to land and water surfaces. *Proc. Roy. Soc. Lond.*. **A 354**. pp 245-268.

Garrant (1992): The atmospheric boundary layer. 315 pp. Cambridge University Press. Cambridge.

Hamer W.J. and Wu Y.C. (1972): Osmotic coefficients and mean activity coefficients of uni-univalent electrolytes in water at 25°C. *J. phys. chem. Ref. Data* **1**. pp 1047-1099.

Hargreaves K.J. and Atkins D.H.F. (1987): The measurement of ammonia in the outdoor environment using passive diffusion tube samplers. *Report AERE-R-12568*. Harwell Laboratory, Didcot, Oxon, UK

Harrison R.M. and Pio C.A. (1983): An investigation of the atmospheric HNO_3-NH_3-NH_4NO_3 equilibrium relationship in a cool, humid climate. *Tellus* **35B**. pp 155-159.

Hough A.M. and Derwent R.G. (1987): Studies of the distribution of photochemical ozone production between different hydrocarbons. *Atmos. Environ.* **21**. pp 2015-2033.

Huebert B.J., Luke W.T., Delany A.C. and Brost R.A. (1988): Measurements of concentrations and dry surface fluxes of atmospheric nitrates in the presence of ammonia. *J. Geophys. Res.* **90**. pp 2085-2090.

Hummelshøj P. (1992): Dry deposition of particles and gases. PhD thesis. Risø National Laboratory, Roskilde, Denmark.

Husted, S. and Schjorring, J.K. (1995): Apoplastic pH and ammonium in leaves of Brassica napus. *Plant Physiology*, in press.

Keller H.B. (1968): Numerical methods for two-point boundary-value problems. Blaisdell Publishing Company. Waltham, Massachusetts, Toronto, London.

Keuken M.P, Schoonebeck C.A.M, van Wensveen-Louter A. and Slanina J. (1988): Simultaneous sampling of NH_3, HNO_3, HCl, SO_2 and H_2O_2 in ambient air by a wet annular denuder system. *Atmos. Environ.* **22** no. 11. pp 2541-2548.

Khlystov A., Wyers G.P. and Slanina J. (1995): The steam-jet aerosol collector. *Atmos. Environ.* **29** no. 17. pp 2229-2234.

Kramm G. and Dlugi. R. (1994): Modelling of the vertical fluxes of nitric acid, ammonia and ammonium nitrate. J. Atmos. Chem. ...

Lamaud E., Chapuis A., Fontan J. and Serie E. (1994): Measurements and parameterization of aerosol dry deposition in a semi-arid area. *Atmos. Environ.* **28** no. 14. pp 2461-2471.

Larson T.V. and Taylor G.S. (1983): On the evaporation of ammonium nitrate. *Atmos. Environ.* **17**. pp 2489-2495.

Lenschow D.H. and Raupach M.R. (1991): The attenuation of fluctuations in scalar concentrations through sampling tubes. *J. Geophys. Res.* **96** no. D8. pp 15259-15268.

Lenschow D.H. and Delany A.C. (1987): An analytic formulation for NO and NO_2 flux profiles in atmospheric surface layer. *J. Atmos. Chem.* **5**. pp 301-309.

Monteith J.L. and Unsworth M.H. (1990): Principles of environmental physics. 2nd edition. Edward Arnold press. London, New York, Melbourne, Auckland 1990.

Mozurkewich M. (1993): The dissociation constant of ammonium nitrate and its dependence on temperature, relative humidity and particle size. *Atmos. Environ.* **27A** no. 2. pp 261-270.

Neumann H.H. and den Hartog G. (1985): Eddy correlation measurements of atmospheric fluxes of ozone, sulphur and particulates during the Champaign intercomparison study. *J. Geophys. Res.* **90** no. D1. pp 2097-2110.

Nihlgård, B. (1985): The ammonium hypothesis - An additional explanation to the forest dieback in Europe. *Ambio* **14**. pp 2-8

Owen P.R. and Thomson W.R. (1963): Heat transfer across rough surfaces. *J. Fluid Mech.* pp 321-334.

Panofsky H.A. (1963): Determination of stress from wind and temperature measurements. *Quart. J. Roy. Meteor. Soc.* **89**. pp 85-94.

Paulson C.A. (1970): The mathematical representation of wind speed and temperature profiles in the unstable atmospheric surface layer. *J. App. Meteor.* **9**. pp 857-861.

Peters K. and Eiden R. (1992): Modelling the dry deposition velocity of aerosol particles to a spruce forrest. *Atmos. Environ.* **26A** no. 14. pp 2555-2564.

Pio C.A. and Harrison R.M. (1987a): The equilibrium of ammonium chloride aerosol with gaseous hydrochloric acid and ammonia under tropospheric conditions. Letter to the editors. *Atmos. Environ.* **21** no. 5. pp 1243-1246.

Pio C.A. and Harrison R.M. (1987b): Vapour pressure of ammonium chloride aerosol: Effect of temperature and humidity. *Amos. Environ.* **21** no.12. pp 2711-2715.

Press W.H., Teukolsky S.A., Vetterling W.T. and Flannery B.P. (1992): Numerical recipes in C - The art of scientific computing. 2nd edition. Cambridge Univ. Press. Cambridge.

Raupach M.R. (1989a): A practical Lagrangian method for relating scalar concentrations to source distributions in vegetation canopies. *Quart. J. Roy. Meteorol. Soc.* **115**. pp 609-632.

Raupach M.R. (1989b): Applying Lagrangian fluid mechanics to infer scalar source distributions from concentration profiles in plant canopies. *Agric. and Forest Meteorol.* **47**. pp 85-108.

Roux A., Musbally G.M., Perron G. and Desnoyers J.E. (1978): Apparent molal heat capacities and volumes of aqueous electrolytes at 25°C: $NaClO_3$, $NaClO_4$, $NaNO_3$, $NaBrO_3$, $NaIO_3$, $KClO_3$, $KBrO_3$, KIO_3, NH_4NO_3, NH_4Cl and NH_4ClO_4. *Can. J. Chem.* **56**. pp 24-28.

Schwartz S.E. (1986): Mass-transport considerations pertinent to aqueous phase reactions of gases in liquid-water clouds. In: *Chemistry of multiphase atmospheric systems* (Ed.: Jaeschke W.). pp 415-471. Springer-Verlag. New York.

Seidl W., Brunnemann G., Kins L., Köhler E., Reußwig K. and Dlugi R. (1995): On the ionic composition of aerosol particles and related gas phase species at two sites during the SANA 2 - campaign. In press.

Seinfeld J.H. (1986): Atmospheric chemistry and physics of air pollution. John Wiley, New York. 738 pp.

Slinn W.G.N. (1982): Predictions for particle deposition to vegetative canopies. *Atmos. Environ.* **16** no. 7. pp 1785-1794.

Stelson A.W. and Seinfeld J.H. (1982): Relative humidity and temperature dependence of the ammonium nitrate dissociation constant. *Atmos. Environ.* **16** no. 5. pp 983-992.

Sutton M.A., Fowler D. and Moncrieff J.B. (1993): The exchange of atmospheric with vegetated surfaces. I: Unfertilized vegetation. *Q. J. R. Meteorol. Soc.* **119**. pp 1023-1045.

Sutton M.A., Burkhardt J.K, Guerin D. and Fowler D. (1995): Measurement and modelling of ammonia exchange over arable croplands. In: *Acid rain research: Do we have enough answers?* (Eds.: Heij G.J. and Erismann J.-W.). Elsevier Science BV. pp 71-80.

Sutton M.A., Schjørring J.K. and Wyers G.P. (1995): Plant-atmosphere exchange of ammonia. *Phil. Trans. R. Soc. Lond.* **A 351**, pp 261-278.

Sutton, M.A. (1990): The surface/atmosphere exchange of ammonia. PhD thesis, Institute of Ecology and Resource Management, University of Edinburgh, Edinburgh, UK, 194 pp

The Royal Society (1983): The nitrogen cycle in the United Kingdom. Report of a Royal Society Study group. Royal Society,. London

Thom A.S. (1975): Momentum, mass and heat exchange of plant communities. *In: Vegetation and the atmosphere. Vol. 1.* (Ed.: Monteith J.L.). pp 57-109. Academic Press. London.

van der Eerden (1982): Toxicity of ammonia to plants. *Agric. and Environ.* **7**, pp 223-235

Wagmann D.D., Evans W.H., Parker V.B., Harlöw I., Baily S.M. and Schumm R.H. (1968): Selected values of chemical thermodynamic properties; tables for the first thirty-four elements in the standard order of arrangement. NBS technical note 270-3.

Wagner H. and Neumann K. (1961): Der Dampfdruck des Ammoniumchlorids zwischen 35 und 90°C. *Zeits. Phys. Chem.* **21**. pp 51-70.

Webb E.K. (1970): Profile relationships: The log-linear range and extension to strong stability. *Quart. J. Roy. Meteor. Soc.* **96**, 67-90.

Webb E.K., Pearman G.I. and Leuning R. (1980): Correction of flux measurements for density effects due to heat and water vapour transfer. *Quart. J. Roy. Meteor. Soc.* **106**. pp 85-100.

Wesely M.L (1989): Parameterization of surface resistances to gaseous dry deposition in regional-scale numerical models. *Atmos. Environ.* **23** no. 6. pp 1293-1304.

Wyers G.P., Otjes R.P. and Slanina J. (1993): A continious-flow denuder for the measurement of ambient concentrations and surface-exchange fluxes of ammonia. *Atmos. Environ.* **27A** no. 13. pp 2085-2090.

Wyers, G.P.; Otjes, R.P.; Vermeulen, A.T.; Wild, P.J. and Slanina, J. (1992): Measurement of vertical concentration gradients of ammonia by continuous-flow denuders. In: *Field measurements and interpretation of species related to acid deposition. Air Pollution Report* **39** (eds.: G. Angeletti, S. Beilke and J. Slanina). pp 173-178. CEC. Brussels

Wyers, G.P.; Otjes, R.P. and Slanina, J. (1993): A continuous-flow denuder for the measurement of ambient concentrations and surface-exchange fluxes of ammonia - Technical Note; *Atmos. Environ.* **27A**, 1993, No. 13, pp 2085-2090

Zhang Y., ten Brink H., Slanina S. and Wyers P.G. (1995): The influence of ammonium nitrate equilibrium on the measurement of exchange fluxes of ammoni and nitric acid. in: *Acid rain research: Do we have enough answers?* (Eds.: G.J. Heij and J.-W. Erisman). Elsevier Science BV. pp 103-112.